Effect of denervation on the regulation of mitochondrial transcription factor A expression in skeletal muscle

Liam D. Tryon

A thesis submitted to the Faculty of Graduate Studies in partial fulfilment of the requirements for the degree of Master of Science

Graduate Program in Kinesiology and Health Science
York University
Toronto, Ontario

July 2014

Abstract

The most rapid decline in myofiber size and mitochondrial content during denervation, a muscle disuse model, occurs during the first week following the onset of the stimulus. In this study, we analyzed the expression of Tfam, a critical mitochondrial transcription factor involved in the orchestration of mitochondrial biogenesis, at multiple levels during denervation. Tfam transcriptional activation was depressed during the early stages of denervation but was counteracted by increases in the stability of the Tfam mRNA, an effect which could not be accounted for by the protein expression of select RNA-binding proteins. Denervation reduced Tfam mitochondrial import, which was associated with reductions in mitochondrial DNA transcription. These data highlight that there are multiple factors affecting the expression and activity of the Tfam transcript and protein during denervation. This work also emphasizes the importance of mitochondrial protein import in the regulation of Tfam function, and subsequently mitochondrial content, during muscle disuse.

Acknowledgements

My parents for their unrelenting support and encouragement.

Stephen Pastore, Matthew Crilly, Jonathan Memme and Eric Desjardins for their technical assistance, support and dedicated work ethic.

Dr. David A. Hood for his continued guidance and advice, as well as giving me more opportunities than I can thank him for.

Table of Contents

List of Tables and Figures
Review of Literature

Manuscript

List of abbreviations

4E-BP1	eukaryotic translation initiation factor 4E binding protein 1
ACh	acetylcholine
ADP	adenosine diphosphate
AICAR	5-Aminoimidazole-4-carboxamide ribonucleotide
Akt	*Other aliases:* PKB (protein kinase B)
AMP	adenosine monophosphate
AMPK	AMP-activated protein kinase
ARE	adenosine-uridine (AU)-rich elements
ATF2	activating transcription factor 2
Atg7	autophagy related protein 7
ATP	adenosine triphosphate
Ca^{2+}	calcium ion
CaMK	Ca^{2+}/calmodulin-dependent protein kinase
CCA	chronic contractile activity
Ccr4-Not	negative regulator of transcription complex
ChIP	chromatin immunopreciptation
COX	cytochrome *c* oxidase
COX I	cytochrome *c* oxidase subunit I
CREB	cyclic AMP-responsive element-binding protein 1
CUGBP1	CUG-binding protein 1
DcpS	decapping scavenger enzyme
Drp1	dynamin-related protein 1
EDL	extensor digitorum longus
Egr-1	early growth response protein-1
eIF2β	eukaryotic initiation factor 2 β
eIF4E	eukaryotic translation initiation factor 4E
EMSA	electrophoretic mobility shift assay
ERK1/2	extracellular-signal-regulated kinases 1/2
ERR	estrogen related receptor
ETC	electron transport chain
Fis1	fission 1
FoxO	forkhead box O
FTR	fast-twitch red
FTW	fast-twitch white
GRE	guanosine-uridine (GU)-rich elements
GSK3β	glycogen synthase kinase 3 β
H_2O_2	hydrogen peroxide
HMG	high motility group
HSP1/HSP2	heavy strand promoter 1/2
Hsp70/Hsp90	heat shock protein 70/90
HuR	human antigen R
IGF-1	insulin growth factor-1
IMF	intermyofibrillar
IMM	inner mitochondrial membrane
KSRP	KH-type splicing regulatory protein
LC3	microtubule-associated protein 1 light chain 3
LON	mitochondrial LON protease
LSP	light strand promoter
m7G	7-methylguanosine
MEF2	myocyte enhancing factor 2
MHC	myosin heavy chain
miRISC	miRNA-mediated silencing complex
miRNA	micro RNA

mRNP	messenger RNA-protein complex
mtDNA	mitochondrial DNA
mtHsp70	mitchondrial heat shock protein 70
mTORC1	mammalian target of rapamycin complex 1
MTS	matrix targeting sequence
Mul1	mitochondrial E3 ubiquitin protein ligase 1
MuRF1	muscle RING finger 1
NFAT	nuclear factor of activated T-cells
NMJ	neuromuscular junction
NRF-1/2	nuclear respiratory factor-1/2
NUGEMP	nuclear gene encoding mitochondrial protein
OMM	outer mitochondrial membrane
Oxa1	oxidative assembly protein 1
OXPHOS	oxidative phosphorylation
p38 MAPK	p38 mitogen activated protein kianse
p62	*Other aliases:* SQSTM1 (sequestosome 1)
p97/VCP	p97/valosin containing protein
PABP	poly(A)-binding protein
PAM	presequence translocase-associated motor
Pan2-Pan3	poly(A)-specific ribonuclease subunit 2/3
PARN	poly(A)-specific ribonuclease
PGC-1α	peroxisome proliferator-activated receptor gamma coactivator-1, alpha
PI3K	phosphoinositide-3-kinase
PINK1	phosphatase and tensin homolog (PTEN) induced putative kinase 1
PKC	protein kinase c
Pol γ	polymerase gamma, mitochondrial (DNA)
POLRMT	polymerase, mitochondrial (RNA)
PPAR	peroxisome proliferator-activated receptor
RIP	RNA immunoprecipitation
RBP	RNA-binding protein
ROS	reactive oxygen species
RRM	RNA-recognition motif
rRNA	ribosomal RNA
S6K	ribosomal protein S6 kinase, 70kDa
SDH	succinate dehydrogenase
Sp1	specificity protein 1
SS	subsarcolemmal
STR	slow-twitch red
TA	tibialis anterior
Tfam	mitochondrial transcription factor A
Tfb2m	mitochondrial transcription factor B2
TIM/Tim	translocase of the inner mitochondrial membrane
TOM/Tom	translocase of the outer mitochondrial membrane
TRAF6	TNF receptor associated factor
tRNA	transfer RNA
UPS	ubiquitin-proteasome system
USER	untranslated sequence elements for regulation
UTR	untranslated region
YY1	yin yang 1

Chapter 1

REVIEW OF LITERATURE

1.0 Skeletal Muscle

Skeletal muscle, along with cardiac and smooth muscle, are the three main forms of muscle present in mammals. As the name suggests, skeletal muscles are responsible primarily for the locomotive function of the mammalian skeleton, through their association with bones via tendons or apopneuroses. Skeletal muscle is under the exclusive control of the central nervous system, which allows for the voluntary recruitment of this tissue for locomotion. Further, skeletal muscle is characterized by having 'striations' (that is, a striped or banded appearance), and can be composed of thousands or more individual myofibers, each spanning the length of the muscle itself. Within a muscle, individual fibers are grouped into bundles surrounded by connective tissue, which receive vascular and neural input. These inputs provide nutrients and oxygen for the production of adenosine triphosphate (ATP) which is required for muscle contraction, as well as nervous innervation at the neuromuscular junction (NMJ), which provides the stimulus for muscle contraction. In concert with these inputs, contraction of this tissue at the most basic level is attributable to the interaction of the myofibrillar actin and myosin proteins in an ATP-dependent process, known as cross-bridge cycling.

Skeletal muscle represents approximately 40% of a non-obese individual's body mass, and is capable of responding with astounding plasticity to both environmental and genetic stimuli. These cues can result in profound functional and phenotypic alterations. Thus, an understanding of the structure and function of skeletal muscle allows for a full appreciation of these changes.

1.1 Skeletal Muscle Fiber Types and Composition

Skeletal muscle is under direct neural control, and this influence is voluntary. Efferent α-motor neurons control the release of the neurotransmitter acetylcholine at the NMJ and allow for

the entry of extracellular calcium and the release of calcium from intracellular stores in the sarcoplasmic reticulum. This calcium release event allows for the ATP-dependent interaction of actin and myosin, which is responsible for the shortening of the sarcomere, the smallest functional unit within skeletal muscle (94), and a resulting muscle contraction.

Diversity exists among muscle fibers, in terms of the coupling between the neurochemical excitation and mechanical contraction. This diversity is predominantly attributable to the differential expression of myosin heavy chain proteins, in addition to the extent of neural innervation and the frequency with which the muscle receives neural input (181, 208) as well as the metabolic pathways employed for the generation of energy require to contract muscle. Skeletal muscle can be grouped into three general categories defined by their principle fiber type: slow-twitch red (STR), fast-twitch red (FTR) and fast-twitch white (FTW). Slow-twitch red fibers have the greatest degree of neural innervation for a given muscle fiber area, allowing them to be active for long periods of time without undergoing substantial fatigue. These fibers are also characterized by their distinct red colouration due to their high mitochondrial content, and are highly reliant on oxidative metabolism for the generation of ATP. On the other hand, fast-twitch white fibers are the largest in size, and have the least amount of neural innervation for a given fiber area. This fiber type has the capacity to contract with great force, but as a result, fatigues quite rapidly. This is a consequence of being highly dependent on glycolysis for the generation of ATP, lacking the mitochondria of the STR fiber type. Fast-twitch red fibers are intermediate to these other types in terms of size, contraction force, fatigability, and dependence on oxidative or glycolytic pathways. While these comparisons are true for human skeletal muscle, rat skeletal muscle is slightly different. In this mammal, fast-twitch red fibers are considered the most oxidative, higher than STR and FTW fibers, respectively (49).

This difference is likely owing to the fact that there are inter-species differences in locomotive, postural and behavioral patterns. Nonetheless, the heterogeneity observed in the composition and source of energy production between these fiber types is suggestive of differential adaptation to stimuli, either internal or external.

Muscle fibers also possess a population of precursor cells, termed “satellite cells”, which can proliferate, and either partake in the formation of new muscle fibers, or donate their nuclei to the existing muscle fibers when there is an increased requirement for transcriptional activity (84). This contributes to the ‘multi-nucleated’ appearance of skeletal muscle fibers, a feature unique to this tissue. This trait of skeletal muscle factors greatly into its adaptive plasticity.

1.2 Skeletal muscle oxidative capacity

The capacity of a muscle to consume oxygen is dependent on both the supply of oxygen to the tissue, and the ability of the tissue to consume that which is delivered to it. Oxygen supply is determined by the vascularity of the tissue, which determines the amount of oxygen which can be supplied by circulating hemoglobin. A large capillary bed allows for greater amounts of oxygen to be delivered. Once supplied to the tissue, a muscle-specific oxygen carrying molecule, termed myoglobin, can act as an intermediate to reversibly bind oxygen and facilitate the delivery of oxygen to the mitochondria from the surface of the muscle cell. This feature is particularly significant in highly oxidative, slow-twitch muscle fibers (35, 251).Once delivered to the mitochondrion, oxygen can be consumed at the end of a series of oxidation-reduction reactions, to power the synthesis of ATP. There is a positive correlation between the amount of mitochondria contained within skeletal muscle and the amount of oxygen that tissue is able to consume (210).

Knowing this, we often regard “oxidative capacity” and “mitochondrial content” as synonymous phrases. Thus, any changes to the mitochondrial content of a muscle, perhaps brought about by chronic endurance training or prolonged muscle disuse, should directly influence the capacity of that muscle to consume oxygen. Fortunately, many established mammalian models exist which recapitulate these alterations and allow for the study of the phenotypic and metabolic alterations that are associated with these changes.

1.3 Muscle Disuse: A model of reduced skeletal muscle contractile activity

Given that skeletal muscle accounts for almost half of the mass of the human body, it is not surprising that the capacity of this tissue to adapt to stimuli is extensive. This is the case in muscle atrophy, which can occur as a product of pathology (ie. disease states) or in the absence of contractile activity. Alterations to muscle during atrophy range from acute changes in molecular signaling to chronic functional, metabolic and morphological adaptations. However, the etiology of the atrophy is often a powerful factor in determining the outcome that is manifested in terms of these changes.

Due to the invasive nature of obtaining skeletal muscle samples from humans to study the mechanisms of inactivity-induced muscle wasting, multiple animal models that mimic muscle disuse in humans can be used. This section will review a few of these models, before exploring disuse-induced adaptations to skeletal muscle and the mechanisms by which these occur.

1.3.1 Experimental models to study disuse-induced skeletal muscle atrophy

Rodent models of limb immobilization have been utilized to investigate the impact of the removal of a weight bearing stimulus to a muscle, specifically that of hindlimb immobilization (ie. casting) or the tail suspension technique. These models provide insight into the mechanisms through which muscle disuse is brought about, and has direct applications to human

circumstances, such as spaceflight or prolonged bed rest. These techniques are non-invasive, and are typically cost-effective. In terms of hindlimb suspension, the technique was developed over 40 years ago by the National Aeronautics and Space Agency for the purpose of weightlessness simulation and alterations in musculoskeletal loading, as experienced during prolonged spaceflight (156, 157). As the opportunities for microgravity exposures are limited, this model provides the best estimate of its effects on muscles. This method utilizes a tail-cast to hang the hindlimbs into an unweighted, suspended position, leaving the head tilted downwards and affording the animal freedom of forelimb movements (161). This provides for an important intra-animal control when analyzing the tissues. While not used for the same extent of extrapolation as hindlimb suspension affords for spaceflight weightlessness, limb casting immobilization provides another paradigm by which non-invasive muscle atrophy can be analyzed and achieved in rodent models. This model allows for a plastic or orthopedic cast to be applied to an animal, fixing a joint in a particular position and stretching the muscle to a predetermined length (161). As these muscles are fixed in a particular position, atrophy and hypertrophy can be achieved in a muscle and its antagonist respectively. Both of these techniques are relatively simple to perform and sufficient to induce disuse. However, the rapidity by which atrophy is achieved is quite slow, and this can act as an obstacle when using these models experimentally.

In contrast to these non-invasive techniques, denervation provides a surgical method to induce muscle disuse. Denervation (or neurotomy) involves the physical interruption of neural innervation, through severing the α-motor neuron supply to the muscle. This effectively removes the nerve-muscle communication and can rapidly induce atrophy, but may also interrupt neural input to vascular beds innervated by the same nerve (161). This technique serves as a model for severe spinal cord injury, where there is no possibility of neural regeneration. Nerve crushing is a

closely related technique that involves the physical application of force to the nerve with adequate pressure to temporarily ablate neural input to the muscle. However, over time this model permits regeneration of the nerve and re-innervation to occur. Alternatively, a chemical approach to denervation can be taken (161), as physical denervation removes both neuromotor and neurotrophic inputs to the muscle. Treatment with the sodium-channel blocker tetrodotoxin maintains both axonal continuity and the flow of possible trophic factors, while eliminating impulse conduction from the nerve to the muscle (148). This approach removes any confounding interruptions to vascular beds supplied by the same nerve during neurotomy.

In addition to the models mentioned, starvation, aging and various disease states (sepsis, cancer cachexia, AIDS, burn injury, heart failure) are all associated with muscle loss. However, the intracellular mechanisms between disuse-induce muscle atrophy and the atrophy induced by these stimuli is comprehensively different. Although all of these models are valid in their own right, conclusions drawn from one model should be applied with caution to the others. Ultimately, the model utilized should reflect the goals of the study.

1.3.2 Mechanisms of disuse-induced skeletal muscle atrophy

Prolonged inactivity of skeletal muscle results in a net loss of muscle protein content and myofiber atrophy. Atrophy is predominantly due to over-activation of the cell's major proteolytic pathways, the ubiquitin-proteasome system (UPS) and the autophagy-lysosome pathway, which control the half-life of awide variety of cellular proteins. Although it is clear that these changes in myofiber size arise from an reduction in muscle protein synthesis and an increase in protein degradation (10, 55, 69, 223, 249), the mechanisms by which this occur as a result of a disuse stimulus continue to be elucidated. In this section, a brief outline of the pathways governing disuse-induced muscle atrophy will be provided.

Muscle mass maintenance and hypertrophy is predominantly controlled through the IGF-1 (insulin growth factor-1)/PI3K/Akt signaling axis (199). Activation of this pathway by circulating IGF allows for Akt to stimulate protein synthesis through its downstream effectors (mammalian target of rapamycin) (117). Simultaneously, Akt maintains an inhibitory phosphorylation on the forkhead box O (FoxO) transcription factor family (202, 219, 261). However, when this inhibitory phosphorylation is removed, FoxO family members can translocate to the nucleus and induce muscle atrophy through a subset of genes that are commonly up- or down-regulated in response to muscle-disuse stimuli (122, 198). The genes that are consistently up-regulated are commonly referred to as atrophy-related genes ("atrogenes") and are transcripts associated with the UPS and autophagy pathways. Thus, Akt appears to be the main point of control in determining the balance between protein synthesis and degradation.

In response to muscle disuse, the UPS is responsible for the removal of muscle sarcomeric proteins. It does so through up-regulating the expression of ubiquitin and ubiquitin-conjugating enzymes, increasing the conjugation of ubiquitin to muscle proteins and the rate of removal of these proteins via the proteasome (121). The rate-limiting step in this system is the conjugation of ubiquitin to proteins by E3 ligases. There are several E3 ubiquitin ligases responsible for this conjugation, which are both muscle-specific and up-regulated during muscle atrophy. The E3 ligases first identified were atrogin-1 and muscle RING finger 1 (MuRF1), and were found to be induced by denervation (21). Interestingly, while it remains to be confirmed, atrogin-1 is suspected to have several muscle proteins as substrates (135). On the other hand, MuRF1 has been reported to interact with and contribute to the degradation of many muscle structural proteins, including troponin I and myosin heavy and light chains (38, 40, 62, 103). Nonetheless, knockout models of both of these ligases are resistant to denervation-induced

muscle atrophy, suggesting a strong importance for ubiquitin-conjugation in UPS-mediated atrophy (21).

In addition to atrogin-1 and MuRF1, knockout of TRAF6 (TNF receptor associated factor 6), a ubiquitin ligase which mediates the conjugation of polyubiquitin chains to target proteins, also provides resistance to denervation-induced muscle loss (113, 152, 178). In a related system, the p97/VCP (valosin containing protein) complex assists in the removal of ubiquitinated proteins from larger intramuscular structures during denervation. Similarly, over-expression of a dominant-negative p97/VCP in skeletal muscle preserves muscle mass and blocks proteolysis during denervation-induced disuse (184).

The autophagy-lysosome system is another pathway which is activated during muscle disuse, and similar to the UPS, is under the regulation of FoxO transcription factors (FoxO3a in particular) (142, 261). This pathway allows for the bulk degradation of proteins and organelles, through sequestration into vacuoles, and delivery of these vacuoles to lysosomes for digestion by lysosomal enzymes (85). In fact, Mammucari et el. demonstrated that autophagy is a required process for myofiber atrophy to occur (142). Interestingly, autophagy appears to serve a basal role in the maintenance of muscle mass, as *Atg7*-null mice (mice unable to initiate autophagy) display several signs of myopathy, including abnormal mitochondria, oxidative stress and a buildup of polyubiquitinated proteins (144).

Apart from activation of the UPS and autophagy-lysosome system, myonuclear apoptosis contributes to muscle atrophy, although not to the extent of these other two systems. This form of apoptosis is distinct from classical apoptosis, as muscle fibers contain multiple nuclei per cell body, each which control a particular domain of cytoplasm. This way, it is possible to undergo a loss of myonuclei without cell death in these multi-nucleated fibers during disuse muscle atrophy

(203). Indeed, denervated skeletal muscle displays greater mitochondrial-associated apoptotic susceptibility, denoted by the increased expression of pro-apoptotic proteins and increased DNA fragmentation, alongside reductions in myofiber size (4, 24, 218). This myonuclear loss with muscle atrophy may be a strategy to maintain a relatively constant and optimal nucleus-to-myofiber ratio.

1.3.3 Disuse-induced adaptations in skeletal muscle

With muscle disuse, there are a variety of morphological, functional and metabolic adaptations which can occur. These changes appear to be species-, stimulus-, muscle- and muscle fiber type-specific, while also sensitive to the duration which the stimulus is applied. Accordingly, the analysis of these adaptations must be interpreted with respect to these these influencing factors.

One of the most evident alterations in skeletal muscle with disuse is the reduction in skeletal muscle mass and myofiber cross-sectional area (4, 23). These reductions occur as an adaptation to a decreased recruitment of the muscle fibers, and the loss of pro-hypertrophic stimuli which basally maintain muscle fiber size. Further, the loss of neural influence by denervation or mechanical unloading has been shown to cause a slow-to-fast fiber type conversion (37). Preferential atrophy for specific fiber types has been shown to occur, however this preference is dependent on the muscle type it is expressed in (177). The exact mechanism of this phenomenon is unknown, but may be due to the neural influences which differ between muscles, in addition to a wide selection of intrinsic properties of myofiber, such as differential gene expression, neural innervation and contractile properties.

Early electron microscopy work has demonstrated that ultra-structural alterations, such as sarcomeric and myofibrillar disruption, along with changes in the size and shape of mitochondria

and the sarcoplasmic reticulum is typical of denervated muscle (72, 86, 138, 179). These ultra-structural changes manifest in functional changes, the most notable being a reduction in muscle contractile strength (63, 246), as myofiber cross-sectional area is directly linked with the capacity to generate force. Associated with this is a super-sensitivity of skeletal muscle to acetylcholine (ACh), in part due to the spreading of ACh receptors all over the muscle, including outside of the NMJ (13). This may be the muscle's attempt to become more sensitive to ACh in response to the fact that ACh is no longer abundant. Muscle capillarization is also impacted by denervation, as capillary regression and reduction in the capillary-to-fiber ratio have been reported (25, 233, 239). Taken together, the multitude of changes to the ultrastructure of the muscle following denervation appears to directly result in functional impairments.

In addition to these morphological alterations, there are metabolic changes brought about altered gene expression and signaling which occurs with muscle disuse. The next sections will address the changes which occur in response to muscle disuse in both the acute (within the first week) and chronic stages of following the cessation of contractile activity.

1.3.3.1 Early disuse-induced alterations to skeletal muscle

With respect to muscle characteristics, muscle mass has been shown to be reduced within the first week of muscle disuse, however, the rate and magnitude of this reduction is dependent on the muscle type studied (4, 69, 79, 92, 246, 249). This is predominantly due to the removal myosin heavy chain (MHC) proteins, which are the major component of the contractile apparatus, as the mRNA and protein expression of all MHC isoforms has been shown to decrease following 3 days of denervation (73, 191). Muscle mitochondrial content has also been shown to rapidly decline within the first week of denervation (4, 216, 246). Electron microscopy studies confirm this and also reveal an increased amount of "abnormal" mitochondria in denervated

muscle during the same time period (45, 86). Markers of a cellular environment laden with oxidative stress is also typical in these muscles (19, 205).

As mentioned previously, muscle disuse is primarily characterized by a shift in the balance between protein synthesis and degradation. As early as 3 hours post-denervation, skeletal muscle amino acid uptake is reduced (78). This is followed by an increase in the conjugation of ubiquitin to proteins and subsequent proteolysis via the UPS within the first 72 hours of denervation (69, 81, 223). Increases in the mRNA of atrogin-1 and MuRF1 E3 ligases are also evident at 24 hours and 3 days of muscle disuse (198, 212). Interestingly, protein synthesis appears to increase as well in response to denervation in a similar time-course, as it is elevated between 48 to 72 hours post denervation (10, 190). Argadine et al. speculate that this is due to an increase in protein synthesis through an ERK1/2/GSK3β/eIF2β-dependent pathway (11), while Quy et al. suggest that this is mediated via an mTORC1/S6K/4E-BP1-dependent mechanism (190). Nonetheless, the magnitude of this increase is synthesis does not match the increase in degradation, allowing the balance to shift in favour of protein degradation.

In addition to these changes in UPS-mediated proteolysis, an up-regulation of a variety of genes in the process of autophagy is observed in muscle denervated for 3 or 7 days (261). Additionally, fluorescence microscopy of single muscle fiber from a hindlimb denervated for 7 days reveals the co-localization of mitochondria with LC3, an autophagy related protein (196). This suggests the removal of mitochondria by autophagy as early as one week post-denervation. As both the UPS and autophagy-lysosome pathways are positively regulated by FoxO transcription factors, it is not surprising that these factors are responsive to conditions of muscle disuse. Accordingly, expression of FoxO1/3a/4 mRNA is up-regulated in response to hindlimb immobilization and denervation, and this is associated with increased FoxO nuclear translocation

and activity, which is highest at 3 days following the cessation of contractile activity (18, 211, 212).

1.3.3.2 Chronic disuse-induced alterations to skeletal muscle

Muscle disuse, denervation in particular, is associated with a rapid reduction in muscle mass initially which persists for 7 to 14 days. This is not sustained however, and the muscle atrophies at a much lower rate at time points beyond this (4, 198, 246). At several weeks of denervation, loss of contractile filaments is apparent and widespread, in addition to sarcomere disruption and myofibrillar disorganization. This is accompanied by enlarged lysosomes and loss of mitochondria, although the rate of this reduction in mitochondrial content is not as substantial as the loss within the first week of denervation (4). Mitochondria that do remain appear to be smaller, globular and sparse, in addition to possessing an altered structure, as cristae disappear (72, 138, 179, 230, 238). Reductions in the capillary-to-fiber ratio are evident by 3 weeks of denervation, and continue to decline beyond this (239).

Functionally, chronically denervated fibers display a reduction in the rate of ADP-stimulated respiration, ATP synthesis, ATP consumption and cross-bridge cycling rate (4, 170, 215), in addition to reductions in the expression and activity of several calcium handling proteins, which play a key role in regulating muscular contraction (1, 209). These alterations result in impairments to muscle performance, as denervated muscle has a substantially progressively lower tension output and poorer endurance capacity beyond 7-8 days of denervation (209, 246).

Chronically denervated muscle is also associated with elevated levels of apoptosis. Reports from Adhihetty et al. and Siu and Alway describe an elevated level of several pro-apoptotic factors, which was associated with increased mitochondrial apoptotic susceptibility and

DNA fragmentation as early as one to two weeks post-denervation (4, 218). It has been suggested that this mitochondria-mediated cell death is due to intra-cellular calcium overload (44). Further, markers of cellular stress are widespread and mitochondrially-produced reactive oxygen species are elevated within the first two weeks of denervation, and remain high for several months subsequent to this (1, 4, 170, 216).

It is evident that muscle disuse induces a wide variety of alterations in skeletal muscle. Of particular interest to this literature review is the regulation of the reduction in mitochondrial content that occurs in response to denervation-induced disuse. The next chapter will describe the structure and function of the mitochondrion, and the molecular pathways by which the biogenesis and degradation of the mitochondrion occurs during basal and disuse-induced conditions.

2.0 Mitochondria in Skeletal Muscle

Mitochondria are dynamic organelles that exist in a variety of morphologies and are the primary site of energy generation in mammalian cells. Additionally, mitochondria participate in apoptosis (5, 187), the generation of oxidative stress (110), calcium signaling (54, 243) and thermogenesis (52). Mitochondria do not exist as individual organelles, but rather as a network which is in equilibrium between fusion and fission events (which add or subtract from the network, respectively). The process by which mitochondrial volume is increased is referred to as mitochondrial biogenesis, which involves the coordinated expression of genes encoded within both the nucleus and the mitochondrial genome (mitochondrial DNA or mtDNA). Conversely, mitochondria can be specifically targeted for degradation and removal from a cell through a process called mitochondrial autophagy, or simply 'mitophagy.' The balance between these two pathways determines the size of the intra-muscular mitochondrial pool, and in turn, reflects the oxidative capacity of the muscle (210).

2.1 Mitochondrial Structure and Function

Mitochondria are double membraned organelles, which arose from the engulfment of a protobacterium by a pre-existing eukaryote several billion years ago (241). These organelles are the site of the aerobic oxidation of metabolic fuels. Mitochondria are separated from the cytoplasm by an outer membrane (OMM), which surrounds the entire organelle. Energy production via oxidative phosphorylation (OXPHOS) is accomplished by the passage of electrons through the multi-protein electron transport chain (ETC), which is embedded in the inner membrane of the mitochondrion (IMM). As electrons are transferred from components of the ETC proteins, hydrogen ions (H+) are driven into the space between the two membranes, termed the intermembrane space (IMS). This buildup of H+ is creates a proton-motive force, and

uses chemiosmosis to drive the phosphorylation of ADP to form ATP at the final protein complex of the ETC, ATP synthase. Additionally, the IMM is repeatedly folded and convoluted (known as the cristae) to increase the surface area so many copies of the ETC can exist within a single mitochondrion, increasing the capacity for ATP synthesis. Enclosed within the IMM is the mitochondrial matrix, which contains enzymes that participate in the Krebs Cycle. This cycle oxidizes pyruvate, a byproduct of glycolysis, which occurs in the cytosol. This reduces coenzymes such as NAD+ and FAD+, which transfer their electrons to ETC protein subunits to power oxygen consumption and ATP synthesis.

Finally, the mitochondrial matrix contains the double-stranded 16.5 kilobase mtDNA, which encodes a small, but crucial fraction of the genes required for the proper functioning of the ETC (13 proteins, 2 rRNAs and 22 tRNAs) (240). Unlike nuclear DNA, this genome is not coated by histones (225) and is located in very close proximity to the IMM, making it highly susceptible to oxidative damage (8, 256). Mitochondrial DNA will be addressed in more detail later on.

2.1.1 Mitochondrial subpopulations: subsarcolemmal and intermyofibrillar mitochondria

As mentioned above, mitochondria do not exist as individual organelles within striated muscle, but rather as a network. This network is a product of a continual cycle of mitochondrial fusion and fission events, which confers substantial plasticity and a means of quality control to the intra-muscular pool of mitochondria. Mitochondrial fusion can be advantageous as it permits sharing and mixing of intra-mitochondrial contents, such as metabolites, enzymes and mtDNA, in an effort to promote a homogeneous and healthy mitochondrial population and protect against dysfunction. Conversely, mitochondrial fission allows for fragmentation to facilitate the specific clearance of dysfunctional portions of the network (60). In essence, mitochondrial networks are

maintained through these opposing processes in order to optimize efficiency of the organelle, assist in adaptations to cellular stress and reduce the harm associated with damaged or dysfunctional components (30).

Electron microscopy work has revealed that mitochondria in striated muscle are divided into two general subpopulations that are morphologically, functionally and biochemically distinct. These subpopulations are titled by the location of the mitochondria, either beneath the sarcolemma, regarded as subsarcolemmal (SS) mitochondria, or dispersed between the myofibrils, termed intermyofibrillar (IMF) mitochondria. Subsarcolemmal mitochondria comprise 10-15% of the total mitochondrial population, but this varies based on species and predominant muscle fiber type (91). Morphologically, these subpopulations differ in both organelle shape and cristae structure (183, 194). These differences point to divergent roles in striated muscle. It has been postulated that due to their cellular location, SS mitochondria supply ATP for membrane transporters and nuclear functions, while IMF mitochondria provide ATP to myosin ATPases for muscular contractions. This is supported by reports confirming that ATP synthesis differs between these groups, as IMF mitochondria respire at a rate 2-3-times that of the SS pool (4, 39, 111, 221) and express greater levels of proteins associated with OXPHOS (61). Interestingly, these subpopulations exhibit differences in reactive oxygen species (ROS) production, as SS produce approximately 3-times that of the IMF (3). Other functional variances include mitochondrial enzyme activity, protein import and synthesis, apoptotic susceptibility and membrane structure (3, 39, 41, 221).

In addition to their inherent functional differences, these groups of mitochondria differ in their capacity to adapt to various stimuli. Comparisons have demonstrated that under conditions of altered muscle contractile activity, such as during chronic use or disuse, SS mitochondria are

consistently more responsive than IMF mitochondria to a common stimulus (2, 4, 20, 90, 109, 111, 216).

2.2 Regulation of mitochondrial content

Mitochondrial content within skeletal muscle is the product of the balance between mitochondrial biogenesis (which increases mitochondrial content) and mitophagy (the specific isolation and degradation of mitochondria, which decreases mitochondrial content). As stated previously, mitochondrial content reflects the oxidative capacity of the muscle, which in turn, is reflective of the muscle's contractile activity**.** As muscle is a very plastic tissue, the ability to appropriately regulate its mitochondrial content is crucial. In this section, molecular mechanisms regulating both mitochondrial biogenesis and mitophagy will be addressed, in addition to reviewing known alterations to these processes during muscle disuse.

2.2.1 Upstream signaling of mitochondrial biogenesis

Gene expression which promotes mitochondrial biogenesis is regulated by physiological demands that require an increase in energy production. Regulation of this gene expression program is predominantly at the transcriptional level. An external stimulus, such as a change in contractile activity, can alter the concentration of a variety of contractile-dependent messengers, such as AMP, cytosolic calcium, or promote transient ROS production. Alterations in these factors can subsequently activate signaling kinases, several of which have been shown to post-translationally modify transcription factors and promote mitochondrial biogenesis. These messengers and their targets will be briefly discussed.

Firstly, muscular contractions are dependent on the hydrolysis of ATP by myosin ATPase. This subsequently leads to an increase in the ADP:ATP ratio in the muscle, and ultimately an increase in AMP formation (89). The rise in AMP concentration can lead to the

allosteric activation of the metabolic sensor, adenosine monophosphate-activated protein kinase (AMPK). Studies have demonstrated that AMPK is indeed activated in response to muscle activity (235, 247) and this activation is mechanistically linked to enhanced mitochondrial biogenesis (17, 100, 248).

Muscle contractions also lead to rapid increases in cytosolic calcium ion (Ca^{2+}) concentration from large intracellular stores in the sarcoplasmic reticulum. These Ca^{2+} transients can activate the Ca^{2+}-dependent phosphatase calcineurin, Ca^{2+}/calmodulin dependent kinases (CaMK), p38 MAPK and protein kinase C (PKC) (36, 195). These signals can post-translationally modify transcription factors, such as NFAT, MEF2 or CREB/ATF2, and subsequently promote the expression of mitochondrial genes (6, 65, 147, 252).

Finally, normal aerobic metabolism is associated with a small fraction of the electrons being transferred to oxygen molecules, instead of being passed to other protein complexes in the ETC. The electrons which escape, termed an "electron leak," forms the reactive superoxide, which is then rapidly transformed into H_2O_2 by anti-oxidant enzymes, such as the superoxide dismutases (67). Under normal physiological conditions, there is a balance between oxidant production and antioxidant function. Exercise and muscle contractions also have the capacity to encourage the production of moderate amounts of oxidants (48, 146). However, in pathological conditions, oxidant production can exceed the cell's capacity to buffer them and can damage proteins, lipids, DNA and other molecules inside the cell, in addition to activating apoptosis (231). Interestingly, reactive oxygen species (ROS) can act as a signaling molecule, as they have the capability to activate the transcription of a mitochondria-associated gene in an AMPK-dependent and independent fashion (98). Other studies have also demonstrated a positive association between ROS and increased mitochondrial mass (123, 124) and elongation (108).

Conversely, ROS production can result in the fragmentation of mitochondrial networks (58, 260) and autophagy (34, 107, 207). While the exact effects of ROS are contentious, they are nonetheless very much implicated in mitochondrial morphology and biogenesis.

2.2.2 Transcription factor activation

Expression of the ~1500 genes required for mitochondrial biogenesis is under almost exclusive control of transcription factors which bind to nuclear DNA, and their co-activating factors. The aforementioned cellular messenger signals can converge upon intermediate signaling kinases, which in turn can modify certain transcription factors implicated in mitochondrial biogenesis. This allows for a cell to respond robustly to varied physiological cues, such as changes in muscle activity. Genes such as specificity protein-1 (Sp1) and early growth response gene-1 (Egr-1) have been shown to respond with great immediacy to contractile activity, and are both known to induce the expression of the mitochondrial protein cytochrome c (42, 97, 255).

However in skeletal muscle, the transcriptional co-activator peroxisome proliferator-activated receptor-γ co-activator-1α (PGC-1α) is regarded as the most significant regulator of mitochondrial biogenesis and function, as well as muscle fiber type (130, 236, 254). As it is a transcriptional co-activator, it lacks the capacity to bind to nuclear DNA directly. Instead, it greatly enhances the activity of transcription factors, as it can recruit factors to modify histones and directly interact with transcription initiation machinery (188, 242). Crucial to its role in regulating the expression of nuclear genes encoding mitochondrial proteins (NUGEMPs), PGC-1α has the capacity to bind to transcription factors such as nuclear respiratory factor (NRF)-1 and -2 (254). The activation of these transcription factors is coupled with the transcriptional control of other genes involved in mitochondrial function and biogenesis, such as subunits of protein

complexes in the ETC and factors involved in their assembly, mtDNA transcription and replication machinery, enzymes participating in heme biosynthesis and mitochondrial protein import (106). Further, PGC-1α co-activates NRF-1 on the promoter of the critical mitochondrial transcription factor Tfam (mitochondrial transcription factor A) (254), which will be addressed in more detail later on. Apart from NRF-1/2, PGC-1α has been shown to co-activate other transcription factors such as peroxisome proliferator-activated receptors (PPARs), estrogen related receptors (ERRs) and ying-yang-1 (YY1), to augment the expression of genes participating in mitochondrial fatty acid oxidation, Krebs cycle and oxidative phosphorylation (46, 53, 141).

Regulation of PGC-1α can occur predominantly at transcriptional, post-transcriptional and post-translational levels. Notably, PGC-1α expression can be induced by administration of pharmacological agents such as 5-Aminoimidazole-4-carboxamide ribonucleotide (AICAR) or thyroid hormone (96, 126, 245) or by contractile activity, both *in vitro* and *in vivo* (96, 185). Metabolic stimuli can also regulate the activity of PGC-1α post-translationally, as it can be phosphorylated (100, 189), (de)acetylated (128, 164) and methylated (227). The ability of this co-activator to be regulated at multiple levels underscores its role as the master regulator of mitochondrial content.

2.2.3 Expression of the mitochondrial genome

While PGC-1α solely participates in the expression of NUGEMPs, we must not forget that the proper functioning of the ETC is dependent on expression of genes coded in both the nuclear and mitochondrial genomes. In order for coordinated expression of these genomes to occur, factors which assist in the expression of the mitochondrial genome must first be transcribed from the nuclear genome, and imported into the mitochondrion. Transcription of

mtDNA only requires the presence of two transcription factors, mitochondrial transcription factors A and B2 (Tfam and Tfb2m), and the mitochondrial RNA polymerase (POLRMT) (132, 257), which are all nuclear encoded and whose expression is regulated by PGC-1α and the NRFs (77, 254).

The mitochondrial genome is a circular, enclosed and double-stranded ~16.5kb molecule, existing in about 2,700 copies per cell (112), although this likely varies between cell type and species. It contains the genetic information for 13 proteins that are essential subunits of protein complexes I, III, IV and V. Additionally, it contains the code for 22 tRNAs and 2 rRNAs which are required for translation of the these proteins within the mitochondrial matrix. Curiously, the only non-coding region of mtDNA, known as the D-loop, contains control elements for the initiation of mtDNA transcription, as mtDNA lacks intron regions. The double strands of mtDNA are referred to as the heavy (H) and light (L) strands, and are named for the variance in the proportion of nucleic acids found in each.

Transcription of mtDNA can initiate on either strand, as both contain promoter regions (154), however the transcriptional product from each site differs. Transcription from heavy-strand promoter 1 (HSP1) yields a molecule containing information for the coding of both rRNAs, while heavy-strand promoter 2 (HSP2) produces a transcript spanning almost the entire heavy strand, including 14 of the 22 tRNAs, 12 mRNAs and both rRNAs. Transcription from the light-strand promoter (LSP) produces the ND6 mRNA, the remaining 8 tRNAs and primers used for replication of the HSPs (12, 206). Regardless of where transcription occurs, nascent transcripts are polycistronic, and thus must be processed in order to form mature mRNA molecules (171) before being translated. As all 13 proteins coded for by mtDNA are destined for the ETC and ATP synthase, a system for the assembly of these proteins into the mitochondrial

membranes must exist. Studies in yeast have demonstrated that concomitant with translation, the oxidative assembly complex, Oxa1, works to correctly construct and insert membrane proteins into the mitochondrial membrane, facilitating the assembly of cytochrome c oxidase and ATP synthase (7, 87, 105).

2.2.4 Tfam and other accessory factors involved in mtDNA transcription

As mentioned previously, mtDNA transcription is regulated by a non-coding region, referred to as the D-loop, which contains the heavy- and light-strand promoters. Transcription initiation from these sites only requires three components, Tfam, Tfb2m and POLRMT, which are collectively referred to as the transcriptional core. Following initiation, elongation of the transcripts is facilitated by transcription elongation factor of mitochondria (TEFM), which interacts with POLRMT and boosts its processivity (149).

Tfam is a multi-functional protein which, in addition to its absolute requirement for transcription initiation (213), plays roles in mitochondrial replication, packaging and maintenance. This protein belongs to the high-motility group (HMG) family of proteins, as it has tandem HMG-box domains separated by a 27-amino acid linker region. This protein family has been characterized by its ability to bend and unwind DNA. Accordingly, Tfam possesses the ability to unwind and distort mtDNA promoters in a U-turn like structure (64, 166, 167, 197), facilitating access of other core components to the promoter region and stimulating mtDNA transcription. Tfb2m and POLRMT interact with each other and Tfam, and participate in promoter melting and proper transcription initiation from H- and L-strand promoters (206).

Tfam also has plays a role in mtDNA replication, as mtDNA transcription from the LSP generates the primers for heavy-strand replication. Along with mtDNA polymerase γ (Pol γ),

mtDNA helicase Twinkle and a mtDNA single-stranded DNA-binding protein, Tfam forms a "replisome" which are the minimal components required for replication (57).

Additionally, Tfam has the capacity to bind, wrap and bend any DNA without sequence specificity (64). Tfam has also been shown to fully coat mtDNA (102), which is supported by measurements estimating the ratio of Tfam molecules : mtDNA to be approximately 1000:1 (112, 118). Experiments have shown that Tfam can cause compaction and twisting of mtDNA, storing them in intracellular complexes called 'nucleoids,' with each nucleoid containing 2-10 copies of mtDNA (112, 127, 204). The coating of mtDNA with Tfam has been likened to the role of histone coating of nuclear DNA, in that it provides a manner in which mtDNA can be protected and maintained (102). This is critical for preservation of the normal expression and function of the ETC. Additionally, the compact packaging of mtDNA is important as the size of mammalian mtDNA precludes existence in its free (non-compacted) form in the mitochondrial matrix.

Complete ablation of Tfam in a mouse model leads to embryonic lethality, owing to a severe mtDNA depletion, whereas heterozygous Tfam knockout mice exhibit an approximate 40% reduction in mtDNA levels (118). On the other hand, experiments inducing moderately high levels of Tfam have been shown to increase the presence of mtDNA transcripts, while excessive overexpression of Tfam appears to inhibit mtDNA transcription (68, 143). Additionally, Tfam degradation is mediated by the mitochondrial LON protease, which is also expressed within mitochondrial nucleoids (22). Intra-mitochondrial phosphorylation of free Tfam prevents Tfam-mtDNA interactions and facilitates its degradation via LON protease, which allows for fine-tuning of Tfam abundance inside the mitochondrion (137, 145). It would then appear that

titration of Tfam protein levels is manner in which a cell can match mtDNA replication and transcription, and consequently respiratory chain expression, with its metabolic requirements.

Accordingly, Tfam levels have been shown to be modified by metabolic stresses, in particular by increases in contractile activity. Williams demonstrated via an *in vivo* model of chronic contractile activity that increases in mtDNA copy number paralleled increases in oxidative capacity. This is likely due to increases in the expression of Tfam, which has been shown to increase in response to both *in vitro* (29, 234) and *in* vivo (82, 115) models of chronic contractile activity, as well as in response to acute exercise (185, 200) and endurance training (16, 176). Skeletal muscle exposed to chronic contractile activity also demonstrated an increase in the amount of Tfam imported into the mitochondrial matrix. This was associated with increased Tfam-mtDNA binding, and preceded the increase in mitochondrial content that accompanies chronic increases in muscle activity (82). The idea that increased Tfam expression precedes changes in mitochondrial content points to a crucial role for Tfam in contractile activity-induced mitochondrial biogenesis. Increased Tfam expression and function in response to contractile is likely mediated by increased activity of the PGC-1α/ NRF-1/2 axis, although recent work by Saleem et al. suggests that increased intra-mitochondrial p53 content is critical for Tfam-mediated mtDNA transcription in response to exercise (200).

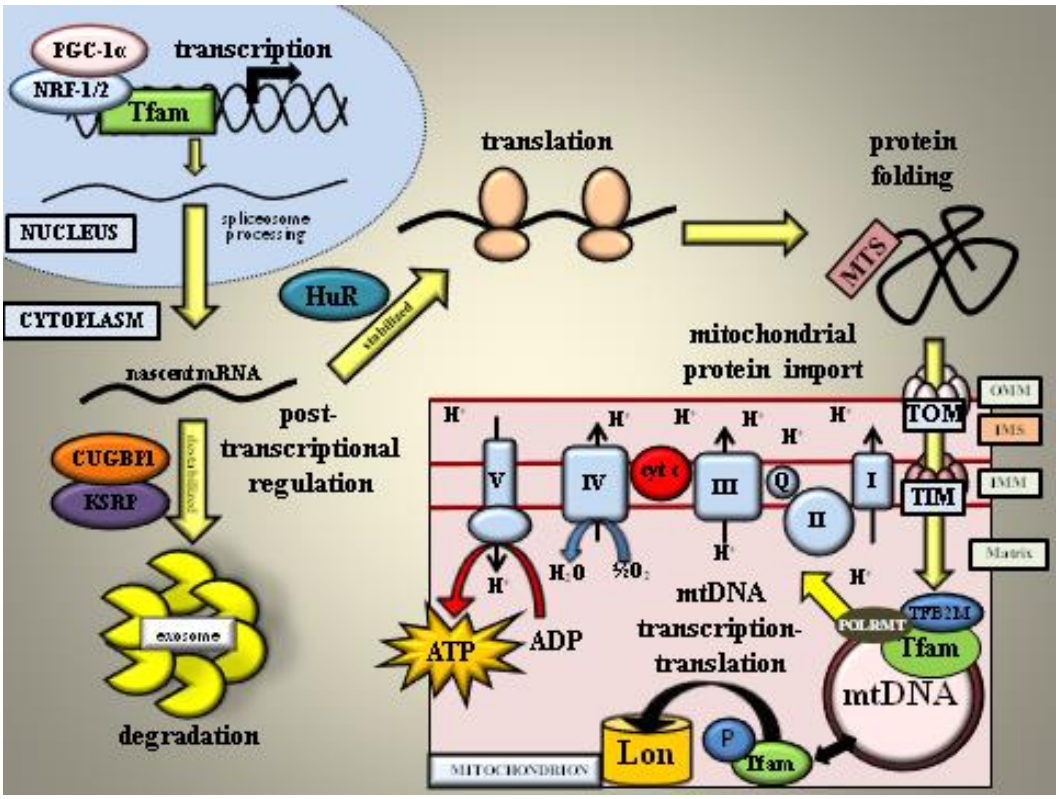

Figure 1. Mitochondrial biogenesis occurs as a result of the complex coordination of gene expression at multiple levels. Owing to its ability to respond to upstream signals influencing nuclear transcription factors, and its ability to communicate and coordinate these with mitochondrial DNA (mtDNA), mitochondrial transcription factor A (Tfam) is often regarded as the "link" between the nuclear and mitochondrial genomes. This mitochondrial transcription factor is vital for the coordinated expression of these genomes during mitochondrial biogenesis. Following transcription and splicing in the nucleus and export into the cytoplasm, Tfam has the ability to interact with RNA-binding proteins or other factors which can influence its fate depending on the state of the cell: to be degraded into its constituent parts or translated into protein. If it is translated, Tfam is targeted to the mitochondrion by the matrix targeting sequence (MTS) and is imported into the matrix, where it can bind to mtDNA and stimulate transcription, replication and compaction this molecule. Tfam can also be phosphorylated in the mitochondrial matrix, and degraded by Lon protease.

2.2.5 Mitochondrial protein import

Newly synthesized NUGEMPs that are destined for the mitochondrion are translated into proteins in the cytoplasm. Less than 1% of all proteins required for mitochondrial function are synthesized from genes encoded in the mitochondrial genome. As mitochondrial biogenesis is actually the expansion of the existing mitochondrial reticulum and not the *de novo* synthesis of

new mitochondria, precursor proteins (pre-proteins) synthesized by ribosomes in the cytosol must be imported into the mitochondrion in order to increase mitochondrial content. Mitochondrial protein import thus serves as another site at which mitochondrial content can be regulated.

As newly synthesized mitochondrial-destined proteins are not in their final conformation, cytosolic chaperones such as heat-shock protein (Hsp) 70 and Hsp90 are thought to stabilize them and position these pre-proteins in the vicinity of mitochondria (259). Further, in order for import into the mitochondrion to be specific for mitochondrially-destined proteins, there must be a system which permits mitochondria to distinguish between the vast numbers of proteins present in the cytosol. Indeed, mitochondrial matrix destined proteins can be identified by a positively charged cleavable N-terminus pre-sequence, called the matrix targeting sequence (MTS). The MTS is a 10-80 amino acid residue, which confers specificity for proteins to traverse the translocases of the outer and inner mitochondrial membranes (TOM and TIM, respectively) prior to entering the matrix.

The TOM complex serves as a universal entry gate for cytosolic proteins to translocate into the mitochondria, as it recognizes precursor sequences, releases these proteins from their cytosolic chaperones and transfers the polypeptide chain across the OMM (165). In short, components of the TOM complex, Tom20 and Tom70 are receptors which recognize pre-proteins and their chaperones, prompting the release of these proteins from the chaperone and passage through the TOM pore (the Tom40 protein) in an ATP-dependent process (259).

Once they have passed through the TOM, pre-proteins are able to engage with the TIM23 complex, which they must pass through in order to enter the mitochondrial matrix. This process is powered by an electrical membrane potential across the inner membrane ($\Delta\psi_{mt}$) and ATP

hydrolysis. Tim50, Tim23 and Tim17 are components of this complex which form a channel through which proteins can pass through the IMM (165). However further action is required for pre-proteins to enter the matrix. This is facilitated by an import "motor," which is comprised of Tim44, Tim14, Tim16 and mitochondrial Hsp70 (mtHsp70). Collectively, these proteins are referred to as the presequence translocase-associated motor (PAM), and they assist in the ATP-dependent translocation of the pre-protein into the matrix, which occurs in a ratchet-lie manner (158, 165, 172). Once the pre-protein enters the matrix, the MTS can be proteolytically cleaved by the mitochondrial-processing peptidase (MPP) (224), and the protein can be directed to its appropriate mitochondrial location. In addition to the TIM23 matrix-associated import pathway, pathways for import and insertion of proteins into the IMM and OMM exist (15, 217), but will not be discussed in detail here.

Protein import into the mitochondrion can also vary depending on the cellular stimulus imposed. Chronic contractile activity for instance, has been demonstrated to increase the expression of protein import machinery components, including cytosolic and mitochondrial chaperones (Hsp70, Hsp90 and mtHsp70), as well as components of both TOM and TIM complexes (101, 173, 220). Increased expression of these proteins allows for enhanced protein import into the mitochondrion and mitochondrial biogenesis (220).

2.2.6 Mitochondria-specific autophagy

Autophagy is the mechanism by which a cell recycles intracellular components as a quality control mechanism, as it can selectively eliminate dysfunctional organelles. Mitophagy is the specific autophagic removal of mitochondria, and is a process which directly opposes mitochondrial biogenesis to determine the size of the intramuscular mitochondrial pool. As excessive ROS production from the ETC can be cytotoxic, the removal of these dysfunctional

organelles is crucial to maintenance of a healthy cell. In fact, mouse models which are defective in the general autophagy pathway display an accumulation of defective mitochondria (253). The process of mitophagy is not only responsible for the elimination of damaged mitochondria, but also appears to be active under basal conditions, as studies have estimated that the mitochondria are turned over every few days (131, 153, 226).

The process of general cellular autophagy in general is broken down into three general stages: the formation and closure of the membrane surrounding the organelle to be degraded (the autophagosome), the delivery and merger of the autophagosome to the lysosome and the degradation of the autophagosomal contents by lysosomal enzymes. Autophagy is normally suppressed during anabolic conditions, as PI3K/mTOR signaling inhibits autophagy activation. However, under catabolic conditions, this inhibition is lost and activation of the ULK1 complex can catalyze downstream signaling for bulk cellular autophagy to occur.

However, the manner in which mitochondria are specifically degraded is mechanistically different from general autophagy. As stated previously, mitochondria are not solitary organelles, but rather exist in a network. Components of the mitochondrial network which are to be removed and recycled must first be separated by mitochondrial fission before undergoing mitophagy. Loss of mitochondrial membrane potential for instance (which is associated with mitochondrial dysfunction) promotes mitochondrial fission, and appears to be essential for mitophagy (232). In addition to mitochondrial fission, depolarization promotes the translocation of the E3 ubiquitin ligase Parkin to the mitochondria, to ubiquitinate mitofusins 1/2 (186, 222), targeting their removal by the proteasome and subsequently preventing re-fusion of damaged mitochondria into the network. Damaged mitochondria also express the PTEN-induced kinase 1 (PINK1) on their outer membrane (119), which acts as marker of damaged mitochondrion. PINK1 is capable of

recruiting Parkin to the mitochondria (163), to subsequently induce mitophagy (162). Parkin also ubiquitinates of other OMM proteins (31), providing a link to autophagic machinery via the ubiquitin-binding adaptor p62. This protein has domains which allow it to interact with ubiquitin chains on the mitochondrion, as well as LC3, which is the main constituent of the autophagosomal membrane. p62 thus provides a physical link between mitochondrial proteins that have been tagged for degradation and the autophagosomal membrane (74).

Although many questions still remain regarding mitophagy and the proteins involved in this process, it is clear that this process is critical to the maintenance of a healthy mitochondrial pool, through the elimination of dysfunctional and surplus mitochondria.

2.3 Muscle-disuse induced mitochondrial alterations

Apart from the substantial reductions in mass evident in muscle subjected to chronic disuse, reductions in mitochondrial content and function are evident. Studies using electron microscopy note preferential loss of mitochondria in the subsarcolemmal region of membrane (72, 95, 134). Although the mitochondrial loss persists with experimental denervation times up to 18 months (138), the rate of reduction in mitochondrial content appears to be the most considerable within the first week of denervation (4). The remaining pool of mitochondria are characterized as being smaller, more fragmented as well as having matrices which are less dense (72, 134, 138, 179, 230, 238). Iqbal et al. postulate that fragmentation of the mitochondrial network is due to a reduction in the ratio of fusion : fission proteins associated with the mitochondria (95). Interestingly, fragmentation of the mitochondrial network, through the over-expression of pro-fission proteins Fis1 and Drp1, is sufficient to induce muscle atrophy (196).

Cardiolipin, a key mitochondrial membrane phospholipid which binds ETC complexes to ensure proper electron transfer, is also reduced with denervation (174, 246). This manifests in

functional impairments to the mitochondria, as the activity and expression of membrane-embedded mitochondrial enzymes such as cytochrome c oxidase and succinate dehydrogenase are reduced with muscle disuse (26, 191, 216, 246). Citrate synthase, a mitochondrial matrix enzyme, exhibits a similar reduction in expression and function (26, 238). Mitochondria that have been isolated from denervated muscle also exhibit a reduction in the rate of ATP synthesis, in addition to elevated levels of ROS production (4, 160, 170, 216). These factors have been suggested to negatively impact mitochondrial protein import, which is also suppressed following denervation (216). These studies highlight the notion that with muscle disuse, mitochondria are not only less prevalent, but also less efficient.

Mitochondrial biogenesis appears to be repressed with chronic muscle disuse, as studies have reported reductions in PGC-1α mRNA content as rapid as 1 day following denervation (198), which persists for weeks following the cessation of muscle activity (88, 198, 201, 238). Reductions in the protein content of PGC-1α and Tfam is also reduced with prolonged muscle inactivity (4, 26). However, the exact signaling mechanisms regulating the expression of these genes during muscle disuse has yet to be determined. Fascinatingly, muscle-specific over-expression of PGC-1α blocks muscle atrophy during denervation (26, 88, 201). However, it is not completely understood whether this is through the preservation of mitochondrial content or mitochondrial biogenesis-independent regulatory roles of this transcriptional co-activator.

On the other hand, mitochondrial degradation appears to be increased with muscle disuse. In response to denervation, the mRNA expression of Parkin, PINK1 and an E3 ubiquitin ligase Mul1 is elevated (136). Mul1 appears to mediate mitochondrial fission and subsequent mitophagy in response to muscle wasting stimuli. Its exact role in muscle disuse, although promising, remains to be determined. However, other evidence exists suggesting an elevation in

mitophagy during muscle disuse. O'Leary et al. recently revealed that key proteins mediating the removal of mitochondria via autophagy, such as the ubiquitin ligase Parkin, the autophagosomal membrane protein LC3 and the ubiquitin-LC3 adaptor protein p62 all show a greater association with mitochondria in denervated muscle (168, 169). Although it appears that mitophagy is augmented during muscle disuse, more work in this field needs to be done.

3.0 Post-Transcriptional Regulation of mRNA

Gene expression can be regulated at a variety of levels, from the transcription of DNA to the translation of protein, and beyond that, with post-translational modifications and control of intracellular localization. In particular, mRNA is capable of being regulated following transcription, in what are simply referred to as "post-transcriptional events." Until recently, these events have been overlooked, and light has been shed on the function of these events on the gene expression. This chapter will briefly summarize these post-transcriptional events, and specifically analyze the role of mRNA stability as an avenue of modulating gene expression.

3.1 mRNA stability

Messenger RNA (mRNA) is composed of a 5' untranslated region (5'-UTR), a coding region and a 3' UTR. The coding region provides the information for the protein to be translated from, while both untranslated regions serve as regulatory components for the mRNA. Newly created mRNAs are also equipped with two inherent stability determinants, the 5' 7-methylguanosine (m7G) cap structure, and the 3' poly(A) tail, a stretch of ~25-200 adenine nucleotides on the 3' end of the transcript. In order for an mRNA to undergo decay, either of these two structures must be compromised. Additionally, the 5' m7G cap affords the transcript the ability to interact with the cytoplasmic eukaryotic initiation factor 4E (eIF4E), while the 3' poly(A) tail has the ability to bind the poly(A) binding protein (PABP). Binding of either of these factors to a transcript assists in cap-dependent translation initiation (99, 151), but also provides stability and protection from exonucleolytic decay.

Following transcription, the newly formed mRNA is spliced by a multi-protein complex called the spliceosome, which removes non-coding intron regions, and unites coding exon regions. This mature mRNA is the exported from the nucleus into the cytoplasm, where mRNA

decay can occur. Independent of how mRNA degradation is executed, the degradative process is usually concentrated in cytoplasmic foci, regarded as processing bodies (P-bodies) (175), as they contain many of the proteins involved in the various stages of the process outlined below.

In mammalian cells, the predominant pathway to the degradation of a nascent mRNA is deadenylation-dependent, that is, exonucelolytic activity proceeds from the 3' end of the transcript towards the 5' end. This first step in the decay of an mRNA is the removal of the poly(A) tail (214), which occurs in two phases (258). It is initially trimmed by the ribonuclease complex Pan2-Pan3 to <100 adenine nucleotides. Following moderate shortening of the tail, the Ccr4-Not complex takes over, and removes the remaining adenines. Deadenylation can also occur with the help of poly(A)-specific ribonuclease (PARN), which can bind to the 5' cap, in turn stimulating its poly(A)-ribonuclease activity (70). The method by which poly(A) tail removal by these deadenylases proceeds appears to be mRNA specific (80). Following deadenylation, 3' to 5' decay is executed by the exosome, which is a 10-12 subunit complex composed of various enzymes and helicases (93, 159). This complex digests the transcript, until only a few 5' nucleotides remain, after which the 5' m7G cap is removed by the decapping enzyme DcpS (133).

mRNA degradation can also be mediated by microRNAs (miRNA). These short RNAs bind to sequences in the 3' UTR of a target mRNA, recruit a host of other proteins to form a miRNA-loaded RNA-induced silencing complex (miRISC), which can silence the target mRNA through triggering deadenlyation of target mRNAs or translational repression (56).

3.2 Factors involved in mRNA stability

It must be reinforced that mRNA decay is not a random process, but rather a product of coordinated events, involving *cis*-acting elements contained within the transcript itself, and

trans-acting factors which can bind to these *cis*-elements and influence mRNA stability. These *trans*-acting factors, such as RNA-binding proteins (RBPs) or miRNAs, associate with specific sequences in the transcript, largely situated in the 3'-UTR. These sequences have been referred to as untranslated sequence elements for regulation (USER) (104), two of which have been widely documented: AU-rich elements and GU-rich elements. These USERs and some of the proteins that bind to them will be addressed below.

3.2.1 *cis*-elements and their role in mRNA stability

3.2.1.1 AU-Rich Elements

Located in the 3'-UTR, adenosine-uridine (AU)-rich elements (AREs) are one of the best characterized USERs and are the most commonly found mRNA regulatory elements in mRNAs. Depending on the protein that binds to these elements, AREs can modulate mRNA stability, or assist in translation, as these RBPs can bring the transcript into the proximity of factors controlling stability or tranlastion. AREs are also found in a wide variety of transcripts, as estimates by Halees et al. suggest that between 2-11% of the transcriptome contains these modulating elements (83).

Traditionally, AREs have been grouped into three general categories (33). Class I AREs contain between 1-3 instances of the AUUUA pentamer, typically found in regions rich in uridylate nucleotides. Class II AREs are characterized by having anywhere between 5-8 overlying copies of the same AUUUA pentamer motif. Finally, class III AREs lack the AUUUA pentamer completely, and instead are simply regions that contain an abundance of uridylate nucleotides. Interestingly, even though these classes are relatively similar in nucleotide composition, it has been suggested that a greater degree of specificity exists, as the flanking sequences to these AREs can impact the overall effect on mRNA transcript stability (71).

Furthermore, deadenylation of the mRNAs that contain AREs appears to be required for the decay of these transcripts, as disruption of the deadenylase complexes precludes the initiation transcript decay by *trans*-acting factors (262). Nonetheless, ARE-containing mRNAs are almost exclusively degraded by the exosome, in a 3' to 5' manner following deadenylation (32).

3.2.1.2 GU-Rich Elements

Although ARE-mediated decay has tradtionally been the most studied pathway in mRNA degradation, it is not applicable for all transcripts. Guanosine-uridine (GU)-rich elements (GREs) are also located in the 3'UTR, however much less focus has been placed on them than AREs. Speculation of the existence of alternative, non-ARE regulatory sequences arose when Raghavan et al. noted an abundance of transcripts which displayed a rapid decay rate, yet lacked AREs or other known regulatory elements (192). Using computational algorithms in a follow-up study, this same group uncovered conserved sequences that were enriched in unstable, short-lived mRNAs. Furthermore, this consensus 11mer UGUUUGUUUGU sequence is sufficient to induce instability when introduced into non-GRE containing mRNAs, suggesting that this element participates in mRNA destabilization (237). Apart from this unique 11mer sequence, similar GU-rich sequences have been discovered, and impart the same destabilizing function (193). Although more work needs to be done to elucidate their full role in mRNA decay, GRE sequences appear to play a crucial role in mRNA stability.

3.2.2 *trans*-acting factors and their role in mRNA stability

As mentioned earlier, *trans*-acting factors, such as proteins, can bind to target *cis*-elements in the 3'-UTR of genes to form mRNA-protein (mRNP) complexes which mediate the decision to degrade or stabilize the target gene. While dozens of RNA-binding proteins exist, a select few with recognized roles in striated muscle tissue will be briefly addressed here.

3.2.2.1 Human antigen R (HuR)

HuR is one of the best characterized RNA-binding proteins, and it is a ubiquitously expressed protein known for targeting mRNAs which contain AREs in their 3'-UTR (139, 140). This protein is part of a family of closely related proteins which contain three RNA recognition motifs (RRMs). Interestingly, HuR is implicated in a variety of post-transcriptional functions. As HuR has been characterized as a protein that can shuttle between the nucleus and the cytoplasm, it is not surprising that it participates in both nuclear and cytoplasmic duties such as the splicing of nascent mRNAs (120), the export of the mature mRNA into the cytoplasm (116) and stabilization of ARE-containing mRNAs in the cytoplasm (59, 180). Furthermore, HuR promotes translation of stabilized mRNAs, as it is capable of interacting with the cellular translation machinery and its target mRNAs simultaneously (116). It is believed that HuR promotes the stabilization of target mRNAs by competing for target binding sites with other RBPs which promote mRNA decay, such as ARE/poly(U)-binding/degradation factor-1 and tristetraprolin (116, 150).

The HuR protein also offers several sites of post-translational modifications which allow for shuttling between nuclear and cytoplasmic locations. Numerous signaling kinases, including p38 MAPK (250), AMPK (244) and PKC (51), have been implicated in the phosphorylation of several residues on HuR. However, the interplay between these and other kinases which can phosphorylate HuR is complex, as phosphorylation of different residues can mediate a variety of effects, often contradictory in nature. Alternatively, HuR is able to be methylated (129), which has been shown to impair the ability of HuR to interact with target mRNAs, and possibly affecting its capacity to move between the nucleus and cytoplasm. Although elucidating the

exact effects of the multitude of modifications to HuR remains, altering the expression and function of this protein appears to play a substantial role in the stability of a host of mRNAs.

3.2.2.2 K-homology splicing regulator protein (KSRP)

KSRP is another protein which plays a key role in modulating the stability of ARE-containing mRNAs, both in vitro and in vivo (75). It contains four K-homology motifs (50), which mediate its ability to recognize and bind to RNA with high affinity, in addition to allowing it to simultaneously interact with the both the exosome and PARN (75). The ability for this protein to interact with two critical components of deadenylation-mediated decay highlights its importance in promoting 3' to 5' mRNA decay.

Similar to HuR, KSRP function can be modulated through post-translational modifications. Work by Amirouche et al. (9) and Briata et al. (27) has demonstrated the ability of p38 MAPK to phosphorylate KSRP in murine C2C12 cells. This phosphorylation prevents the binding of KSRP to ARE-containing muscle specific mRNAs. Furthermore, phosphorylation simultaneously downregulates KSRP protein expression and enhances the sequestration of KSRP with 14-3-3 proteins. Other work has highlighted KSRP as a target of the PI3K/Akt signaling axis, which is of particular importance during skeletal muscle growth in myogenesis and hypertrophy. Interestingly, activation of PI3K/Akt in C2C12 cells causes phosphorylation KSRP, which displaces it from mRNA destabilizing complexes and target mRNAs (28, 76). Thus it appears that KSRP phosphorylation by multiple upstream kinases is critical in preventing both its ability to interact with the machinery which degrades mRNAs and its target mRNAs themselves.

3.2.2.3 CUG-binding protein 1 (CUGBP1)

CUGBP1 is a member of a family of similar RNA-binding proteins, containing 3 RRMs (228), allowing it to bind to a variety of 3'-UTR elements, including GC-rich and GU-rich

elements, in addition to AREs (155, 193). While studies have described the role of CUGBP1 in mRNA splicing (182) and translation control (229), more focus has been placed on the role of CUGBP1 as a deadenylation accessory factor, as it recruits PARN deadenylase to target mRNAs, and consequently promoting their decay (155). Work by Lee et al. has identified that CUGBP1 has numerous transcript targets in muscle cells, and principally binds to mRNAs that have 3'-UTRs enriched with GREs (125). These authors also note that several of the identified target sequences of CUGBP1 overlap with sequences bound by the mRNA stabilizing protein HuR. This perhaps alludes to the existence of mRNPs containing both stabilizing and destabilizing factors, and likely competitive binding for these sites to determine the fate of the target transcript.

Along with the other RNA binding factors addressed above, the function of CUGBP1 can be altered by phosphorylation. Using an animal model of myotonic dystrophy, Kuyumcu-Martinez et al. demonstrated that CUGBP1 is under the regulatory control of the PKC signaling pathway, which hyperphosphorylates CUGBP1 (114). This post-translational modification increases the half-life of this protein and nuclear localization, leading to aberrant splicing and dysregulated translational control. While an effect of phosphorylation or other post-translational modifications on the ability to CUGBP1 to function as an mRNA decay promoting factor was not examined, future work should address this interaction.

3.3 mRNA stability and skeletal muscle

Research evaluating changes in gene expression often examines alterations to transcriptional networks and protein abundance, however, very little focus has been placed on examining events following transcription. While the extent of transcriptional activity provides information regarding changes in upstream signaling in gene expression, mRNA stability

provides a link to possible changes in gene expression to the steady-state concentration of mRNA. In a recent review, Balagopal et al. suggest that while changes in transcription may provide insight into the direction of the net response of a gene to a stimulus, regulation of transcript stability seems to be an important factor in the kinetics of this response (14). In other words, control of transcript stability may be important for a cell to "accelerate" or "brake" while adjusting to new steady state conditions.

An example of this is presented in a study by Freyssenet et al., who examined the role of stability in mitochondrial biogenesis in a model of chronic contractile activity (CCA). Following CCA, mRNA of the mitochondrial protein cytochrome c was elevated, but this preceded changes in transcriptional activation of the cytochrome c promoter. This suggests that in this paradigm, augmented stability contributed to the early elevation in mRNA (66). Using the same experimental model, Lai et al. examined the effect of CCA on primary regulators of mitochondrial biogenesis, namely PGC-1α and Tfam. Interestingly, despite no change in the mRNA of these genes with CCA, their stability was markedly decreased. The authors suggested that this is a beneficial effect, with a higher turnover rate providing a more favourable, plastic environment for the cellular response to contractile activity (115). Considering this, D'Souza et al. hypothesized that the stability of these regulators of mitochondrial biogenesis is inversely proportional to the mitochondrial content of muscle, that is, higher mitochondrial content was correlated to higher transcript turnover rates. By analyzing different striated muscle fiber types which have inherently different mitochondrial densities, they surmised that stability of these factors, along with RBPs which play a role in the control of transcript decay, is regulated in a transcript- and tissue-specific fashion (47). This is not surprising, as divergent tissue-specific mechanisms controlling the stability of mitochondrially-associated mRNAs have been previously

implied (43). Altogether, it appears that differences in transcript structure, coupled with tissue- and stimulus-specific regulation of stability illustrate an increasingly complex picture of post-transcriptional regulatory mechanisms. Additional examination of the relationship between mitochondrial content and mRNA stability is merited in order to clarify previously observed relationships.

Thesis Objectives

Thus, based on my review of literature, the objectives of my thesis are to:

1. Establish a time course for the reduction of muscle mass and mitochondrial content in response to denervation-induced muscle disuse;
2. Characterize the impact of denervation on various levels of Tfam expression throughout this time course, by examining the relationship between the *in vivo* Tfam promoter activity, steady-state mRNA concentration, mRNA stability and intracellular protein distribution;
3. Examine mechanisms contributing to mRNA stability, by quantifying specific RNA binding proteins in denervated skeletal muscle;
4. Assess activity of upstream signaling kinases pertinent to both mitochondrial biogenesis and RNA binding proteins in response to denervation.

Hypotheses

I hypothesized that:

1. In response to denervation, the activity of the Tfam promoter *in vivo* would be reduced, with a subsequent reduction in Tfam mRNA expression;
2. Tfam mRNA turnover would be unaltered at early denervation time-points, but would be characterized by reduced turnover as denervation progressed and mitochondrial content is reduced;
3. Whole tissue expression of RBPs would be unaltered at early denervation time points, but would favour a more "stabilizing" environment as denervation proceeded;
4. The concentration of intramitochondrial Tfam protein would be reduced with denervation;
5. Kinase signaling known to promote mitochondrial biogenesis would be reduced prior to the reduction of mitochondrial content with denervation.

Chapter 2

MANUSCRIPT

Manuscript Author Contributions

Liam D. Tryon performed the animal surgeries, experiments and assays, and collected and analyzed the data, and authored the manuscript.

Matthew J. Crilly performed some of the COX activity assays and western blotting.

Dr. David A. Hood proposed, designed and supervised this project. He is the principal investigator and editor of the manuscript.

This manuscript has been submitted for publication in a peer-reviewed journal.

Prefix

The purpose of this study was to determine how the expression of mitochondrial transcription factor A (Tfam), a vital protein which coordinates mitochondrial content by controlling the transcription and replication of mitochondrial DNA (mtDNA), is regulated during a state of reduced organelle content imposed by muscle disuse. We measured Tfam expression at multiple levels following unilateral denervation for 8 hours, 16 hours, 24 hours, 3 days or 7 days, and hypothesized that decreases in Tfam expression would precede reductions in mitochondrial content. Muscle mass was lowered by 13% and 38% at 3 and 7 days post-denervation, while COX activity fell by 33 and 39% at the same time points. Activation of the Tfam promoter *in vivo* was reduced by 30-65% between 8h and 3 days of denervation. mRNA stability assays revealed that Tfam mRNA was stabilized during short-term denervation, enhancing its transcript's half-life following 8-24 hours of denervation. Protein expression of RNA-binding proteins involved in modulating mRNA decay in skeletal muscle (KSRP and CUGBP1) was elevated at 3 and 7 days of denervation. Tfam localization within subsarcolemmal mitochondria was reduced after 3 and 7 days of denervation, and this was associated with a suppression of COX I mRNA, suggesting that denervation impairs both Tfam import into mitochondria, as well as mtDNA transcription. Finally, AMPK phosphorylation increased 16 hours after denervation ($p=0.06$), and was repressed after 7 days of denervation, providing support for an early pro-autophagy signal, but an anti-mitochondrial biogenesis signal with more prolonged denervation. These data suggest that putative signals regulate the Tfam promoter during the earliest stages following denervation, but that these are counteracted by increases in the stability of the Tfam transcript. Import of Tfam into the mitochondrion seems to be the most critical point of regulation of this protein during denervation, an impairment which is crucial for the loss of mitochondria brought about by muscle disuse.

Introduction

Chronic muscle disuse, such as that brought about by denervation, is a potent inducer of muscle atrophy (2, 46, 51). This phenomenon arises as a result of the shift in the balance between protein synthesis and degradation, favouring muscle catabolism (5, 20), in addition to the activation of pathways mediating macroautophagy (37, 38, 55). Concomitant with the reduction in muscle fiber size, mitochondrial content is also diminished, which likely accounts for observed impairments in muscle endurance performance (2, 51).

The regulation of mitochondrial content has been well documented, and is primarily stimulated by the activity of the transcriptional coactivator PPARγ coactivator-1α (PGC-1α) (23, 44). PGC-1α is capable of controlling the expression of a variety of aspects of mitochondrial biogenesis, through the coactivation of key nuclear transcription factors, such as nuclear respiratory factors (NRF)-1 and -2 (53), which in turn can promote the expression of mitochondrial transcription factor A (Tfam). Mitochondrial biogenesis requires the coordinated expression of genes encoded within the nuclear and mitochondrial genomes (mtDNA). In order to properly orchestrate mitochondrial biogenesis, factors which promote the transcription and expression of mtDNA must be transcribed from the nuclear genome, and imported into mitochondria. Tfam is a required component of the mitochondrial transcription machinery, along with mitochondrial transcription actor B2 (Tfb2m) and mitochondrial RNA polymerase (POLRMT) (45, 54). Tfam is unique in that is has the ability to bind to mtDNA and distort it into a U-turn like structure, facilitating access of other accessory components to promote mtDNA transcription (36, 41). Beyond this, Tfam also has essential roles in the replication and compaction of mtDNA into nucleoid structures (17, 27)

The necessity of Tfam has been highlighted by Larsson et al., who demonstrated that whole body homozygous Tfam ablation results in embryonic lethality, whereas viable heterozygous Tfam knockout mice display reductions in mtDNA levels and compromised electron transport chain function (31). Muscle-specific knockouts of Tfam display similar mitochondrial impairments (52). Conversely, the transient overexpression of Tfam is sufficient to induce mtDNA expression and mitochondrial mRNAs (34). Furthermore, increases in the expression and mitochondrial import of Tfam in response to contractile activity have been shown to precede increases in mitochondrial content, suggesting a crucial role for this protein in the regulation of contractile activity-induced mitochondrial biogenesis (22). These reports underscore the vital role of Tfam in mtDNA expression and content, as well as mitochondrial function.

However, the significance of regulating Tfam expression during denervation-induced atrophy has not been fully explored. Previous work has documented that denervation-induced disuse reduces mitochondrial content quite rapidly, depleting the mitochondrial pool by approximately 40% following five days of denervation (2). This is associated with considerable reductions in the expression of factors regulating mitochondrial biogenesis (2, 42, 43, 49), including PGC-1α and Tfam, along with an impairment in protein import into the mitochondrial matrix (46).

Thus, the purpose of this study was to investigate the relationship between the expression of Tfam and mitochondrial content during denervation-induced disuse. We examined the expression of Tfam at the transcriptional and post-transcriptional levels during the first week of denervation, as this is the time frame in which the most substantial loss of mitochondrial content occurs. We hypothesized that a decline in Tfam content would precede reductions in

mitochondrial content, as a result of a diminished drive for mitochondrial biogenesis. Moreover, consistent with earlier work from our laboratory in mRNA stability, we hypothesized that a decline in mitochondrial content would favour a more stabilizing environment for Tfam mRNA.

Methods

Animals and Experimental Design. Animal care and experimental procedures were approved by the York Animal Care Committee, and were in accordance with the Canadian Council of Animal Care. Male Sprague-Dawley rats (300-400g, Charles River, St. Constant, QC, Canada) were randomly assigned to one of five time-course groups: 8 hours, 16 hours, 24 hours, 3 days or 7 days. Prior to denervation in a subset of animals, the tibialis anterior (TA) of both hindlimbs was electrotransfected with the rTfam-pGL3 vector. Four days following electrotransfection, rats underwent surgery to induce unilateral hindlimb denervation, while the contralateral hindlimb was sham-operated. At each of these time points, animals were sacrificed and the TA muscles were excised from the denervated and contralateral, sham-operated limb. TA muscles from both limbs of these animals were used for a selection of biochemical analyses. In a separate set of experiments, a subset of male Sprague-Dawley rats was randomly assigned to one of three time-course groups: 24 hours, 3 days or 7 days. These animals were denervated as described below, and at each time point, animals were sacrificed. The TA muscles from these animals were used to isolate subsarcolemmal mitochondria from freshly excised tissue, while the extensor digitorum longus (EDL) was fixed and frozen for cross-sectional area analyses.

Denervation surgery protocol. Rats were anesthetized using gaseous isofluorane. The fast-twitch tibialis anterior and extensor digitorum longus muscles were denervated by exposing the left common peroneal nerve and transecting a 5-mm section. The contralateral hindlimb underwent the exact same procedure, whereby the right common peroneal nerve was exposed, but no transection was performed. Following the administration of sterile ampicillin, the incision was sutured and closed with metal clips. The day of surgery represented *day 0* of the time course. Animals were given amoxicillin in their drinking water following the surgery (0.025% wt/vol).

At the conclusion of the time-course for each group, animals were anesthetized with an intraperitoneal injection of ketamine-xylazine (0.2ml/100g of body weight) and both sham-operated and denervated TA muscles were excised, clamped frozen in liquid nitrogen and stored at -80°C. Muscle samples used for biochemical analyses were then pulverized at the temperature of liquid nitrogen, while samples used for cross-sectional analyses were prepared as described below.

Intramuscular DNA injection and electroporation in vivo. Male Sprague Dawley rats (300-400g) were anesthetized as described above. Electrotransfection experiments were performed as previously described (12, 14). The lower hindlimbs were shaved and sterilized, prior to the injection of a Tfam promoter-firefly luciferase reporter containing plasmid (rTfam1-pGL3 vector, ref. (12)). TA muscles were injected from the distal portion of the leg, with the syringe being inserted so that its orientation paralleled that of fiber orientation. Approximately 30µl of the plasmid solution (containing 50µg of the rTfam1-pGL3 and 1µg of pRL-CMV to normalize for electrotransfection efficiency in 0.9% sterile saline solution) was injected into the TA of both hindlimbs using a short 29-gauge insulin syringe (BD Ultra-Fine). Immediately after the DNA injection, transcutaneous electrical pulses were applied using the ECM 830 Electroporation system (BTX Harvard Apparatus). The muscle was held on either side of the injection site by the tweezertrodes (BTX Harvard Apparatus) at the level of the skin, and a total of eight pulses was delivered with anode and cathode electrode orientation being reversed after four pulses (100 V/cm, 20ms, 1Hz per pulse). Four days after treatment, the animals were subject to the denervation protocol as described below. At the conclusion of the denervation time-course, muscles were excised, clamped frozen and stored. All muscles were then powdered at the temperature of liquid N_2 until further molecular analyses were performed.

pGL3 and pRL-CMV luciferase reporter assay. Muscle powders from the denervated and sham-operated hindlimbs (30-50 mg) were diluted seven-fold (wt/vol) in 1x passive lysis buffer. Homogenates were sonicated on ice (3 X 10 seconds) and subsequently centrifuged at 16,100 *g* for 5 minutes at 4°C. After centrifugation, 20µl of the supernate were used to assess pGL3 luciferase activity using an EG&G Berthold Luminometer (Lumat LB9507). pGL3 firefly luciferase values were corrected for electrotransfection efficiency by simultaneously assessing pRL renilla luciferase activity.

Cytochrome c oxidase (COX) activity. Pulverized frozen TA muscle was diluted in muscle extraction buffer (100mM KH_2PO_4, 100mM Na_2HPO_4, 2mM EDTA, pH 7.2) and sonicated 3 x 5 seconds on ice. Supernates were added to a solution containing fully reduced cytochrome c. This reaction was performed in a 96-well plate at 30°C using a Synergy-HT microplate reader. COX activity was determined by the maximal rate of cytochrome c reduction, assessed by measuring the change in absorbance at 550nm. Data were compiled with KC4 software.

In vitro cytosolic protein extraction. Frozen powders (50mg) from sham-operated and denervated TA muscles were homogenized separately in 500µl sterile homogenization buffer (25% glycerol, 0.42M NaCl, 1.5mM $MgCl_2$, 0,2mM EDTA, 20mM HEPES pH 7.9, 0.5mM 1,4-DTT, 0.5mM PMSF and RNase-free water) at 30% power output for 3x10s. Homogenates were subsequently centrifuged at 5000 *g* for 15 minutes at 4°C. The supernate was transferred to a sterile Eppendorf tube, and further centrifuged at 15,000 *g* for 15 minutes at 4°C to produce mitochondria-free (S15) crude cytosolic fractions. Protein concentrations were determined by the Bradford colorimetric protein assay.

In vitro RNA isolation. Total RNA was isolated using TRIzol reagent (Life Technologies), whereby muscle tissue powders were derived from TA of either the sham-operated or denervated

animals (approximately 100mg tissue/ml TRI-reagent). RNA isolation was performed as previously described (12, 29). Briefly, RNA was precipitated overnight at -20°C with isopropanol, and subsequently pelleted, washed, dried and resuspended in sterile water. RNA concentration and purity were assessed using spectrophotometry, while RNA quality was affirmed through separation on a 1% agarose-formaldehyde gel to visualize 28S and 18S rRNA.

In vitro mRNA decay assay. Total RNA (35µg) derived from the TA muscle of the Sprague-Dawley rats of SD rats was combined with 20µg of S15 cytosolic extracts derived from either the denervated or control TA of animals subjected to the time-course denervation protocol. To allow for assessment of the degradation of RNA within the incubated tubes as a percentage of the original RNA content, a tube containing 35µg of RNA and 5µl of sterile homogenization buffer in a 100µl reaction volume served as a baseline measure at the zero time-point. This sample does not contain the cytosolic proteins, and it allowed us to determine the amount of RNA present in the sample without the influence of cytosolic factors. Reaction volumes were set at 100µl, and samples were incubated at 37°C for 15 or 45 minutes. At the completion of each incubation time-point, phenol was added to each sample and it was shaken vigorously. Total RNA was then reisolated using a phenol-chloroform-isoamyl alcohol extraction procedure as previously described (29). The reisolated RNA was pelleted, washed, dried and resuspended in sterile water. RNA concentration and purity were determined via spectrophotometry, and RNA quality was assessed by examining the separation and intensity of 28S and 18S rRNAs on a 1% agarose-formaldehyde gel.

Reverse transcription-polymerase chain reaction (RT-PCR). For the purpose of assessment of mRNA decay kinetics, cDNA was reverse transcribed from 1.5µg of total RNA, which was isolated following the in vitro decay assay, using SuperScript III reverse transcriptase in a 20µl

reaction. Subsequently, cDNA was amplified by semi-quantitative polymerase chain reaction (PCR) using *GoTaq* Flexi DNA polymerase (Promega) with the required reagents and sequence-specific sense and anti-sense primers in a 50µl reaction. Primer sequences and PCR cycle count for Tfam and ribosomal protein S12 (Rps12) are listed in Table 1. PCR products (40µl) were visualized on ethidium bromide-stained 1.8% agarose gels under UV light, and quantified using Sigma Scan Pro (v.5) software. For usage in real-time PCR, oligonucleotide primers were designed using sequences from GenBank using Primer3 (v.0.4.0) software (MIT, Cambridge, MA) and primer specificity was confirmed using OligoAnalyzer 3.1 (Integrated DNA Technologies). Real-time PCR primer sequences for Tfam, COX I, ribosomal protein S12 and cytoskeletal protein B-actin (Actb) are also listed in Table 1.

Real-Time PCR. Gene expression was quantified in a 96-well plate using the StepOnePlus® Real-Time PCR System (Applied Biosystems), along with SYBR® Green chemistry (PerfeCTa SYBR® Green SuperMix, ROX, Quanta BioSciences). Each well contained: SYBR® Green SuperMix, forward and reverse primers (20 µM), 2 µg of cDNA diluted 30-fold in DEPC-treated water, resulting in a final reaction volume of 25 µL per well. The PCR program consisted of a holding stage (95°C for 10 min), followed by 40 cycles of annealing (60°C for 1 min) and extension (95°C for 15 s), then by a final melting stage (95°C for 15 s, 60°C for 1 min, 95°C for 15 s). Samples were tested in duplicates to ensure accuracy. Analyses of melt curves generated by the instrument were used to determine the presence of non-specific amplification and primer dimers. Negative control wells contained DEPC-treated water in place of cDNA.

Real-time PCR quantification. The threshold cycle (CT) number for the endogenous control genes were averaged, in lieu of a single reference gene. The average CT values for these genes, Rps12 and Actb, did not change between sham-operated and denervated muscles within time

points, as well as between time points. This average was subtracted from the CT number of the gene of interest (ΔCT=CT(target gene)-CT(endogenous control)). The ΔCT value of the sham-operated tissue was then subtracted from the ΔCT value of the denervated tissue (ΔΔCT=ΔCT(denervated)-ΔCT(sham-operated)). Results were reported as fold-changes using the ΔΔCT method, calculated as $2^{-\Delta\Delta CT}$.

Subsarcolemmal mitochondrial isolation. Animals were anesthetized, and both denervated and sham-operated contralateral TA muscles were excised, minced and briefly homogenized using an Ultra-Turrax polytron at 40% power output. The subsarcolemmal (SS) mitochondria were isolated using differential centrifugation as previously described (10), and resuspended in medium (100 mM KCl, 10 mM MOPS, 0.2% BSA). Further, cytosolic fractions of these same muscles were isolated via centrifugation. The concentrations of isolated mitochondria and cytosolic fractions were determined by Bradford colorimetric protein assay, prior to immunoblotting.

Protein Extraction and Immunoblotting. For whole muscle protein extraction, twenty micrograms of powdered tissue were added to Sakamoto buffer (20mM HEPES, 2 mM EGTA, 1% Triton X-100, 10% glycerol, 50mM beta-glycerolphosphates, 1 mM phenylmethanesulphonylflouride, 1 mM dithiothreitol, 1 mM sodium orthovanadate, 10 µm leupeptin, 5 µm pepstatin A, 10 mg/ml aprotinin) and were subject to a 20-fold dilution. Samples were rotated for one hour, sonicated (3 x 3 seconds, 30% power) and centrifuged for 10 mins at 12,000 x *g*. Supernates were recovered and protein concentration was determined by Bradford protein assay. Whole muscle or isolated SS mitochondrial and cytosolic extracts were separated by SDS-PAGE and subsequently electrotransferred onto nitrocellulose membranes. Membranes were then blocked for one hour in 1X TBST [Tris-buffered saline-Tween 20, 25 mM Tris·HCl

(pH 7.5), 1 mM NaCl, 0.1% Tween 20] containing 5% skim milk, before being incubated at 4°C overnight in blocking buffer with antibodies directed towards Tfam (1:3000; manufactured in house, ref. (22)), GAPDH (1:100,000; ab9485), Porin (1:1000; MitoSciences MSA03), HuR (1:2000; sc5261), CUGBP1 (1:1000; sc20003), KSRP (1 ml prediluted antibody serum), total AMPK (1:500; Cell Signaling #2532), phosphorylated AMPK (Thr172) (1:3000; Cell Signaling #2535S), total p38 (1:1000; Cell Signaling #9212) and phosphorylated p38 (Thr180/Tyr182) (1:500; Cell Signaling #9211S). The KSRP antibody was a generous gift from Dr. Bernard Jasmin (University of Ottawa). Following incubation, blots were washed in 1X TBST (3 x 5 minutes) to remove excess primary antibody, and incubated with the appropriate secondary antibody coupled to horseradish peroxidase at room temperature for 1 hour. After this, membranes were washed with 1X TBST again to remove excess secondary antibody, and antibody-bound protein was revealed by the enhanced chemiluminescence method. Films were scanned and analyzed using Carestream Molecular Imaging Software Standard Edition v.5.4.2. To control for loading, protein quantifications were corrected either with GAPDH or Porin immunoblotting or Ponceau staining where noted. There was no effect of time or denervation on the loading controls utilized.

Cross-sectional analyses and succinate dehydrogenase (SDH) Staining. EDL muscles from the sham-operated and denervated hindlimb were excised from the animal, mounted in Cryomatrix (Thermo Scientific) and frozen in isopentane at the temperature of liquid nitrogen. These muscles were then cryo-sectioned into 10μm sections, transferred to glass slides and were incubated with an SDH staining solution (0.2M sodium succinate, 0.2M phosphate buffer pH 7.4, nitroblue tetrazolium) at 37°C for 20 minutes. Slides were then rinsed in distilled water, after which a microscope cover glass was mounted on slides using DPX Mountant for histology

(Fluka BioChemika no. 44581). Photos of muscle sections were taken using a Nikon Eclipse 90i camera and QCapture software. Muscle cross-sectional areas were determined using ImageJ software.

Statistical Analyses. Data were produced and analyzed with GraphPad 4.0 Software, and values (where indicated) are reported as ± SE. Student's paired t-test was employed to assess differences between conditions. The nonlinear regression equation $50 = 100e^{(-kx)}$ was used to calculate mRNA half-lives. A two-way ANOVA was performed to determine differences in Tfam half-life.

Results

Effect of denervation on muscle mass, muscle fiber cross-sectional area and mitochondrial content. Denervation of the tibialis anterior (TA) muscle did not influence muscles within the first 24 hours, however significant reductions of muscle mass of 13% and 38% were observed following 3 and 7 days of denervation, when compared to the contralateral, sham-operated hindlimb ($p < 0.05$; Fig. 1A). To ensure that the lack of change in muscle mass within the first 24 hours of denervation was not masked by local tissue inflammation and edema, we compared the wet and dry tissue masses of the TA muscle within this time period. There was no difference in the ratio of wet mass to dry mass of this muscle within this time period, confirming that tissue edema did not confound our measures of muscle mass during the period immediately following denervation (Fig. 1B). Cytochrome *c* oxidase activity, a common marker indicative of the mitochondrial content of a tissue, declined by 33 and 39% after 3 and 7 days of denervation, respectively (Fig. 1C). We also assessed the effect of denervation on the muscle mass and cross-sectional area of the extensor digitorum longus. Denervation reduced the mass of the EDL by 4 and 30% after 3 and 7 days, respectively (Fig 2A). Individual fiber cross-sectional area of the EDL was decreased by 20, 22 and 50% following 24 hours, 3 days or 7 days of denervation (Fig. 2B, 2C). The frequency distribution of fiber sizes measured in these cross-sections, illustrates the left-ward shift in the distributions with continued denervation (Fig 2D). These data verify that our denervation paradigm was sufficient to induce a reduction in muscle mass, cross-sectional area and mitochondrial content.

Effect of denervation on Tfam transcriptional activation, mRNA content and stability. We assessed the transcriptional activity of the Tfam promoter by electrotransfecting a 1.1kb rat Tfam promoter-luciferase reporter into the TA prior to denervation. Activity of the promoter was

reduced by 30-65% between 8h and 3 days of denervation, but was not significantly different from the contralateral, sham-operated TA after 7 days of denervation (Fig 2A). Tfam mRNA was not different between denervated and sham-operated muscles between 8h and 3 days of denervation, but was increased 1.9-fold after 7 days of denervation (Fig. 2B). We also measured the stability of Tfam mRNA using an established *in vitro* cell free mRNA decay assay (12, 29). Tfam mRNA was stabilized during short-term denervation, as transcript half-life ($t_{½}$) was enhanced 1.8-fold following 8 hours ($p < 0.05$), and 3-fold after 24 hours of denervation ($p = 0.08$) (Fig. 3C). However, after 7 days of denervation Tfam transcript stability was decreased by ~40% when compared to its half-life in the sham-operated muscle ($p < 0.05$) (Fig. 3C). Thus, despite the early reduction in Tfam transcriptional activity following denervation, mRNA content is maintained at a constant level as stability is increased during the same time period.

Expression of RNA-binding proteins during denervation. To gain further insight into the mechanisms mediating Tfam mRNA half-life during denervation, we measured the expression of several RNA binding proteins that have been implicated in the regulation of mRNA stability. In whole muscle protein extracts, no effect of denervation was observed on the expression of HuR, a protein which promotes the stability and translation of target mRNAs (30) (Fig 4A). Expression of CUGBP1, an mRNA destabilizing protein which can interact with GC-, GU- and AU-rich elements (35, 40), was elevated 1.4-, 1.9- and 4.3-fold by 24 hours, 3 days and 7 days following denervation, respectively. KSRP, a protein which has role in the modulation of ARE-containing mRNAs (21), was increased by 2.1- and 2.8-fold at 3 and 7 days post-denervation (Fig. 4C).

Abundance of Tfam subsarcolemmal (SS) mitochondria and function following denervation. We have previously shown that the import of the mitochondrial matrix-destined protein OCT is

diminished in response to denervation (46). To evaluate the idea that denervation reduces global matrix-destined protein import, we measured the protein abundance of Tfam in isolated SS mitochondria, as well as in the cytosolic fractions of the same muscles (Fig. 5A). Our Tfam antibody detects two bands, a 27 kDa, full-length precursor Tfam which was present exclusively in the cytosol, and a 24 kDa mature Tfam which was localized in mitochondria. The difference in molecular weight is accounted for by the proteolytic removal of the mitochondrial targeting sequence during protein import (47). In line with our previous measurements, SS mitochondrial Tfam content was reduced by 63 and 67% after 3 and 7 days of denervation ($p < 0.05$, Fig 5A). To determine whether this had an impact of mtDNA transcription, we measured the mRNA content of the mtDNA-encoded cytochrome *c* oxidase subunit 1 (COX I), as an indirect index of Tfam function inside the mitochondria. Denervation significantly reduced COX I mRNA by 36 and 25% after 3 and 7 days of denervation ($p < 0.05$, Fig 5B).

Activation of kinases associated in mitochondrial biogenesis. We wanted to assess the impact of denervation on the signaling of kinases implicated in promoting the maintenance of muscle mitochondria. Following 16 hours of denervation, phosphorylation of AMPK on the Thr172 residue was increased ($p = 0.06$) 2.3-fold. However, after 3 and 7 days of denervation, phosphorylation of AMPK at the Thr172 residue was reduced by 35 ($p = 0.09$) and 74% respectively (Fig. 6A). No significant differences in the phosphorylation of p38 on its Thr170/Tyr172 residues were detected in response to denervation (Fig. 6B). Denervation did not alter the total protein content of either AMPK or p38 over the 7 day period.

Discussion

It is well documented that chronic denervation-induced muscle atrophy is associated with a concomitant reduction in muscle mitochondrial content (2, 46, 51). Interestingly, this decrease in mitochondrial content appears to proceed in two phases, starting with a rapid, substantial reduction which occurs during the first week subsequent to denervation, and followed by a slower, more gradual decline in the weeks which follow (2, 51). Previous work has highlighted the reduction in the expression of factors implicated in mitochondrial biogenesis with prolonged muscle denervation (2, 42, 50). However, given the extensive decrease in muscle mitochondrial content during the early stages, we wished to determine if this was a by-product of a diminished drive for mitochondrial biogenesis. To do so, we examined the impact of denervation on the expression of mitochondrial transcription factor A (Tfam), an essential nuclear-encoded mitochondrial transcription factor noted for its role in controlling mitochondrial DNA copy number, transcription and compaction (16, 28, 34, 52). Thus, the primary purposes of this study were to investigate the influence of short term denervation-induced disuse on the control of various levels of Tfam expression, and to determine if the large reduction in mitochondrial content could be attributed to alterations in the regulation of this transcription factor. We hypothesized that Tfam transcriptional activity, mRNA and intra-mitochondrial protein content would decline, and that these changes would precede the lessening of mitochondrial content.

Our first goal was to determine how rapidly and to what extent muscle mass and mitochondrial content were reduced during the very early stages of denervation. Our data illustrate that muscle mass of both the tibialis anterior (TA) (Fig. 1A, 2A) and extensor digitorum longus were reduced as soon as 3 days following denervation, and declined further thereafter. This was paralleled by a reduction in COX activity, an index of mitochondrial content (Fig. 1C)

after 3 and 7 days of denervation. To ensure that muscle atrophy at the earliest time points following denervation was not masked by inflammation and edema, we determined that there were no differences in the water content of the muscles from either the sham-operated or denervated hindlimbs (Fig. 1B). Furthermore, we confirmed that the reduction in muscle mass was indeed a consequence of the reduction in muscle fiber size, a hallmark of atrophy, by quantifying fiber cross-sectional area (Fig, 2C). The leftward shift in the fiber size distribution (Fig. 2C) with increasing time of denervation indicates that this was certainly the case.

Consistent with our hypothesis, Tfam transcription in the TA muscle was reduced as early as 8 hours following the denervation surgery, and remained depressed for up to 3 days after the removal of the neural stimulus (Fig. 3A). This provides evidence that factor(s) interacting with the 1.1kb proximal rat promoter of this gene are either less active in the induction, or more active in the repression of the transcription of this gene, and that this occurs well before the reduction of mitochondrial content is observed. Unexpectedly, the mRNA content of Tfam was unaltered during this same time period (Fig. 3B), which exposed a dissociation between transcription and steady state mRNA levels.

Previous work in our labortatory has utilized a cell-free *in vitro* decay assay (12, 19, 29) to determine relative mRNA degradation rates between multiple divergent skeletal muscles. In this case, we sought to compare the degradation rate of Tfam mRNA between skeletal muscle that had been either sham-operated or denervated. Our observations indicate that Tfam mRNA decay was attenuated at the early time points following denervation (Fig. 3C). This suggests that the lack of change in the steady state Tfam mRNA could be accounted for by concomitant decreases in mRNA transcription, along with increases in mRNA stability. We have previously documented that tissue-specific mechanisms exist which control the stability of mitochondrially-

associated mRNAs (11, 12, 29). The current work highlights the notion that in addition tissue-specific mechanisms, mRNA stability is also reliant on time-dependent factors following the onset of an adaptive stimulus (Fig 3C). Interestingly, we have previously documented an opposing change, that is, a reduction in mRNA stability in response to chronic muscle use (29), indicating that the influence of mRNA stability is also stimulus-dependent.

In an attempt to reveal possible mechanisms accounting for the different half-lives between sham-operated and denervated muscles, we investigated possible factors contributing to the change Tfam transcript stability. The stability of mRNAs is mediated primarily by sequence elements found in the 3'-untranslated regions (UTRs) of transcripts, most notably those rich in adenosine and uridine (AU-rich elements – AREs) and guanosine and uridine (GU-rich elements – GREs) (9, 48). RNA binding proteins (RBPs) bind to these elements, and promote either the stabilization or the degradation of the target mRNAs. We chose to measure several RBPs which have been characterized in skeletal muscle to have a role either in facilitating transcript stabilization, as is the case with human antigen R (HuR) (18, 32), or in promoting transcript destabilization, such as CUG binding protein 1 (CUGBP1) (32) and K homology splicing regulator protein (KSRP) (4, 8).

Our results indicate that HuR expression remained unaltered over the denervation time-course (Fig. 4A), while whole cell protein expression of CUGBP1 and KSRP was elevated with progressive denervation (Fig. 4B, C). This suggests that the overall cellular expression of these factors may not control the alterations in stability at the early denervation time points. While not examined in this study, alterations in the activity or intracellular localization of these proteins may also contribute the observed changes in Tfam stability. Furthermore, other proteins or non-coding RNAs (micro-RNAs) may also play a role in explaining our data. Nonetheless, it remains

possible that the increased expression of both of the measured destabilizing RBPs contributes to the reduction in Tfam transcript stability after 7 days of denervation. We have identified multiple putative sequence elements in the 3'-UTR of the rat Tfam gene (data not shown), which, based on sequence specificity of the above mentioned RBPs, may represent binding sites for these proteins. Future work will examine possible interactions between RBPs and these elements in the Tfam 3'-UTR.

We have previously shown that with six weeks of denervation, Tfam protein levels are reduced by 60% (2). Additionally, the import of ornithine carbamoyltransferase, a mitochondrial matrix-destined protein, was decreased as early as 3 days following denervation (46). Thus, we hypothesized that denervation would result in a reduction of Tfam within mitochondria. To test this, we examined the protein content of Tfam in isolated subsarcolemmal (SS) mitochondria, as import into the mitochondrial matrix is required for it to interact with mtDNA. We chose to specifically investigate SS mitochondria, as this mitochondrial subpopulation has been shown to adapt to physiological stimuli with greater rapidity when compared to the intermyofibrillar population (2, 7, 26, 46). In line with previous data, our current work reveals that intra-mitochondrial Tfam content was reduced as early as 3 days of denervation (Fig. 5A), concomitant with a reduction in COX I transcript (Fig. 5B). We interpret the reduction in COX I transcript to be an indirect indication that transcription of mtDNA is reduced, and that this is due to the decrease in Tfam imported and localized within this subset of mitochondria.

Finally, we analyzed the phosphorylation of p38 MAPK and AMP-activated protein kinase (AMPK) to initiate the study of signaling kinase activation which may be implicated in the reduction in mitochondrial biogenesis observed (3, 6, 24). We were unable to detect changes in the phosphorylation of p38 on the Thr180 and Tyr182 residues (Fig. 6B), the phosphorylation

of which has been implicated in the induction of the PGC-1α gene and mitochondrial biogenesis through the activation of ATF2 and MEF2 (3), as well as the activation E3 ubiquitin ligases atrogin1/muscle atrophy F-box (MAFbx) and muscle ring finger protein 1 (MuRF1) (1, 33). Phosphorylation of p38 has been previously shown to occur in response to muscle disuse in rodents (13, 39), however, our inability to detect alterations in our current model may be due to differences in the species studied or in the length of the treatment.

On the other hand, the activation of AMPK by phosphorylation on its Thr172 residue followed an interesting pattern during the denervation time course (Fig. 6A). We observed an increase in AMPK phosphorylation at 16 hours following denervation ($p = 0.06$). As activation of AMPK has been implicated in the induction of macroautophagy and mitophagy (15, 25), our data suggest that AMPK-signaling to induce autophagy may be involved in the very immediate response to denervation. Interestingly, we observed a reduction in the phosphorylation of AMPK by 3 days ($p = 0.09$) and 7 days after denervation, likely contributing to the diminution in the drive for mitochondrial biogenesis with sustained muscle disuse. Although AMPK phosphorylation stimulates mitochondrial biogenesis through PGC-1α and NRF-1 (6, 24), we did not detect a reduction in the transcriptional control of Tfam, a known target of NRF-1 following seven days of denervation. This suggests either that other mechanisms, independent of AMPK activation of the PGC-1α/NRF-1 pathways, are involved in the regulation of Tfam transcription at this point in time, or that the effect of AMPK activity on the Tfam promoter during denervation was not captured by the 1.1kb proximal promoter construct we utilized. Nonetheless, monitoring and modulating the activity of AMPK during denervation may be an interesting avenue for future research.

In sum, it appears that there are factors, albeit unknown at this time, regulating the Tfam promoter during the earliest stages following denervation. These effects are counteracted by alterations in the stability of the Tfam transcript. Ultimately, import of Tfam into the mitochondrion appears to be a crucial point in the regulation of Tfam activity during denervation. Reductions in Tfam import occurred in concert with the decline in mitochondrial content, suggesting that Tfam import is critically involved in the loss of mitochondria during muscle disuse. Indeed, we have previously shown that COX activity is positively correlated with the rate of mitochondrial protein import (46). Future studies should strive to determine the upstream signals regulating the Tfam promoter during denervation, and could seek to further elucidate the processes which contribute to the reduction in mitochondrial content within the first 72 hours of denervation.

Table 1. PCR primers

Usage	Transcript	Forward	Reverse	Product Size (bp)	PCR Cycle Count
Semi-quantitative PCR	**Tfam**	5'-ATGGCGCTGTTCCGGGGAATGTGG-3'	5'-TTAATTCTCAGAGATGTCTCCCGGG-3'	735	34
	S12	5'-GGAAGGCATAGCTGCTGG-3'	5'-CCTCGATGACATCCTTGG-3'	638	26
Real-time PCR	**Tfam**	5'-CGCCTGTCAGCCTTATCTGTA-3'	5'-TGCATCTGGGTGTTTAGCTTA-3'	131	n/a
	COX I	5'-GCCAGTATTAGCAGCAGGTAT-3'	5'-TGTTGATAAAGGATTGGGTCT-3'	102	n/a
	S12	5'-ATGGACGTCAACACTGCTCT-3'	5'-ATCTCTGCGTGCTTGCAT-3'	127	n/a
	B-actin	5'-CCCCATTGAACACGGCAT-3'	5'-GCCAACCGTGAAAAGATGACC-3'	154	n/a

Tfam, mitochondrial transcription factor A; S12, ribosomal protein 12 (Rps12); COX I, cytochrome c oxidase subunit 1; B-actin, cytoskeletal protein beta-actin; bp, base pairs

Future Work

1. We noted that the *in vivo* transcription of the Tfam gene from the 1.1kb promoter was repressed as early as 8 hours following the removal of a neural stimulus, and remained repressed up to 3 days following denervation. We have mapped the 1.1kb promoter and have identified putative binding sites for numerous transcription factors. The Foxo3a transcription factor is well characterized as having a role in the activation of autophagy, mitophagy and the ubiquitin-proteasome system during muscle atrophy. Interestingly, the 1.1kb proximal promoter region of Tfam we utilized in this study contains 4 putative Foxo3a binding motifs. Previous studies have suggested a role for Foxo3a in the reducing of Tfam mRNA content *in vitro*. Furthermore, work analyzing the kinetics of Foxo3a nuclear-cytoplasmic shuttling during denervation notes that Foxo3a is localized in the nucleus to the greatest degree 3 days following denervation, while it is excluded from the nucleus after 7 days of denervation. Future work should utilize chromatin immunoprecipitation (ChIP) assays to determine if Foxo3a does indeed interact with its putative binding motifs on the Tfam promoter *in vivo*, and to evaluate the dynamics of this interaction during denervation.
2. In the current study, we have only evaluated two upstream signaling kinases involved mitochondrial biogenesis, p38 MAPK and AMP-activated protein kinase. Numerous other factors (either kinases or transcription factors) are involved in promoting or inhibiting either mitochondrial biogenesis or mitochondrial degradation via mitophagy. Future work should evaluate the activation or de-activation of other signaling kinases, or the nuclear-cytoplasmic shuttling dynamics of transcription factors involved in the control of mitochondrial content. Emphasis should be placed on the first 72 hours following denervation, as mitochondrial content is reduced to almost two-thirds of control levels during this time-frame.

3. We noted an increase in the stability of Tfam mRNA at two distinct time-points during the first 24 hours following denervation. While we noted that there was an increase in the expression of KSRP and CUGBP1 proteins in whole cell fractions primarily at 3 and 7 days following denervation, there was no difference in the expression of these proteins (or HuR) at the earliest time points following denervation. These proteins have been described to have the capacity to shuttle between the nucleus and the cytoplasm, and their intracellular compartmentalization, rather than overall expression may be more crucial to their function at the onset of a stimulus. Future work should evaluate the intracellular localization of these or other RBPs during denervation.
4. We have measured three RBPs that have well-described roles in promoting transcript stability or instability in skeletal muscle in this study. However, whether or not HuR, CUGBP1 or KSRP are actually capable of binding directly to the 3'-UTR of the Tfam transcript, and thus directly impacting the stability of this transcript, is unknown. It is of interest to determine if these or other RBPs physically interact with the Tfam transcript, which can be ascertained through RNA-immunoprecipitation (RIP) assays. Once it is known which RBPs bind to the 3'-UTR of the Tfam transcript, the specific influence of these proteins on Tfam stability can be determined through knockdown or overexpression expressions. Furthermore, it is well known that non-coding RNAs (specifically microRNAs) are capable of affecting mRNA stability. Monitoring the expression pattern of microRNAs known to alter Tfam expression may also shed light on how Tfam stability is modulated.
5. Tfam localization within the subsarcolemmal mitochondria was decreased at 3 and 7 days following denervation. While we have previously shown that import into subsarcolemmal mitochondria is impaired following denervation, it is also known that Tfam is proteolytically

degraded inside the mitochondrial matrix by Lon protease. While mitochondrial localization of Tfam appears to be critical in the reduction of mitochondrial content during denervation, the reduction in this localization may be solely a product of reduced import, or may be coupled with an increased rate of intramitochondrial degradation. Assessment of the protein content or proteolytic activity of Lon protease during denervation may provide a more thorough depiction of how intramitochondrial Tfam protein content is reduced with muscle disuse.

6. We observed a reduction in COX I mRNA expression, indicating a reduction in overall mtDNA transcription with denervation. As Tfam is vital for transcription of mtDNA, we interpret the reduction in COX I mRNA as a reduction in the interaction between Tfam and mtDNA. This can be assessed through an electrophoretic mobility shift assay (EMSA), and would affirm our interpretation of the data.

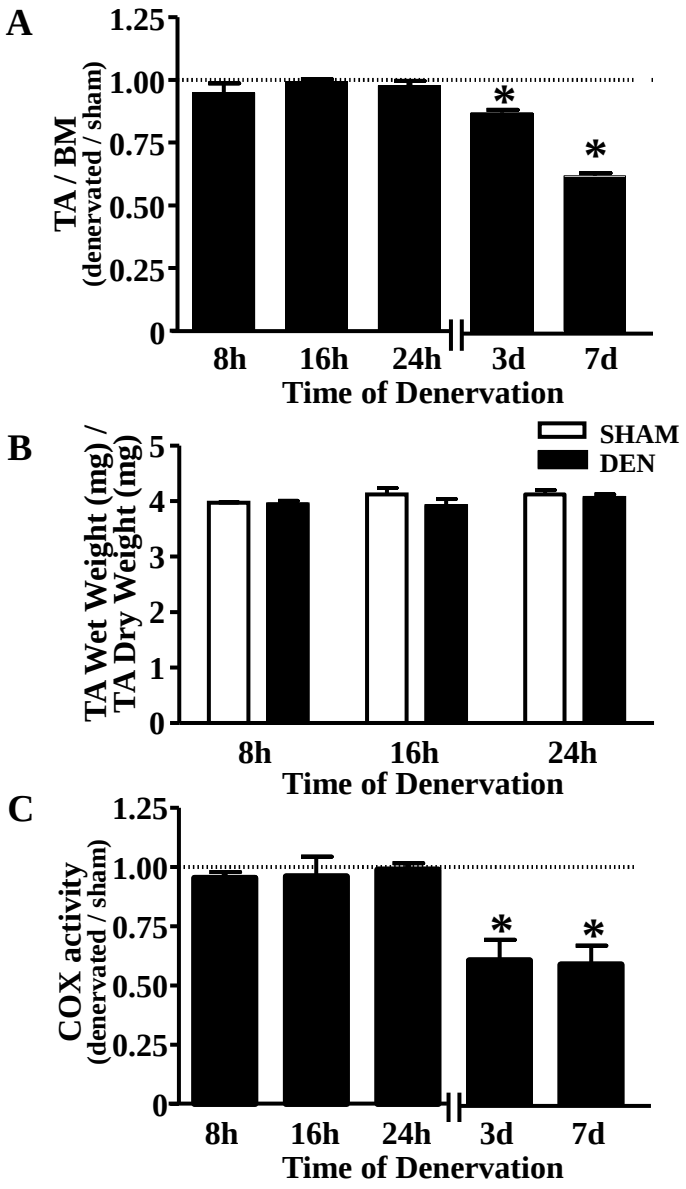

Figure 1. Effect of denervation on tibialis anterior (TA) muscle mass and mitochondrial content. *A.* TA muscle mass corrected for body mass (n = 5 -7 per time point). *B.* TA wet weight corrected for dry weight (n = 3 per time point). *C.* TA Cytochrome *c* oxidase (COX) activity in response to different durations of denervation (n = 5 per time point). * $p < 0.05$ DEN vs. SHAM of the same time point. Values are ± SEM.

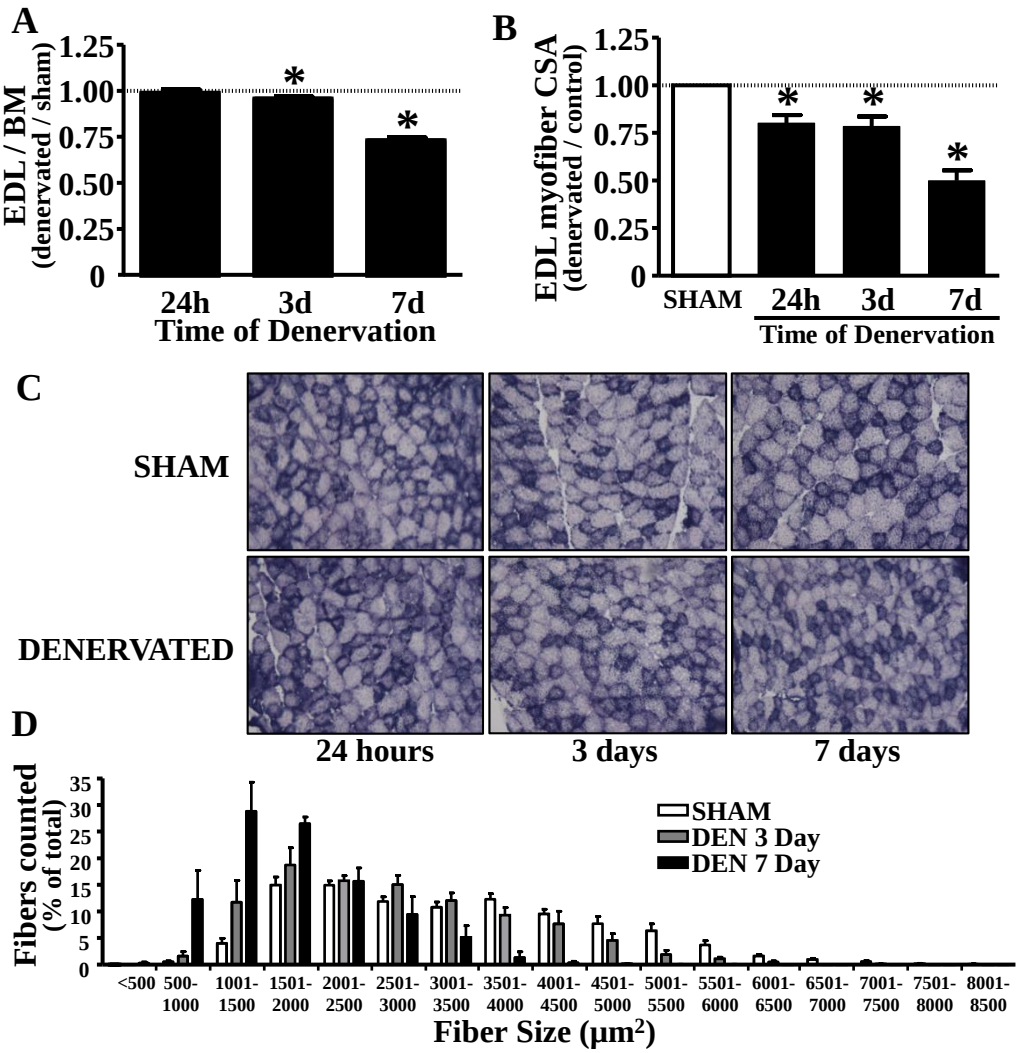

Figure 2. Effect of denervation on extensor digitorum longus (EDL) muscle mass and myofiber cross-sectional area. *A.* EDL muscle mass corrected for body mass (n = 4 per time point). *B.* Fold-change in EDL myofiber cross-sectional area in response to different time points of denervation (n = 4 per time point). *C.* Succinate dehydrogenase (SDH) staining of sham-operated and denervated EDL muscles for different lengths of denervation. *D.* Fiber size distributions from sham-operated, 3 day or 7 day denervated EDL muscles. Cross sections for the sham-operated hindlimbs are the pooled results of all sham-operated muscles analyzed. (n = 4 per time point). * $p < 0.05$ DEN vs SHAM of the same time point. Values are ± SEM.

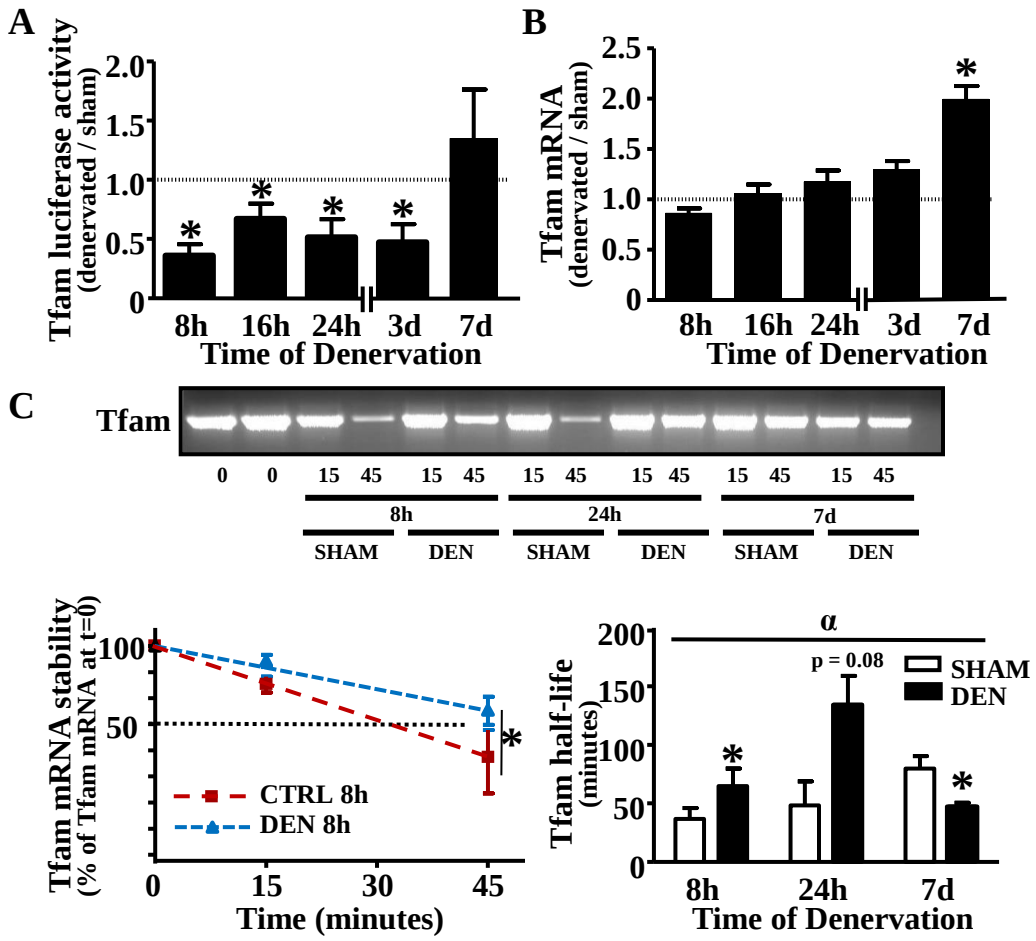

Figure 3. Effect of denervation on Tfam transcription, steady-state mRNA content and mRNA stability. *A.* Tfam transcriptional activity in response to different lengths of denervation, determined using a 1.1kb proximal Tfam promoter-luciferase reporter construct in TA muscle (n = 4-7 per time point). *B.* Tfam mRNA content in response to denervation was measured using qPCR (n = 6 per group). *C.* Degradation of Tfam mRNA in sham-operated (SHAM) or denervated (DEN) TA muscle, either 8 hours, 24 hours or 7 days post-surgery. A representative EtBr gel is shown, as well as a graphical representation of the slopes used to calculate the half-life of Tfam at a given time-point. Half-lives were calculated as described in the methods section (n = 5 per time point). ***** $p < 0.05$ DEN vs. SHAM at the same time point, α $p < 0.05$ main effect of treatment. Values are ± SEM.

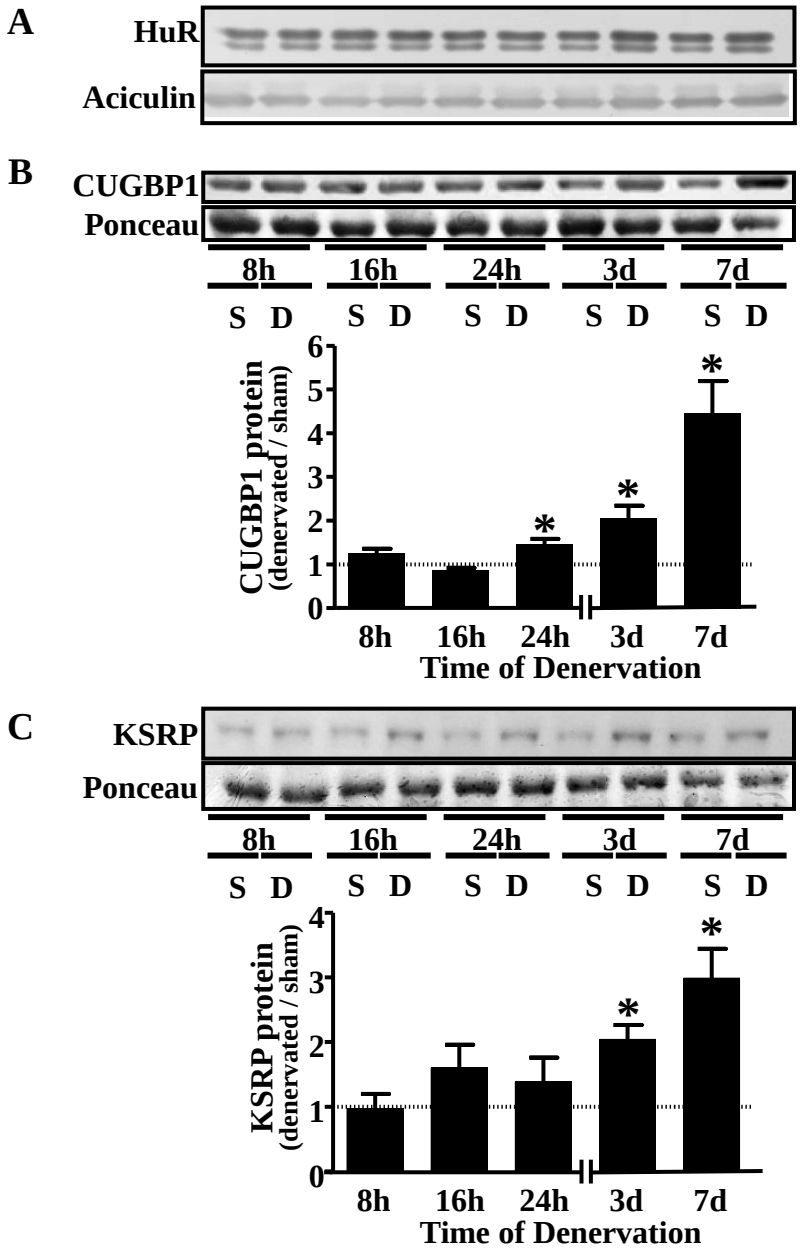

Figure 4. HuR, CUGBP1 and KSRP protein expression in denervated muscle. A representative western blot and graphical representation of *(A)* HuR, *(B)* CUGBP1 and *(C)* KSRP protein expression in sham-operated and denervated muscle. Aciculin was used as a loading control for HuR measurements, while ponceau stains served as loading control for CUGBP1 and KSRP measurements. (n = 4 per time point for all experiments) * $p < 0.05$ DEN vs. SHAM of the same time point. Values are ± SEM.

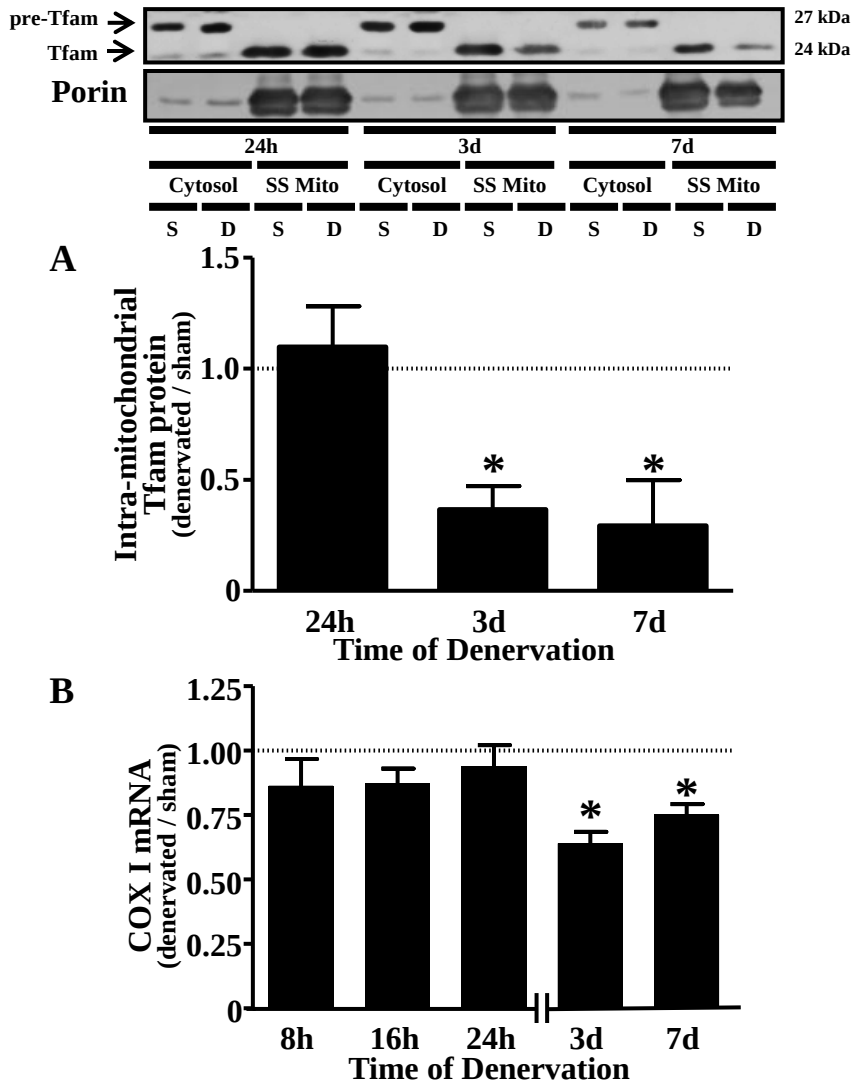

Figure 5. Effect of denervation on Tfam subsarcolemmal (SS) mitochondria content and mtDNA transcription. *A.* SS mitochondria were and cytosols were isolated from TA muscle denervated for different lengths of time. A representative western blot is shown, highlighting both the cytosolic form of Tfam ("pre-Tfam") and the cleaved mitochondrial Tfam, along with a graphical representation of this data (n = 3-4 per time point). *B.* As an indirect index of mtDNA transcriptional activity and Tfam function in response to denervation, mRNA content of the mtDNA-encoded COX I was measured using qPCR (n = 6 per time point). * $p < 0.05$ DEN vs. SHAM of the same time point. Values are ± SEM.

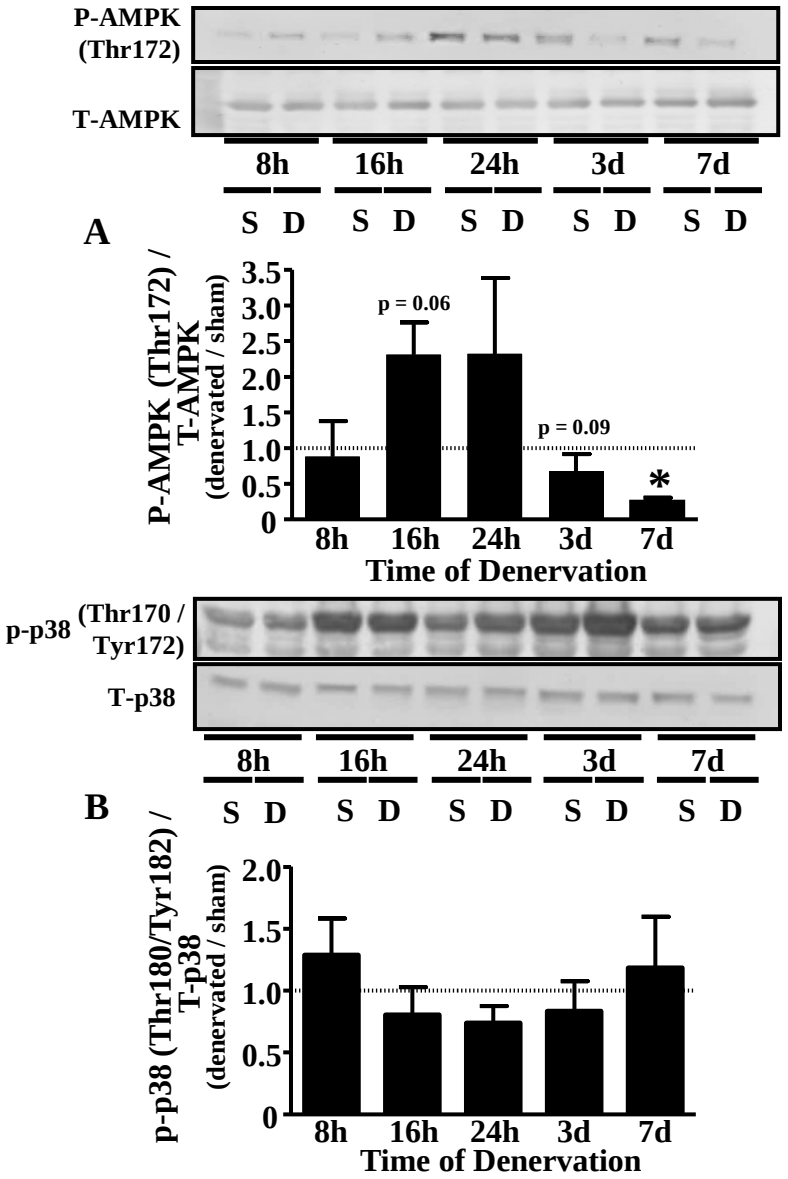

Figure 6. Effect of denervation on intracellular kinase signaling. *A.* A representative western blot and graphical representation of phosphorylated (Threonine 172) and total AMP kinase in response to different durations of denervation (n = 5-6 per time point). *B.* A representative western blot and graphical representation of phosphorylated (Threonine 180 and Tyrosine 182) and total p38 MAPK (n = 4 per time point). For both experiments, the phosphorylated form of each protein was divided by the total protein content of that same protein, as both total AMPK and total p38 were shown not to be altered in response to this duration of denervation. Values are ± SEM.

Appendix A

Raw Data and Statistics for Thesis Figures

Tibialis Anterior Mass (mg) / Body Mass (g)

		Time of Denervation														
		8 hours			16 hours			24 hours			3 days			7 days		
	Sample Set	SHAM	DEN	Fold-Change (DEN / SHAM)	SHAM	DEN	Fold-Change (DEN / SHAM)	SHAM	DEN	Fold-Change (DEN / SHAM)	SHAM	DEN	Fold-Change (DEN / SHAM)	SHAM	DEN	Fold-Change (DEN / SHAM)
	1	1.85	1.85	**1.00**	1.95	1.93	**0.99**	1.90	1.75	**0.92**	1.80	1.60	**0.89**	1.79	1.07	**0.60**
	2	1.76	1.75	**0.99**	1.65	1.59	**0.97**	1.94	1.95	**1.00**	1.94	1.73	**0.89**	1.76	1.11	**0.63**
	3	1.90	1.85	**0.97**	1.70	1.70	**1.00**	1.83	1.82	**0.99**	1.91	1.62	**0.85**	1.81	1.10	**0.61**
	4	1.91	1.61	**0.84**	1.82	1.87	**1.03**	1.76	1.75	**0.99**	2.14	1.82	**0.85**	1.79	1.15	**0.64**
	5	1.73	1.78	**1.02**	1.80	1.81	**1.00**	1.64	1.63	**0.99**	1.75	1.53	**0.87**	1.73	1.08	**0.62**
	6				1.85	1.78	**0.96**	1.88	1.87	**0.99**	1.81	1.62	**0.89**	1.77	1.13	**0.64**
	7				1.71	1.71	**1.00**				1.67	1.62	**0.97**	1.68	0.96	**0.57**
Average		**1.86**	**1.76**	**0.95**	**1.78**	**1.77**	**1.00**	**1.86**	**1.82**	**0.98**	**1.95**	**1.69**	**0.87**	**1.79**	**1.11**	**0.62**
SEM		**0.04**	**0.04**	**0.03**	**0.04**	**0.04**	**0.01**	**0.05**	**0.05**	**0.01**	**0.06**	**0.04**	**0.02**	**0.02**	**0.02**	**0.01**
Paired T-Test				**0.331**			**0.495**			**0.228**			**0.001**			**0.001**

Tibialis Anterior Wet Mass (mg)

		Time of Denervation								
		8 hours			16 hours			24 hours		
	Sample Set	SHAM	DEN	Fold-Change (DEN / SHAM)	SHAM	DEN	Fold-Change (DEN / SHAM)	SHAM	DEN	Fold-Change (DEN / SHAM)
	1	60.5	159.3	**2.63**	42.7	71.6	**1.68**	57.3	60.9	**1.06**
	2	53.4	221.6	**4.15**	72.9	80.8	**1.11**	77.8	94.5	**1.21**
	3	49.8	69.2	**1.39**	26.5	47.8	**1.80**	84.2	75.5	**0.90**

Tibialis Anterior Dry Mass (mg)

		Time of Denervation								
		8 hours			16 hours			24 hours		
	Sample Set	SHAM	DEN	Fold-Change (DEN / SHAM)	SHAM	DEN	Fold-Change (DEN / SHAM)	SHAM	DEN	Fold-Change (DEN / SHAM)
	1	15.2	41.2	**2.71**	9.9	17.5	**1.77**	13.4	14.6	**1.09**
	2	13.5	56.9	**4.21**	18.6	20.3	**1.09**	19.4	23.9	**1.23**
	3	12.5	17	**1.36**	6.4	13	**2.03**	20.6	18.6	**0.90**

Tibialis Anterior Wet Mass / Dry Mass

		Time of Denervation								
		8 hours			16 hours			24 hours		
	Sample Set	SHAM	DEN	Fold-Change (DEN / SHAM)	SHAM	DEN	Fold-Change (DEN / SHAM)	SHAM	DEN	Fold-Change (DEN / SHAM)
	1	3.98	3.87	**0.97**	4.31	4.09	**0.95**	4.28	4.17	**0.98**
	2	3.96	3.89	**0.98**	3.92	3.98	**1.02**	4.01	3.95	**0.99**
	3	3.98	4.07	**1.02**	4.14	3.68	**0.89**	4.09	4.06	**0.99**
Average		**3.97**	**3.94**	**0.99**	**4.12**	**3.92**	**0.95**	**4.12**	**4.06**	**0.98**
SEM		**0.01**	**0.06**	**0.02**	**0.11**	**0.12**	**0.04**	**0.08**	**0.06**	**0.01**
Paired T-Test				**0.672**			**0.303**			

COX Activity (20 Second Vmax)

		Time of Denervation														
		8 hours			16 hours			24 hours			3 days			7 days		
	Sample Set	SHAM	DEN	Fold-Change (DEN / SHAM)	SHAM	DEN	Fold-Change (DEN / SHAM)	SHAM	DEN	Fold-Change (DEN / SHAM)	SHAM	DEN	Fold-Change (DEN / SHAM)	SHAM	DEN	Fold-Change (DEN / SHAM)
	1	13.06	13.37	**1.024**	11.74	15.13	**1.289**	12.40	12.63	**1.019**	13.65	7.69	**0.564**	14.69	8.39	**0.571**
	2	16.98	15.20	**0.895**	16.37	14.83	**0.906**	11.55	18.21	**1.577**	13.42	12.01	**0.895**	13.96	5.23	**0.374**
	3	17.93	17.95	**1.001**	20.36	18.21	**0.894**	19.13	19.08	**0.997**	17.71	11.92	**0.673**	15.71	11.70	**0.745**
	4	11.50	10.74	**0.934**	12.53	11.00	**0.878**	13.47	12.26	**0.910**	10.78	5.72	**0.531**	7.32	7.34	**1.003**
	5	20.73	19.00	**0.916**	21.81	18.14	**0.832**	20.60	21.21	**1.029**	15.18	5.62	**0.370**	22.68	15.07	**0.665**
Average		**16.04**	**15.25**	**0.95**	**16.56**	**15.46**	**0.96**	**15.43**	**16.68**	**1.11**	**14.15**	**8.59**	**0.61**	**14.87**	**9.54**	**0.67**
SEM		**1.67**	**1.50**	**0.02**	**2.02**	**1.33**	**0.08**	**1.85**	**1.80**	**0.12**	**1.14**	**1.43**	**0.09**	**2.45**	**1.73**	**0.10**
Paired T-Test				**0.142**			**0.407**			**0.420**			**0.013**			**0.026**

EDL Mass (mg) / Body Mass (g)

		Time of Denervation								
		24 hours			3 days			7 days		
	Sample Set	SHAM	DEN	Fold-Change (DEN / SHAM)	SHAM	DEN	Fold-Change (DEN / SHAM)	SHAM	DEN	Fold-Change (DEN / SHAM)
	1	0.411	0.401	**0.977**	0.470	0.467	**0.994**	0.436	0.304	**0.698**
	2	0.576	0.522	**0.907**	0.508	0.495	**0.973**	0.410	0.313	**0.763**
	3	0.491	0.479	**0.977**	0.493	0.470	**0.952**	0.444	0.302	**0.680**
	4	0.519	0.516	**0.994**	0.495	0.477	**0.962**	0.443	0.285	**0.643**
Average		**0.499**	**0.480**	**0.964**	**0.492**	**0.477**	**0.970**	**0.433**	**0.301**	**0.696**
SEM		**0.03**	**0.03**	**0.02**	**0.01**	**0.01**	**0.01**	**0.01**	**0.01**	**0.02**
Paired T-Test				**0.192**			**0.044**			**0.002**

Distribution of fiber sizes from sham operated and denervated hind limbs

	Time of Denervation			
	SHAM (combined)	24 hours of denervation	3 days of denervation	7 days of denervation
Fiber Size Range (μm^2)	% of total fibers counted (average)			
<500	0	0.11	0	0.27
500-1000	0.42	2.90	1.61	12.26
1001-1500	4.75	17.09	11.75	28.83
1501-2000	16.25	22.86	18.74	26.49
2001-2500	15.81	19.15	15.76	15.69
2501-3000	12.67	13.72	15.04	9.43
3001-3500	11.41	11.32	12.05	5.12
3501-4000	12.00	7.38	9.30	1.34
4001-4500	9.11	3.46	7.67	0.37
4501-5000	6.87	1.38	4.54	0.14
5001-5500	5.26	0.50	1.88	0.03
5501-6000	2.99	0.13	1.09	0.03
6001-6500	1.18	0.00	0.47	0.00
6501-7000	0.71	0.00	0.00	0.00
7001-7500	0.40	0.00	0.11	0.00
7501-8000	0.11	0.00	0.00	0.00
8001-8500	0.05	0.00	0.00	0.00

All presented values for % of total fibers counted are the average values calculated from four sample sets. As the cross-sectional areas of the sham operated hind limbs from all time points were shown to be <u>not different</u>, the values for the % of total fibers counted for all of the sham operated hind limbs were combined for the purpose of display in the fiber size distribution graph.

Fiber Cross-Sectional Area (μm^2) / Animal Body Mass (g)

	Time of Denervation								
	24 hours			3 days			7 days		
Sample Set	SHAM	DEN	Fold-Change	SHAM	DEN	Fold-Change	SHAM	DEN	Fold-Change
1	9.75	6.77	**0.694**	8.98	6.10	**0.679**	9.08	3.93	**0.433**
2	11.25	8.74	**0.777**	10.12	9.33	**0.922**	10.52	4.39	**0.417**
3	9.78	8.65	**0.885**	9.75	7.80	**0.800**	10.56	5.25	**0.497**
4	9.30	7.92	**0.851**	10.53	7.75	**0.736**	9.71	6.34	**0.653**
Average	**10.02**	**8.02**	**0.80**	**9.85**	**7.75**	**0.78**	**9.97**	**4.98**	**0.50**
Paired T-test			**0.020**			**0.023**			**0.003**
One-way ANOVA (between SHAM muscles)	**0.944 (F < F-Crit)**								

Fiber Cross-Sectional Area (μm^2) / Animal Body Mass (g)

	Time of Denervation		
	24 hours	3 days	7 days
Sample Set	SHAM	SHAM	SHAM
1	9.75	8.98	9.08
2	11.25	10.12	10.52
3	9.78	9.75	10.56
4	9.30	10.53	9.71

ANOVA

Source of Variation	*SS*	*df*	*MS*	*F*	*P-value*	*F crit*
Between Groups	0.064	2	0.032	0.058	0.944	4.256
Within Groups	4.974	9	0.553			
Total	5.038	11				

As F < F crit, there is no difference in the cross-sectional areas between sham-operated hindlimbs at the measured time-points.

1.1kb proximal rat Tfam promoter activity

	Time of Denervation														
	8 hours			16 hours			24 hours			3 days			7 days		
	SHAM	DEN	Fold-Change (DEN / SHAM)	SHAM	DEN	Fold-Change (DEN / SHAM)	SHAM	DEN	Fold-Change (DEN / SHAM)	SHAM	DEN	Fold-Change (DEN / SHAM)	SHAM	DEN	Fold-Change (DEN / SHAM)
	0.310	0.163	**0.526**	8.57	5.286	**0.617**	2.573	0.738	**0.287**	1.417	1.289	**0.910**	9.405	1.035	**0.110**
	1.135	0.408	**0.359**	8.281	3.94	**0.476**	1.354	1.650	**1.219**	1.171	0.529	**0.452**	3.535	6.623	**1.874**
	1.772	0.337	**0.190**	3.877	2.263	**0.584**	0.365	0.193	**0.529**	1.369	0.295	**0.215**	1.917	5.551	**2.896**
	0.782	0.105	**0.134**	3.289	2.192	**0.666**	3.055	0.401	**0.131**	1.138	0.347	**0.305**	1.649	1.422	**0.862**
	1.681	0.258	**0.153**	4.392	1.684	**0.383**	5.712	2.580	**0.452**				0.880	0.562	**0.639**
	1.098	0.779	**0.709**	3.278	1.787	**0.545**	3.101	1.449	**0.467**				1.590	0.771	**0.485**
				0.13	0.184	**1.415**							2.339	6.025	**2.575**
Average	**1.130**	**0.342**	**0.345**	**4.545**	**2.477**	**0.670**	**2.693**	**1.168**	**0.541**	**1.274**	**0.615**	**0.470**	**3.045**	**3.141**	**1.349**
SEM	**0.22**	**0.10**	**0.10**	**1.22**	**0.68**	**0.13**	**0.69**	**0.34**	**0.20**	**0.06**	**0.19**	**0.15**	**1.81**	**1.42**	**0.41**
Paired T-Test			**0.02**			**0.01**			**0.04**			**0.04**			**0.95**

Percent of Tfam mRNA remaining at each time point following decay assay

		Time of Denervation								
		8 hours			24 hours			7 days		
Sample Set	**Gene**	**Treatment & Length of Incubation for Decay Assay**	**Band Intensity**	**% of initial**	**Treatment & Length of Incubation for Decay Assay**	**Band Intensity**	**% of initial**	**Treatment & Length of Incubation for Decay Assay**	**Band Intensity**	**% of initial**
1	**Tfam**	0	449606	**100.00**	0	449606	**100.00**	0	449606	**100.00**
		SHAM 15	330460	**73.50**	SHAM 15	432442	**96.18**	SHAM 15	414374	**92.16**
		SHAM 45	86754	**19.30**	SHAM 45	93782	**20.86**	SHAM 45	327291	**72.80**
		DEN 15	378632	**84.21**	DEN 15	426480	**94.86**	DEN 15	284282	**63.23**
		DEN 45	230217	**51.20**	DEN 45	347032	**77.19**	DEN 45	264045	**58.73**
2	**Tfam**	0	277923	**100.00**	0	277923	**100.00**	0	277923	**100.00**
		SHAM 15	221542	**79.71**	SHAM 15	227863	**81.99**	SHAM 15	224563	**80.80**
		SHAM 45	170358	**61.30**	SHAM 45	221850	**79.82**	SHAM 45	181062	**65.15**
		DEN 15	265952	**95.69**	DEN 15	244139	**87.84**	DEN 15	231546	**83.31**
		DEN 45	190159	**68.42**	DEN 45	236230	**85.00**	DEN 45	155088	**55.80**
3	**Tfam**	0	16051161	**100.00**	0	16051161	**100.00**	0	16051161	**100.00**
		SHAM 15	11341597	**70.66**	SHAM 15	12522490	**78.02**	SHAM 15	13686862	**85.27**
		SHAM 45	4482983	**27.93**	SHAM 45	5000622	**31.15**	SHAM 45	11814331	**73.60**
		DEN 15	14200173	**88.47**	DEN 15	14811241	**92.28**	DEN 15	12808387	**79.80**
		DEN 45	8272214	**51.54**	DEN 45	14162324	**88.23**	DEN 45	9031082	**56.26**
4	**Tfam**	0	15723066	**100.00**	0	15723066	**100.00**	0	15723066	**100.00**
		SHAM 15	12569118	**79.94**	SHAM 15	15402924	**97.96**	SHAM 15	14214074	**90.40**
		SHAM 45	9839869	**62.58**	SHAM 45	13714359	**87.22**	SHAM 45	11655313	**74.13**
		DEN 15	15483792	**98.48**	DEN 15	17418422	**110.78**	DEN 15	14007916	**89.09**
		DEN 45	12008884	**76.38**	DEN 45	12592899	**80.09**	DEN 45	8463635	**53.83**
5	**Tfam**	0	263537	**100.00**	0	263537	**100.00**	0	263537	**100.00**
		SHAM 15	138679	**52.62**	SHAM 15	251254	**95.34**	SHAM 15	184881	**70.15**
		SHAM 45	42020	**15.94**	SHAM 45	46066	**17.48**	SHAM 45	144724	**54.92**
		DEN 15	189242	**71.81**	DEN 15	195022	**74.00**	DEN 15	146040	**55.42**
		DEN 45	96133	**36.48**	DEN 45	166695	**63.25**	DEN 45	143744	**54.54**

Values of Best Fit (k) for Tfam SHAM and DEN muscle

		Time of Denervation														
		8 hours					24 hours					7 days				
	Sample Set	SHAM Values of Best Fit (k)	Half-Life (minutes)	DEN Values of Best Fit (k)	Half-Life (minutes)	Fold Change in Half-Life (DEN/SHAM)	SHAM Values of Best Fit (k)	Half-Life (minutes)	DEN Values of Best Fit (k)	Half-Life (minutes)	Fold Change in Half-Life (DEN/SHAM)	SHAM Values of Best Fit (k)	Half-Life (minutes)	DEN Values of Best Fit (k)	Half-Life (minutes)	Fold Change in Half-Life (DEN/SHAM)
	1	0.0306	**22.65**	0.0146	**47.48**	**2.10**	0.0250	**27.74**	0.0058	**119.55**	**4.31**	0.0071	**97.56**	0.0156	**44.40**	**0.46**
	2	0.0119	**58.30**	0.0084	**82.61**	**1.42**	0.0063	**110.06**	0.0045	**155.48**	**1.41**	0.0106	**65.64**	0.0131	**52.87**	**0.81**
	3	0.0269	**25.75**	0.0142	**48.78**	**1.89**	0.0238	**29.15**	0.0033	**207.96**	**7.13**	0.0076	**91.06**	0.0135	**51.34**	**0.56**
	4	0.0115	**60.48**	0.0061	**114.14**	**1.89**	0.0264	**26.22**	0.0121	**57.28**	**2.19**	0.0069	**99.91**	0.0134	**51.88**	**0.52**
	5	0.0424	**16.35**	0.0227	**30.60**	**1.87**						0.0156	**44.32**	0.0190	**36.46**	**0.82**
Average			**36.71**		**64.72**	**1.83**		**48.29**		**135.07**	**3.76**		**79.70**		**47.39**	**0.63**
SEM			**9.4**		**15.0**	**0.1**		**20.6**		**31.7**	**1.3**		**10.7**		**3.1**	**0.1**
Paired T-Test of Half-Lives						**0.014**					**0.08**					**0.025**

Half-lives were calculated using the formula **$t_{1/2}$=(ln(0.5))/-(rate of decay)**, where the "rate of decay" is the value of best fit (*k*). The value of best fit was obtained by plotting a graph of the % of initial band intensity for each condition (sham-operated or denervated) and each length of denervation (8 hours, 24 hours or 7days), and a line of best fit was fit to these points.

ANOVA

Source of Variation	*SS*	*df*	*MS*	*F*	*P-value*	*F crit*
Interaction	15840	2	7922	6.741	0.005	4.300
Time	7645	2	3823	3.253	0.058	
Treatment	5235	1	5235	4.454	0.046	
Residual	25850	22	1175			

As F > F crit for both interaction and treatment sources of variation, this denotes an interaction effect of the between treatment and time. This also indicates a main effect of the treatment at all time points.

qPCR - Tfam

		Time of Denervation													
		8 hours			16 hours			24 hours			3 days			7 days		
	Sample Set	SHAM	DEN	Fold Change (DEN / SHAM)	SHAM	DEN	Fold Change (DEN / SHAM)	SHAM	DEN	Fold Change (DEN / SHAM)	SHAM	DEN	Fold Change (DEN / SHAM)	SHAM	DEN	Fold Change (DEN / SHAM)
	1	88.8	91.7	1.03	78.7	60.3	0.77	69.8	73.4	1.05	81.9	76.2	0.93	47.5	86.4	1.82
	2	83.2	63.6	0.76	67.5	59.2	0.88	49.0	63.8	1.30	67.2	81.3	1.21	33.4	64.2	1.92
	3	48.8	41.6	0.85	41.1	40.5	0.99	31.2	52.1	1.67	60.1	66.9	1.11	32.0	71.2	2.22
	4	51.0	40.8	0.80	30.0	39.8	1.32	48.6	46.7	0.96	53.8	46.6	0.87	25.0	60.1	2.40
	5	49.1	36.7	0.75	38.1	50.0	1.31	55.1	50.4	0.91	54.3	79.5	1.46	35.2	74.4	2.11
	6	51.0	49.5	0.97	60.6	64.3	1.06	52.2	59.8	1.15	59.8	68.3	1.14	48.5	71.4	1.47
Average		61.98	53.98	0.86	52.68	52.35	1.05	50.99	57.70	1.17	62.86	69.81	1.12	36.93	71.28	1.99
SEM		7.6	8.5	0.0	7.8	4.3	0.1	5.1	4.1	0.1	4.3	5.2	0.1	3.8	3.7	0.1
Paired T-Test				0.058			0.947			0.154			0.222			0.001

qPCR - COX I mRNA

		Time of Denervation													
		8 hours			16 hours			24 hours			3 days			7 days		
	Sample Set	SHAM	DEN	Fold Change (DEN / SHAM)	SHAM	DEN	Fold Change (DEN / SHAM)	SHAM	DEN	Fold Change (DEN / SHAM)	SHAM	DEN	Fold Change (DEN / SHAM)	SHAM	DEN	Fold Change (DEN / SHAM)
	1	853.6	1068.0	1.25	755.3	602.0	0.80	553.2	610.2	1.10	1629.7	823.7	0.51	688.0	452.3	0.66
	2	977.1	763.5	0.78	491.9	438.0	0.89	990.1	1204.6	1.22	1070.7	796.6	0.74	864.1	799.3	0.93
	3	300.7	170.2	0.57	237.6	173.3	0.73	141.9	309.6	2.18	331.0	171.0	0.52	787.3	592.2	0.75
	4	424.1	280.3	0.66	597.0	658.2	1.10	832.8	519.9	0.62	1028.2	753.6	0.73	722.6	568.5	0.79
	5	351.2	291.1	0.83	346.8	334.8	0.97	476.0	395.5	0.83	1199.4	718.6	0.60	907.7	582.5	0.64
	6	325.0	351.9	1.08	1143.0	846.3	0.74	394.9	358.8	0.91	859.0	633.1	0.74	754.1	558.5	0.74
Average		538.61	487.49	0.86	595.27	508.76	0.87	564.81	566.43	1.14	1019.65	649.44	0.64	787.31	592.23	0.75
SEM		121.4	143.0	0.1	132.4	98.8	0.1	125.0	135.4		173.9	99.5	0.0	34.4	46.3	0.0
Paired T-Test				0.452			0.150			0.984			0.013			0.003

qPCR - S12

		Time of Denervation														
		8 hours			16 hours			24 hours			3 days			7 days		
	Sample Set	SHAM	DEN	Fold Change (DEN / SHAM)	SHAM	DEN	Fold Change (DEN / SHAM)	SHAM	DEN	Fold Change (DEN / SHAM)	SHAM	DEN	Fold Change (DEN / SHAM)	SHAM	DEN	Fold Change (DEN / SHAM)
	1	23.0	22.8	**0.99**	22.8	23.5	**1.03**	22.6	23.0	**1.01**	22.7	22.1	**0.97**	22.7	21.8	**0.96**
	2	19.0	23.4	**1.23**	21.9	23.3	**1.06**	24.8	23.0	**0.93**	23.5	21.9	**0.93**	22.6	21.1	**0.93**
	3	23.8	23.7	**1.00**	23.8	23.8	**1.00**	24.6	23.6	**0.96**	23.0	22.9	**1.00**	23.8	22.6	**0.95**
	4	22.8	25.7	**1.13**	24.6	23.6	**0.96**	23.7	24.3	**1.02**	24.5	24.2	**0.99**	24.6	22.9	**0.93**
	5	23.3	23.5	**1.01**	23.4	23.3	**1.00**	23.7	23.6	**0.99**	23.8	22.0	**0.92**	23.4	22.4	**0.96**
	6	21.9	22.7	**1.04**	22.1	22.5	**1.02**	22.9	22.9	**1.00**	22.9	19.9	**0.87**	22.8	21.8	**0.96**
Average		**22.28**	**23.63**	**1.07**	**23.10**	**23.33**	**1.01**	**23.73**	**23.37**	**0.99**	**23.40**	**22.14**	**0.95**	**23.31**	**22.10**	**0.95**
SEM		**0.71**	**0.45**	**0.04**	**0.41**	**0.18**	**0.01**	**0.35**	**0.22**	**0.01**	**0.29**	**0.58**	**0.02**	**0.32**	**0.26**	**0.01**
Paired T-Test				**0.140**			**0.502**			**0.361**			**0.039**			**0.0003**

qPCR - B-actin mRNA

		Time of Denervation														
		8 hours			16 hours			24 hours			3 days			7 days		
	Sample Set	SHAM	DEN	Fold Change (DEN / SHAM)	SHAM	DEN	Fold Change (DEN / SHAM)	SHAM	DEN	Fold Change (DEN / SHAM)	SHAM	DEN	Fold Change (DEN / SHAM)	SHAM	DEN	Fold Change (DEN / SHAM)
	1	23.0	22.5	**0.98**	22.3	22.2	**1.00**	22.4	22.7	**1.02**	22.5	23.2	**1.03**	21.5	23.0	**1.07**
	2	18.2	22.4	**1.24**	21.3	22.3	**1.05**	23.0	22.2	**0.97**	22.4	22.6	**1.01**	20.4	22.0	**1.08**
	3	22.6	22.6	**1.00**	22.5	22.4	**1.00**	22.7	22.6	**1.00**	21.9	23.4	**1.07**	22.0	23.6	**1.07**
	4	22.8	25.3	**1.11**	23.5	23.0	**0.98**	23.1	23.6	**1.02**	23.2	24.7	**1.07**	22.5	23.3	**1.03**
	5	22.8	22.5	**0.99**	22.6	22.6	**1.00**	22.9	22.8	**0.99**	22.5	22.4	**1.00**	21.9	22.9	**1.05**
	6	22.0	22.3	**1.02**	22.0	22.7	**1.03**	22.1	22.3	**1.01**	22.0	20.4	**0.93**	21.1	22.2	**1.05**
Average		**21.86**	**22.93**	**1.05**	**22.37**	**22.55**	**1.01**	**22.68**	**22.70**	**1.00**	**22.42**	**22.77**	**1.02**	**21.56**	**22.83**	**1.06**
SEM		**0.75**	**0.47**	**0.04**	**0.31**	**0.11**	**0.01**	**0.16**	**0.21**		**0.19**	**0.59**	**0.02**	**0.31**	**0.25**	**0.01**
Paired T-Test				**0.228**			**0.499**			**0.924**			**0.496**			**0.0004**

qPCR - average of S12 + B-actin

		Time of Denervation														
		8 hours			16 hours			24 hours			3 days			7 days		
	Sample Set	SHAM	DEN	Fold Change (DEN / SHAM)	SHAM	DEN	Fold Change (DEN / SHAM)	SHAM	DEN	Fold Change (DEN / SHAM)	SHAM	DEN	Fold Change (DEN / SHAM)	SHAM	DEN	Fold Change (DEN / SHAM)
	1	23.0	22.7	**0.99**	22.6	22.9	**1.01**	22.5	22.8	**1.01**	22.6	22.6	**1.00**	22.1	22.4	**1.02**
	2	18.6	22.9	**1.23**	21.6	22.8	**1.06**	23.9	22.6	**0.95**	23.0	22.2	**0.97**	21.5	21.6	**1.00**
	3	23.2	23.2	**1.00**	23.1	23.1	**1.00**	23.6	23.1	**0.98**	22.4	23.1	**1.03**	22.9	23.1	**1.01**
	4	22.8	25.5	**1.12**	24.1	23.3	**0.97**	23.4	23.9	**1.02**	23.9	24.5	**1.02**	23.6	23.1	**0.98**
	5	23.0	23.0	**1.00**	23.0	23.0	**1.00**	23.3	23.2	**0.99**	23.1	22.2	**0.96**	22.7	22.7	**1.00**
	6	21.9	22.5	**1.03**	22.1	22.6	**1.02**	22.5	22.6	**1.00**	22.4	20.1	**0.90**	21.9	22.0	**1.00**
Average		**22.07**	**23.28**	**1.06**	**22.74**	**22.94**	**1.01**	**23.21**	**23.03**	**0.99**	**22.91**	**22.46**	**0.98**	**22.43**	**22.46**	**1.00**
SEM		**0.73**	**0.45**	**0.04**	**0.35**	**0.09**	**0.01**	**0.24**	**0.21**	**0.01**	**0.23**	**0.58**	**0.02**	**0.31**	**0.24**	**0.01**
Paired T-Test				**0.178**			**0.486**			**0.551**			**0.369**			**0.808**

HuR

		Time of Denervation														
		8 hours			16 hours			24 hours			3 days			7 days		
	Sample Set	SHAM	DEN	Fold-Change (DEN / SHAM)	SHAM	DEN	Fold-Change (DEN / SHAM)	SHAM	DEN	Fold-Change (DEN / SHAM)	SHAM	DEN	Fold-Change (DEN / SHAM)	SHAM	DEN	Fold-Change (DEN / SHAM)
	1	402246	476883	**1.19**	348487	660833	**1.90**	687771	765739	**1.11**	765345	830543	**1.09**	697598	817584	**1.17**
	2	512004	611997	**1.20**	728884	721814	**0.99**	698749	712471	**1.02**	631812	973757	**1.54**	695496	940573	**1.35**
	3	421109	386993	**0.92**	356603	400923	**1.12**	521149	467611	**0.90**	436898	533537	**1.22**	617320	850745	**1.38**
	4	678047	567274	**0.84**	502709	545308	**1.08**	638814	741250	**1.16**	683947	826169	**1.21**	993878	1366484	**1.37**
Average		**503352**	**510786**	**1.01**	**484170**	**582219**	**1.20**	**636621**	**671768**	**1.06**	**629501**	**791001**	**1.26**	**751073**	**993847**	**1.32**
SEM		**62968**	**49924**	**0.09**	**88934**	**70650**	**0.21**	**40635**	**68917**	**0.06**	**69833**	**92416**	**0.10**	**83063**	**126900**	**0.05**

Aciculin

		Time of Denervation														
		8 hours			16 hours			24 hours			3 days			7 days		
	Sample Set	SHAM	DEN	Fold-Change (DEN / SHAM)	SHAM	DEN	Fold-Change (DEN / SHAM)	SHAM	DEN	Fold-Change (DEN / SHAM)	SHAM	DEN	Fold-Change (DEN / SHAM)	SHAM	DEN	Fold-Change (DEN / SHAM)
	1	487692	559028	**1.15**	498205	466701	**0.94**	599759	577097	**0.96**	569912	579224	**1.02**	651140	630608	**0.97**
	2	618885	537030	**0.87**	456741	490939	**1.07**	238580	650468	**2.73**	634437	851658	**1.34**	784276	904263	**1.15**
	3	456737	532417	**1.17**	469852	521493	**1.11**	529828	484565	**0.91**	517856	559830	**1.08**	647237	823342	**1.27**
	4	303831	489258	**1.61**	408416	523728	**1.28**	425184	488062	**1.15**	513087	517663	**1.01**	602763	620591	**1.03**
Average		**466786**	**529433**	**1.13**	**458303**	**500715**	**1.09**	**448338**	**550048**	**1.23**	**558823**	**627094**	**1.12**	**671354**	**744701**	**1.11**
SEM		**64696**	**14596**	**0.15**	**18745**	**13583**	**0.07**	**78583**	**39735**	**0.43**	**28300**	**75950**	**0.08**	**39207**	**70749**	**0.07**

HuR corrected for aciculin

		Time of Denervation														
		8 hours			16 hours			24 hours			3 days			7 days		
	Sample Set	SHAM	DEN	Fold-Change (DEN / SHAM)	SHAM	DEN	Fold-Change (DEN / SHAM)	SHAM	DEN		SHAM	DEN	Fold-Change (DEN / SHAM)	SHAM	DEN	Fold-Change (DEN / SHAM)
	1	0.82	0.85	**1.03**	0.70	1.42	**2.02**	1.15	1.33	**1.16**	1.34	1.43	**1.07**	1.07	1.30	**1.21**
	2	0.83	1.14	**1.38**	1.60	1.47	**0.92**	2.93	1.10	**0.37**	1.00	1.14	**1.15**	0.89	1.04	**1.17**
	3	0.92	0.73	**0.79**	0.76	0.77	**1.01**	0.98	0.97	**0.98**	0.84	0.95	**1.13**	0.95	1.03	**1.08**
	4	2.23	1.16	**0.52**	1.23	1.04	**0.85**	1.50	1.52	**1.01**	1.33	1.60	**1.20**	1.65	2.20	**1.34**
Average		**1.20**	**0.97**	**0.81**	**1.07**	**1.17**	**1.10**	**1.64**	**1.23**	**0.75**	**1.13**	**1.28**	**1.14**	**1.14**	**1.39**	**1.22**
SEM		**0.34**	**0.11**	**0.18**	**0.21**	**0.17**	**0.28**	**0.44**	**0.12**	**0.17**	**0.12**	**0.14**	**0.03**	**0.17**	**0.28**	**0.05**
Paired T-Test				**0.495**			**0.656**			**0.448**			**0.029**			**0.094**

CUGBP1

		Time of Denervation														
		8 hours			16 hours			24 hours			3 days			7 days		
	Sample Set	SHAM	DEN	Fold-Change (DEN / SHAM)	SHAM	DEN	Fold-Change (DEN / SHAM)	SHAM	DEN	Fold-Change (DEN / SHAM)	SHAM	DEN	Fold-Change (DEN / SHAM)	SHAM	DEN	Fold-Change (DEN / SHAM)
	1	350318	367902	**1.05**	386637	346324	**0.90**	323056	377199	**1.17**	266456	411731	**1.55**	224835	774268	**3.44**
	2	290398	337212	**1.16**	283265	310097	**1.09**	287425	371358	**1.29**	373714	470423	**1.26**	489869	925766	**1.89**
	3	187958	239995	**1.28**	214132	178192	**0.83**	243457	280204	**1.15**	280015	368529	**1.32**	222376	540653	**2.43**
	4	223594	314053	**1.40**	335556	313986	**0.94**	306162	313483	**1.02**	306728	631009	**2.06**	293010	856383	**2.92**
Average		**263067**	**314791**	**1.20**	**304897**	**287150**	**0.94**	**290025**	**335561**	**1.16**	**306728**	**470423**	**1.53**	**307523**	**774268**	**2.52**
SEM		**36008**	**27262**	**0.08**	**36887**	**37216**	**0.06**	**17144**	**23393**	**0.05**	**23844**	**57456**	**0.18**	**62947**	**83801**	**0.33**

Ponceau

		Time of Denervation														
		8 hours			16 hours			24 hours			3 days			7 days		
	Sample Set	SHAM	DEN	Fold-Change (DEN / SHAM)	SHAM	DEN	Fold-Change (DEN / SHAM)	SHAM	DEN	Fold-Change (DEN / SHAM)	SHAM	DEN	Fold-Change (DEN / SHAM)	SHAM	DEN	Fold-Change (DEN / SHAM)
	1	280947	243974	**0.87**	187207	232219	**1.24**	201932	204996	**1.02**	285857	205592	**0.72**	203480	117121	**0.58**
	2	303407	297516	**0.98**	215298	284518	**1.32**	284652	202831	**0.71**	140089	145499	**1.04**	145134	75943	**0.52**
	3	208874	254820	**1.22**	148979	140825	**0.95**	143384	114682	**0.80**	121683	74621	**0.61**	86961	39060	**0.45**
	4	272797	246138	**0.90**	208431	191410	**0.92**	221863	164030	**0.74**	185841	143945	**0.77**	177301	186381	**1.05**
Average		**266506**	**260612**	**0.98**	**189979**	**212243**	**1.12**	**212957**	**171635**	**0.81**	**183367**	**142414**	**0.78**	**153219**	**104626**	**0.68**
SEM		**20272**	**12523**	**0.08**	**14917**	**30492**	**0.10**	**29128**	**21189**	**0.07**	**36729**	**26769**	**0.09**	**25103**	**31572**	**0.14**

CUGBP1 corrected for ponceau

		Time of Denervation														
		8 hours			16 hours			24 hours			3 days			7 days		
	Sample Set	SHAM	DEN	Fold-Change (DEN / SHAM)	SHAM	DEN	Fold-Change (DEN / SHAM)	SHAM	DEN		SHAM	DEN	Fold-Change (DEN / SHAM)	SHAM	DEN	Fold-Change (DEN / SHAM)
	1	1.25	1.51	**1.21**	2.07	1.49	**0.72**	1.60	1.84	**1.15**	0.93	2.00	**2.15**	1.10	6.61	**5.98**
	2	0.96	1.13	**1.18**	1.32	1.09	**0.83**	1.01	1.83	**1.81**	2.67	3.23	**1.21**	3.38	12.19	**3.61**
	3	0.90	0.94	**1.05**	1.44	1.27	**0.88**	1.70	2.44	**1.44**	2.30	4.94	**2.15**	2.56	13.84	**5.41**
	4	0.82	1.28	**1.56**	1.61	1.64	**1.02**	1.38	1.91	**1.38**	1.65	4.38	**2.66**	1.65	4.59	**2.78**
Average		**0.98**	**1.21**	**1.24**	**1.61**	**1.37**	**0.85**	**1.42**	**2.01**	**1.41**	**1.89**	**3.64**	**1.93**	**2.17**	**9.31**	**4.29**
SEM		**0.09**	**0.12**	**0.11**	**0.16**	**0.12**	**0.06**	**0.15**	**0.15**	**0.14**	**0.38**	**0.65**	**0.30**	**0.50**	**2.21**	**0.75**
Paired T-Test				**0.074**			**0.158**			**0.021**			**0.050**			**0.030**

KSRP

		Time of Denervation														
		8 hours			16 hours			24 hours			3 days			7 days		
	Sample Set	SHAM	DEN	Fold-Change (DEN / SHAM)	SHAM	DEN	Fold-Change (DEN / SHAM)	SHAM	DEN	Fold-Change (DEN / SHAM)	SHAM	DEN	Fold-Change (DEN / SHAM)	SHAM	DEN	Fold-Change (DEN / SHAM)
	1	60705	39895	**0.66**	43822	127342	**2.91**	106899	88290	**0.83**	107202	103896	**0.97**	169020	254854	**1.51**
	2	48211	77060	**1.60**	106081	150116	**1.42**	81977	179587	**2.19**	119964	275811	**2.30**	175407	288129	**1.64**
	3	163591	187904	**1.15**	266399	231155	**0.87**	236399	148808	**0.63**	175729	231667	**1.32**	159854	238250	**1.49**
	4	115188	63547	**0.55**	78444	110568	**1.41**	148533	208567	**1.40**	125298	233319	**1.86**	116866	489581	**4.19**
Average		**96924**	**92101**	**0.95**	**123686**	**154795**	**1.25**	**143452**	**156313**	**1.09**	**132048**	**211173**	**1.60**	**155287**	**317704**	**2.05**
SEM		**26556**	**32845**	**0.24**	**49246**	**26712**	**0.44**	**33887**	**25748**	**0.35**	**15047**	**37190**	**0.29**	**13199**	**58223**	**0.66**

Ponceau

		Time of Denervation														
		8 hours			16 hours			24 hours			3 days			7 days		
	Sample Set	SHAM	DEN	Fold-Change (DEN / SHAM)	SHAM	DEN	Fold-Change (DEN / SHAM)	SHAM	DEN	Fold-Change (DEN / SHAM)	SHAM	DEN	Fold-Change (DEN / SHAM)	SHAM	DEN	Fold-Change (DEN / SHAM)
	1	157212	141917	**0.90**	132676	148317	**1.12**	142483	163179	**1.15**	197506	138207	**0.70**	155913	82703	**0.53**
	2	172309	170320	**0.99**	162729	170103	**1.05**	184334	187664	**1.02**	152793	157889	**1.03**	112779	102224	**0.91**
	3	208874	254820	**1.22**	148979	140825	**0.95**	143384	114682	**0.80**	121683	74621	**0.61**	86961	39060	**0.45**
	4	272797	246138	**0.90**	208431	191410	**0.92**	221863	164030	**0.74**	185841	143945	**0.77**	177301	186381	**1.05**
Average		**202798**	**203299**	**1.00**	**163204**	**162664**	**1.00**	**173016**	**157389**	**0.91**	**164456**	**128665**	**0.78**	**133239**	**102592**	**0.77**
SEM		**25730**	**27906**	**0.07**	**16279**	**11418**	**0.05**	**18983**	**15325**	**0.09**	**17115**	**18483**	**0.09**	**20445**	**30893**	**0.15**

KSRP corrected for ponceau

		Time of Denervation														
		8 hours			16 hours			24 hours			3 days			7 days		
	Sample Set	SHAM	DEN	Fold-Change (DEN / SHAM)	SHAM	DEN	Fold-Change (DEN / SHAM)	SHAM	DEN		SHAM	DEN	Fold-Change (DEN / SHAM)	SHAM	DEN	Fold-Change (DEN / SHAM)
	1	0.386	0.281	**0.73**	0.330	0.859	**2.60**	0.750	0.541	**0.72**	0.543	0.752	**1.38**	1.084	3.082	**2.84**
	2	0.280	0.452	**1.62**	0.652	0.883	**1.35**	0.445	0.957	**2.15**	0.785	1.747	**2.22**	1.555	2.819	**1.81**
	3	0.783	0.737	**0.94**	1.788	1.641	**0.92**	1.649	1.298	**0.79**	1.444	3.105	**2.15**	1.838	6.100	**3.32**
	4	0.422	0.258	**0.61**	0.376	0.578	**1.53**	0.669	1.272	**1.90**	0.674	1.621	**2.40**	0.659	2.627	**3.99**
Average		**0.47**	**0.43**	**0.92**	**0.79**	**0.99**	**1.26**	**0.88**	**1.02**	**1.16**	**0.86**	**1.81**	**2.10**	**1.28**	**3.66**	**2.85**
SEM		**0.11**	**0.11**	**0.22**	**0.34**	**0.23**	**0.36**	**0.26**	**0.18**	**0.37**	**0.20**	**0.49**	**0.23**	**0.26**	**0.82**	**0.46**
Paired T-Test				**0.662**			**0.237**			**0.610**			**0.050**			**0.036**

Tfam (subsarcolemmal mitochondria)

		Time of Denervation					
		24 hr		3 days		7 days	
	Sample Set	SHAM	DEN	SHAM	DEN	SHAM	DEN
	1	389728	449855	254765	119012	427172	320633
	2	466357	721282	278644	94211	768982	538805
	3	222791	146403	138146	10759	533397	23584
	4	961264	995391	818749	472594	498814	56361
Average		**510035**	**578233**	**372576**	**174144**	**557091**	**234846**
SEM		**158771**	**181989**	**151858**	**102142**	**74013**	**121188**

Porin

		Time of Denervation					
		24 hr		3 days		7 days	
	Sample Set	SHAM	DEN	SHAM	DEN	SHAM	DEN
	1	1096883	1096883	417691	417691	505767	365841
	2	1271382	1271382	1119369	1119369	977419	977419
	3	1562228	1562228	1255156	1219237	1475704	989613
	4	1638261	1638261	1424313	1424313	1365097	1365097
Average		**1392188**	**1392188**	**1054132**	**1045152**	**1080997**	**924492**
SEM		**126249**	**126249**	**221125**	**218572**	**219493**	**206814**

Tfam corrected for Porin

		Time of Denervation								
		24 hr			3 days			7 days		
	Sample Set	SHAM	DEN	Fold-Change (DEN / SHAM)	SHAM	DEN	Fold-Change (DEN / SHAM)	SHAM	DEN	
	1	35.53	41.01	**1.15**	30.50	14.25	**0.47**			
	2	36.68	56.73	**1.55**	24.89	8.42	**0.34**	78.67	55.13	**0.70**
	3	14.26	9.37	**0.66**	11.01	0.88	**0.08**	36.15	2.38	**0.07**
	4	58.68	60.76	**1.04**	57.48	33.18	**0.58**	36.54	4.13	**0.11**
Average		**36.29**	**41.97**	**1.10**	**30.97**	**14.18**	**0.37**	**50.45**	**20.55**	**0.29**
SEM		**9.07**	**11.67**	**0.18**	**9.74**	**6.90**	**0.11**	**14.11**	**17.30**	**0.20**
Paired T-Test				**0.359**			**0.010**			**0.011**

Phophorylated AMPK (Thr172)

		Time of Denervation													
		8 hours			16 hours			24 hours			3 days			7 days		
	Sample Set	SHAM	DEN	Fold-Change (DEN / SHAM)	SHAM	DEN	Fold-Change (DEN / SHAM)	SHAM	DEN	Fold-Change (DEN / SHAM)	SHAM	DEN	Fold-Change (DEN / SHAM)	SHAM	DEN	Fold-Change (DEN / SHAM)
	1	164907	56019	**0.34**	59657	122998	**2.06**	424	33148	**78.18**	171017	128123	**0.75**	139001	46595	**0.34**
	2	16410	22827	**1.39**	17261	43098	**2.50**	47606	2657	**0.06**	18360	2386	**0.13**	348	32571	**93.59**
	3	18892	59464	**3.15**	11846	90811	**7.67**	335158	276349	**0.82**	225114	41432	**0.18**	167974	39807	**0.24**
	4	21899	237863	**10.86**	187408	7530	**0.04**	261529	68038	**0.26**	133810	2676	**0.02**	340737	203424	**0.60**
	5	405675	28492	**0.07**	23294	76341	**3.28**	16166	75596	**4.68**	131256	32040	**0.24**	26555	11642	**0.44**
	6	65102	9107	**0.14**	14140	12064	**0.85**	5980	36979	**6.18**	27726	50496	**1.82**	61644	24189	**0.39**
	7	48134	991	**0.02**	21297	34751	**1.63**	91825	27593	**0.30**	65926	67586	**1.03**	55216	91470	**1.66**
Average		**105860**	**59252**	**2.28**	**47843**	**55370**	**2.58**	**108384**	**74337**	**12.93**	**110458**	**46391**	**0.60**	**113068**	**64242**	**13.89**
SEM		**53671**	**30897**	**1.49**	**24050**	**16190**	**0.94**	**51059**	**34937**	**10.91**	**28909**	**16348**	**0.25**	**44105**	**25069**	**13.28**

Total AMPK

		Time of Denervation													
		8 hours			16 hours			24 hours			3 days			7 days		
	Sample Set	SHAM	DEN	Fold-Change (DEN / SHAM)	SHAM	DEN	Fold-Change (DEN / SHAM)	SHAM	DEN	Fold-Change (DEN / SHAM)	SHAM	DEN	Fold-Change (DEN / SHAM)	SHAM	DEN	Fold-Change (DEN / SHAM)
	1	165804	192543	**1.16**	598320	705848	**1.18**	518162	481967	**0.93**	511243	488141	**0.95**	433720	591925	**1.36**
	2	244254	180520	**0.74**	291469	477921	**1.64**	683779	673734	**0.99**	683142	561613	**0.82**	463990	547389	**1.18**
	3	182276	198066	**1.09**	108797	196581	**1.81**	155607	88925	**0.57**	160566	186199	**1.16**	259308	392586	**1.51**
	4	243532	209090	**0.86**	263105	206784	**0.79**	230400	309572	**1.34**	225662	148149	**0.66**	68675	171611	**2.50**
	5	350011	308481	**0.88**	322220	320068	**0.99**	355155	340953	**0.96**	266101	205116	**0.77**	302722	315678	**1.04**
	6	476656	584473	**1.23**	383058	576412	**1.50**	503018	637411	**1.27**	591334	605022	**1.02**	444634	701891	**1.58**
	7	23343	24305	**1.04**	27751	31284	**1.13**	36427	54758	**1.50**	30873	39684	**1.29**	49246	66576	**1.35**
Average		**240839**	**242497**	**1.00**	**284960**	**359271**	**1.29**	**354650**	**369617**	**1.04**	**352703**	**319132**	**0.95**	**288899**	**398237**	**1.50**
SEM		**54316**	**65162**	**0.07**	**70190**	**89997**	**0.14**	**86382**	**92476**	**0.12**	**91989**	**85508**	**0.08**	**65987**	**87311**	**0.18**

p-AMPK (Thr172) / T-AMPK

		Time of Denervation													
		8 hours			16 hours			24 hours			3 days			7 days		
	Sample Set	SHAM	DEN	Fold-Change (DEN / SHAM)	SHAM	DEN	Fold-Change (DEN / SHAM)	SHAM	DEN	Fold-Change (DEN / SHAM)	SHAM	DEN	Fold-Change (DEN / SHAM)	SHAM	DEN	Fold-Change (DEN / SHAM)
	1	0.99	0.29	**0.29**	1.00	1.74	**1.75**				0.33	0.26	**0.78**	0.32	0.08	**0.25**
	2	0.67	1.26	**1.88**	0.59	0.90	**1.52**				0.27	0.04	**0.16**			
	3	0.10	0.30	**2.90**	0.11	0.46	**4.24**	2.15	3.11	**1.44**	1.40	0.22	**0.16**	0.65	0.10	**0.16**
	4							1.14	0.22	**0.19**				0.50	0.12	**0.24**
	5	1.16	0.09	**0.08**	0.72	2.39	**3.30**	0.46	2.22	**4.87**	0.49	0.16	**0.32**	0.88	0.37	**0.42**
	6	1.37	0.16	**0.11**				0.12	0.58	**4.88**	0.05	0.08	**1.78**	1.39	0.34	**0.25**
	7	2.06	0.04	**0.02**	0.77	1.11	**1.45**	2.52	0.50	**0.20**	2.14	1.70	**0.80**			
Average		**1.06**	**0.36**	**0.88**	**0.64**	**1.32**	**2.45**	**1.28**	**1.33**	**2.32**	**0.78**	**0.41**	**0.67**	**0.75**	**0.20**	**0.26**
SEM		**0.27**	**0.19**	**0.50**	**0.15**	**0.34**	**0.56**	**0.47**	**0.57**	**1.07**	**0.33**	**0.26**	**0.25**	**0.18**	**0.06**	**0.04**
Paired T-Test				**0.133**			**0.057**			**0.946**			**0.091**			**0.016**

Phosphorylated p38 (Thr180 / Tyr182)

		Time of Denervation													
		8 hours			16 hours			24 hours			3 days			7 days		
	Sample Set	SHAM	DEN	Fold-Change (DEN / SHAM)	SHAM	DEN	Fold-Change (DEN / SHAM)	SHAM	DEN	Fold-Change (DEN / SHAM)	SHAM	DEN	Fold-Change (DEN / SHAM)	SHAM	DEN	Fold-Change (DEN / SHAM)
	1	116329	89223	**0.77**	218450	91003	**0.42**	115530	144314	**1.25**	329137	227239	**0.69**	97708	44237	**0.45**
	2	114830	120096	**1.05**	169923	173177	**1.02**	259424	162845	**0.63**	207780	186865	**0.90**	284593	233037	**0.82**
	3	213859	273629	**1.28**	425102	316769	**0.75**	560981	300126	**0.54**	417288	452184	**1.08**	435784	391389	**0.90**
	4	460573	482463	**1.05**	1483501	1192825	**0.80**	440280	761404	**1.73**	828375	952027	**1.15**	642576	931349	**1.45**
Average		**226398**	**241353**	**1.03**	**574244**	**443444**	**0.75**	**344054**	**342172**	**1.04**	**445645**	**454579**	**0.96**	**365165**	**400003**	**0.90**
SEM		**81424**	**89918**	**0.10**	**308093**	**254112**	**0.12**	**98193**	**143999**	**0.28**	**134611**	**175787**	**0.10**	**115459**	**190799**	**0.21**

Total p38

		Time of Denervation													
		8 hours			16 hours			24 hours			3 days			7 days		
	Sample Set	SHAM	DEN	Fold-Change (DEN / SHAM)	SHAM	DEN	Fold-Change (DEN / SHAM)	SHAM	DEN	Fold-Change (DEN / SHAM)	SHAM	DEN	Fold-Change (DEN / SHAM)	SHAM	DEN	Fold-Change (DEN / SHAM)
	1	117338	107801	**0.92**	199139	154175	**0.77**	173689	237931	**1.37**	267444	407413	**1.52**	496558	283815	**0.57**
	2	110319	125688	**1.14**	134258	92952	**0.69**	107255	130532	**1.22**	156260	162248	**1.04**	165733	60083	**0.36**
	3	85921	51426	**0.60**	42153	60497	**1.44**	43274	47092	**1.09**	36179	78005	**2.16**	28117	76580	**2.72**
	4	179278	149433	**0.83**	184049	215246	**1.17**	149528	249928	**1.67**	248022	188564	**0.76**	315606	337752	**1.07**
Average		**123214**	**108587**	**0.87**	**139900**	**130717**	**1.02**	**118436**	**166371**	**1.34**	**176976**	**209058**	**1.37**	**251503**	**189558**	**1.18**
SEM		**19864**	**20874**	**0.11**	**35408**	**34220**	**0.17**	**28569**	**47971**	**0.13**	**52824**	**70197**	**0.31**	**100589**	**70931**	**0.53**

p-p38 (Thr180 / Tyr182) / T-p38

		Time of Denervation													
		8 hours			16 hours			24 hours			3 days			7 days		
	Sample Set	SHAM	DEN	Fold-Change (DEN / SHAM)	SHAM	DEN	Fold-Change (DEN / SHAM)	SHAM	DEN	Fold-Change (DEN / SHAM)	SHAM	DEN	Fold-Change (DEN / SHAM)	SHAM	DEN	Fold-Change (DEN / SHAM)
	1	0.99	0.83	**0.83**	1.10	0.59	**0.54**	0.67	0.61	**0.91**	1.23	0.56	**0.45**	0.20	0.16	**0.79**
	2	1.04	0.96	**0.92**	1.27	1.86	**1.47**	2.42	1.25	**0.52**	1.33	1.15	**0.87**	1.72	3.88	**2.26**
	3	2.49	5.32	**2.14**	10.08	5.24	**0.52**	12.96	6.37	**0.49**	11.53	5.80	**0.50**	15.50	5.11	**0.33**
	4	2.57	3.23	**1.26**	8.06	5.54	**0.69**	2.94	3.05	**1.03**	3.34	5.05	**1.51**	2.04	2.76	**1.35**
Average		**1.77**	**2.58**	**1.29**	**5.13**	**3.31**	**0.80**	**4.75**	**2.82**	**0.74**	**4.36**	**3.14**	**0.83**	**4.86**	**2.98**	**1.18**
SEM		**0.44**	**1.07**	**0.30**	**2.32**	**1.23**	**0.23**	**2.78**	**1.29**	**0.14**	**2.44**	**1.33**	**0.24**	**3.57**	**1.06**	**0.42**
Paired T-Test				**0.33**			**0.23**			**0.31**			**0.50**			**0.56**

Appendix B

Additional Figures

Rat Tfam 3'-UTR:

GAUUGAAGACAGAGUUGUCAUUGGGAUUGGGCACAAGAAGCUGG
UUAAGUCUCAAAGCCUUAAGUUGUCAAACUUGAAAGGAUAAAGG
GGUUAACCUUUGACACUCAGUUCA**UUUUU**CUGUAGCCCAUGGACU
UCUGCCCACUGAAUGCAUUUCUGUUGACCUUUUGAGCCUUGACAG
UAGAUCAUGACGAGUUCUGCCGUUUGCUUAAGAACUGGAAUCAA
GACUGUGCGUGCAUCUGCAUGCAGUGGUGAAUUGUUCUGCAUUU
GAUGGUGUAGACAGACUGAAGUGACUUUCACACUGGUGACAGUU
UCGUGCGGGUUUGUGAAGUUCUUACACUGAUGGCCAUUACAUGU
GGGUGCCCCCUUGUCCCAGGCCCAGAGCUGCUCACAGCUGUGGCA
GAGCCAUUGCAGUUUCUAAGAACCUUCCGGGCUUUACUAGAUGAC
GUGGUUUCUAGACAUAAUCAUGUGUAGAGUUGA**UGUUUGU**ACAC
AAUAAGUGAUCAUCGAUGUCCUAACAGCAUUUUAUAGUAGGAGA
G**AUUUA**CAAGUCUUUCUCAAAUUAAGAAAUUAUGUACCAGGUCU
AUGCAUAUGUUUUUAUUGCAUAGAAUAAAAACUCUAAUUUUCCA
AAC

AUUUA : putative AU-rich element
UGUUUGU & **UUUUU :** putative GU-rich elements

Supplementary Figure 1. Identification of *cis*-elements mediating mRNA decay
Putative elements which serve as binding sites for RBPs in the 3'-UTR of the Tfam transcript are highlighted.

Rat 1.1kilobase proximal Tfam promoter:

-1100bp

NRF-2

ACTCCCAAGAGAGAATGAAACCGGAAGCGGTGCTAAGCCTGTGCTAAGGAGTGG

GCTTAGAGGAGTGGGCGTGGTACTCTGCGGCTTGAAGGAGACAATGTTTCAAAGC

PPARα

TGCAGAAAGGAAGTAGACTCTCGGTTCAGTGTTACACTATTAAGATTTTGCTTTCT

TTCCGGTAAAAAAAAAAAGTACAGGTATGCAACAGAAGAGGCTGTTGTTGTTAGG

ATCTCACTATGTTAACTCTGGCCAACATGGAACTTGTATATAGACCAAACTCTAAT

TCACAGAGCTCTACCTGCCTCTTGCCTCCAGAGTGCTGGGAGTAAAAGCATCCACT

Foxo3a

ACCAAGCCGGATGAATGAGACGGTTGTTTTAAATGTTATTTATTTATTAATTTAGT

PPARα

TTACTTTTGAAACAAGGTCTCTAGCCTGACTGTTTGAATGCCTGGCACCACCTCCA

PPARα **Foxo3a**

AATGCTGTAATTACAGGTTTGCACCACCAACCTGGGTTCAGTCTATTTATTTTTGT

GACATGTTTTCTTTTGTGTACATGTTTGTGTGTGTATGTCAAAGTTAGACAGCAAC

PPARα **NF-κβ**

TTGCTTGAGTTGGTTCACTCTTACAATCATGTAGGTCCTGGGGATTGCAAGGCTCT

IL-6 RE-BP

GGGCCATCCTGGAAACTCCTATTCCTTTCTATTAATTTTTAAAGATTAGATAAACA

AAGCGATACATTTCATGACCACTCCTCTCTATCTCTTCCACCCCTCAGTTGCCCCGT

NF-κβ **PPARδ**

GTGTTTTCCTTCGGACTCAGATGAAACAGGCAGTTTGCTGCTGGGTCATCAGCAGT

PPARα

ACCACTGATCGCTGATTTCAAGAGCCACGCACTGTGACACGAGCCGCAGAACCGG

CGTCACGAAGCTGAGCTGGCAGAGGAGGACCCTGGCCCAGCAACAGCCTGCAGG

IL-6 RE-BP

CCTTCCAGCAGAATACTCAGAGGGGCCTGCGGCTATGGCGCGGCTCAGCAACACC

CTTGCCAAACTAAACCGGCTCTGCCTAGCCGCAGGCTCCGCCCCCACTCAGCCCCG

NRF-2

CCCACTGAACGGTGGGGGACACACTCCGCCTCCCGTTTGCCCCGCCTCCTGCTGCA

NRF-2

GACCGGAAGTCTGGGCCTCCCACAGTGCCCCGCGCGCGCGGCG

Transcription start site

Supplementary Figure 2. Identification of putative transcription factor binding sites in the 1.1kb proximal Tfam promoter in rat.

Putative binding sites for a selection of transcription factors relevant to mitochondrial biogenesis and muscle atrophy are highlighted. Foxo3a has 3 overlapping, putative binding sites

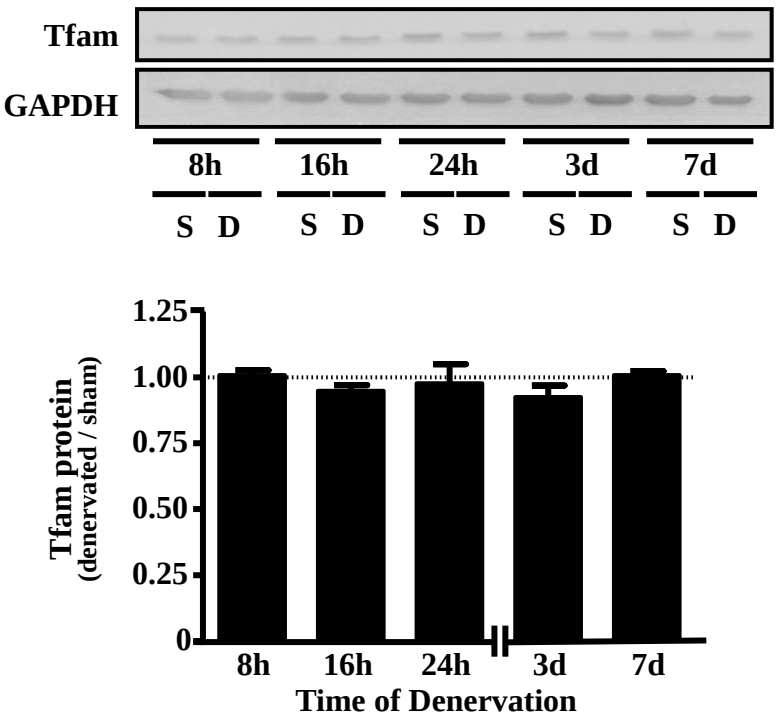

Supplementary Figure 3. Tfam protein expression in denervated muscle. *A.* A representative western blot and graphical representation of Tfam protein expression in denervated muscle, using whole muscle cell extracts. GAPDH served as a loading control (n = 4 per time point). Values are SEM.

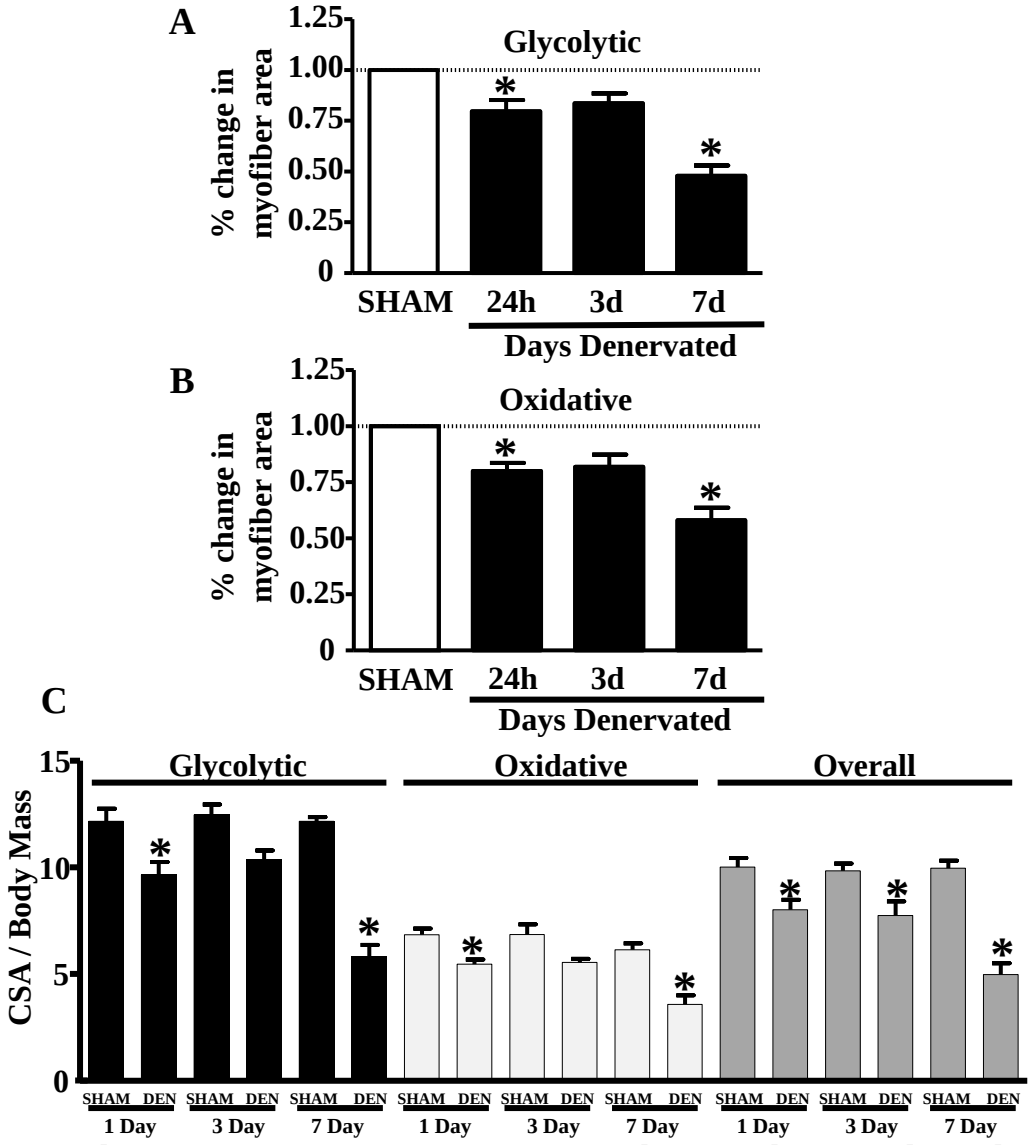

Supplementary Figure 4. EDL cross-sectional area in denervated muscle. Quantification of *(A)* glycolytic and *(B)* oxidative myofiber cross-sectional areas from the same sham-operated and denervated EDL muscle, expressed as a percentage change from the sham-operated hind-limb, the cross-sectional area of which was shown to not change. *(C)* Absolute cross-sectional areas of sham-operated and denervated EDL muscle, corrected for animal body mass. (n = 4 per time point for all experiments) * $p < 0.05$ DEN vs. SHAM of the same time point. Values are SEM.

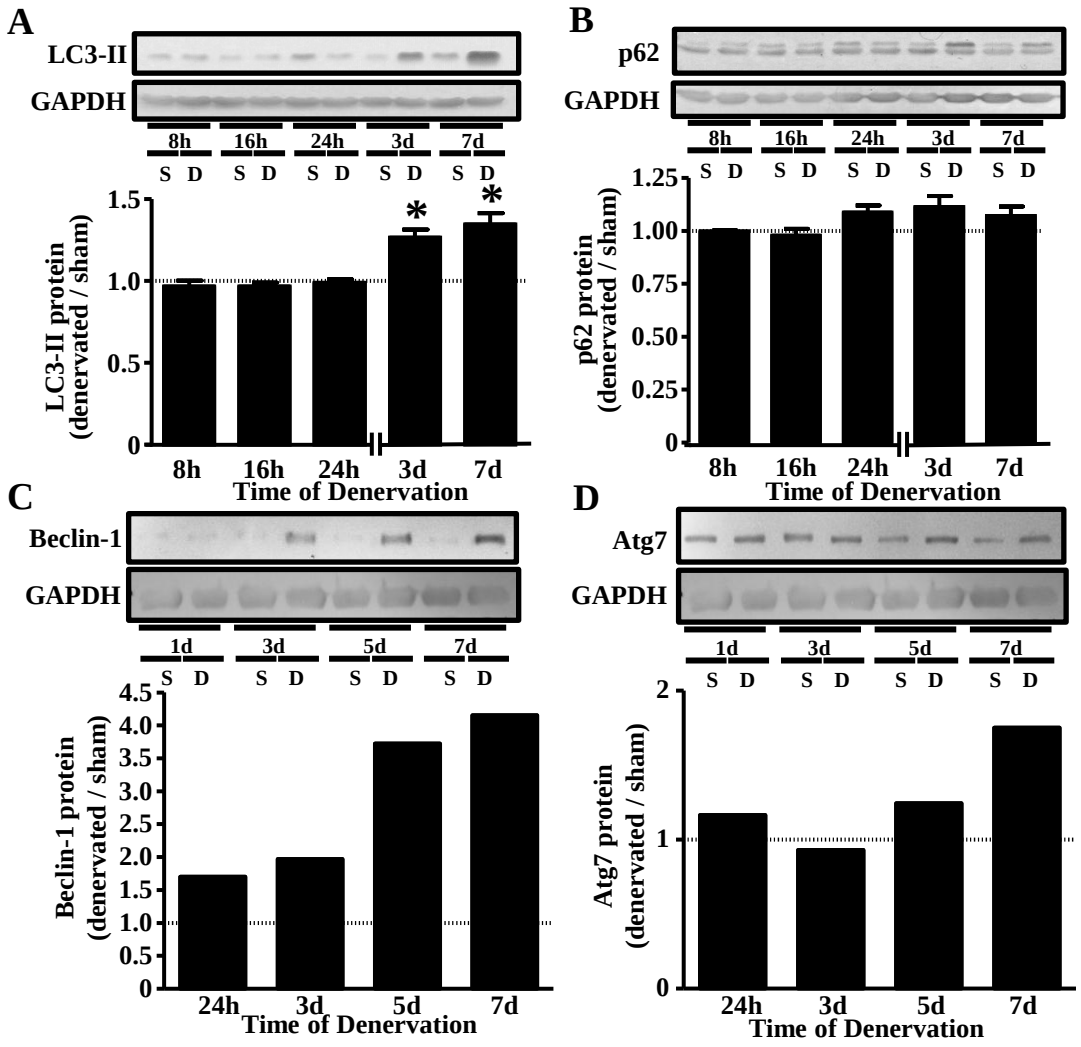

Supplementary Figure 5. Autophagy-related protein expression in denervated muscle. A representative western blot and graphical representation of *A)* LC3-II, *(B)* p62, *(C)* Beclin-1 and *(D)* Atg7 protein expression in sham-operated and denervated muscle. GAPDH was used as a loading control for both measurements. (n = 4 per time point for experiments A and B, n = 1 per time point for experiments C and D) * $p < 0.05$ DEN vs. SHAM of the same time point. Values are SEM.

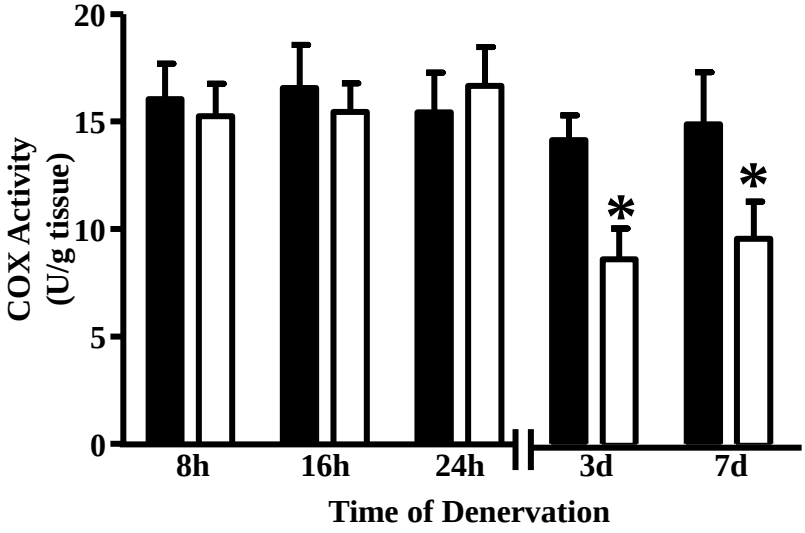

Supplementary Figure 6. COX activity in sham-operated and denervated muscle. A graphical representation of COX activity in sham-operated and denervated muscle. (n = 5 per time point). One-way ANOVA analyses revealed that there were no differences in the COX activity of the sham-operated hindlimbs at all time points. * $p < 0.05$ DEN vs. SHAM of the same time point. Values are SEM.

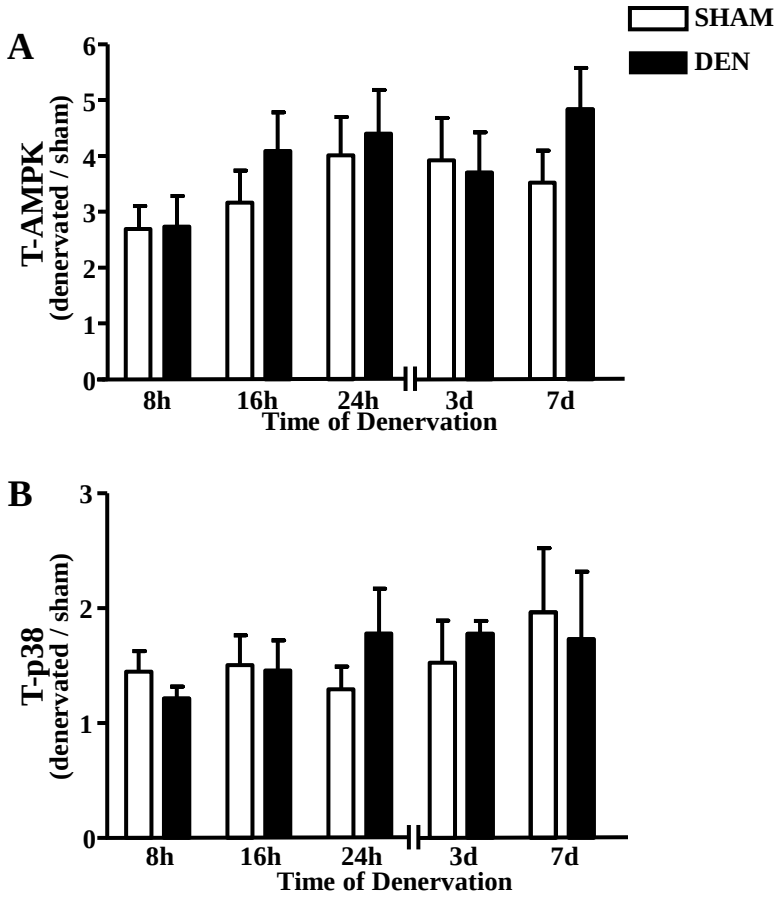

Supplementary Figure 7. Total AMPK and p38 protein expression in denervated muscle. A representative western blot and graphical representation of *A)* Total AMPK alpha and *(B)* total p38 protein expression in sham-operated and denervated muscle. (n = 7 per time point for experiment A, n = 4 per time point for experiment B). Two-way ANOVA analyses revealed no effect of treatment or time in either experiment. Values are SEM.

Appendix C

Raw Data and Statistics for Additional Figures

Tfam

		Time of Denervation													
		8 hours			16 hours			24 hours			3 days			7 days		
	Sample Set	SHAM	DEN	Fold-Change (DEN / SHAM)	SHAM	DEN	Fold-Change (DEN / SHAM)	SHAM	DEN	Fold-Change (DEN / SHAM)	SHAM	DEN	Fold-Change (DEN / SHAM)	SHAM	DEN	Fold-Change (DEN / SHAM)
	1	153	153	**1.00**	157	153	**0.97**	151	149	**0.98**	145	139	**0.96**	138	141	**1.02**
	2	167	173	**1.03**	173	176	**1.01**	168	171	**1.02**	172	172	**1.00**	171	171	**1.00**
	3	125	128	**1.03**	148	143	**0.97**	144	127	**0.88**	129	152	**1.18**	134	150	**1.13**
	4	144	153	**1.06**	159	162	**1.02**	162	158	**0.97**	158	163	**1.03**	158	153	**0.97**
Average		**147**	**151**	**1.03**	**159**	**158**	**0.99**	**156**	**151**	**0.97**	**151**	**156**	**1.04**	**150**	**154**	**1.02**
SEM		**9**	**9**	**0.01**	**5**	**7**	**0.01**	**5**	**9**	**0.03**	**9**	**7**	**0.05**	**9**	**6**	**0.03**

GAPDH

		Time of Denervation													
		8 hours			16 hours			24 hours			3 days			7 days		
	Sample Set	SHAM	DEN	Fold-Change (DEN / SHAM)	SHAM	DEN	Fold-Change (DEN / SHAM)	SHAM	DEN	Fold-Change (DEN / SHAM)	SHAM	DEN	Fold-Change (DEN / SHAM)	SHAM	DEN	Fold-Change (DEN / SHAM)
	1	144	153	**1.06**	150	142	**0.95**	144	138	**0.96**	138	134	**0.97**	136	133	**0.98**
	2	140	144	**1.03**	149	151	**1.02**	157	157	**1.00**	159	154	**0.97**	152	159	**1.05**
	3	86	87	**1.01**	92	106	**1.15**	112	102	**0.91**	95	94	**0.99**	96	99	**1.03**
	4	92	93	**1.02**	94	102	**1.08**	107	96	**0.90**	84	93	**1.11**	96	89	**0.92**
Average		**116**	**119**	**1.03**	**121**	**125**	**1.03**	**130**	**123**	**0.95**	**119**	**119**	**1.00**	**120**	**120**	**1.00**
SEM		**15**	**17**	**0.01**	**16**	**13**	**0.04**	**12**	**15**	**0.02**	**18**	**15**	**0.03**	**14**	**16**	**0.03**
Paired T-Test				**0.127**			**0.445**			**0.073**			**0.894**			**0.982**

Tfam corrected for GAPDH

		Time of Denervation													
		8 hours			16 hours			24 hours			3 days			7 days		
	Sample Set	SHAM	DEN	Fold-Change (DEN / SHAM)	SHAM	DEN	Fold-Change (DEN / SHAM)	SHAM	DEN	Fold-Change (DEN / SHAM)	SHAM	DEN	Fold-Change (DEN / SHAM)	SHAM	DEN	Fold-Change (DEN / SHAM)
	1	1.06	1.00	**0.94**	1.04	1.07	**1.03**	1.05	1.07	**1.02**	1.05	1.04	**0.99**	1.02	1.06	**1.04**
	2	1.19	1.19	**1.00**	1.17	1.17	**1.00**	1.07	1.09	**1.02**	1.08	1.12	**1.04**	1.13	1.08	**0.95**
	3	1.45	1.47	**1.02**	1.62	1.36	**0.84**	1.28	1.25	**0.97**	1.35	1.61	**1.19**	1.39	1.52	**1.10**
	4	1.58	1.63	**1.04**	1.69	1.59	**0.94**	1.51	1.64	**1.09**	1.88	1.74	**0.93**	1.64	1.72	**1.05**
Average		**1.32**	**1.33**	**1.01**	**1.38**	**1.30**	**0.94**	**1.23**	**1.26**	**1.03**	**1.34**	**1.38**	**1.03**	**1.29**	**1.34**	**1.04**
SEM		**0.12**	**0.14**	**0.02**	**0.16**	**0.11**	**0.04**	**0.11**	**0.13**	**0.02**	**0.19**	**0.18**	**0.06**	**0.14**	**0.17**	**0.03**
Paired T-Test				**0.787**			**0.294**			**0.396**			**0.676**			**0.285**

Glycolytic Fiber CSA (um^2) / Body Mass (g)

	Time of Denervation								
	24 hours			3 days			7 days		
Sample Set	**CTRL**	**DEN**	**Fold-Change (DEN / SHAM)**	**CTRL**	**DEN**	**Fold-Change (DEN / SHAM)**	**CTRL**	**DEN**	**Fold-Change (DEN / SHAM)**
1	11.79	7.97	**0.68**	12.00	11.13	**0.93**	11.98	4.65	**0.39**
2	13.85	10.11	**0.73**	12.21	11.02	**0.90**	12.72	5.35	**0.42**
3	11.90	10.73	**0.90**	11.74	9.39	**0.80**	12.21	6.01	**0.49**
4	11.15	9.81	**0.88**	13.90	9.95	**0.72**	11.75	7.25	**0.62**
Average	**12.17**	**9.66**	**0.80**	**12.46**	**10.37**	**0.84**	**12.16**	**5.82**	**0.48**
Paired T-test			**0.041**			**0.057**			**0.003**

Oxidative Fiber CSA (um^2) / Body Mass (g)

	Time of Denervation								
	24 hours			3 days			7 days		
Sample Set	**CTRL**	**DEN**	**Fold-Change (DEN / SHAM)**	**CTRL**	**DEN**	**Fold-Change (DEN / SHAM)**	**CTRL**	**DEN**	**Fold-Change (DEN / SHAM)**
1	6.75	4.99	**0.74**	6.10	5.77	**0.95**	5.29	3.15	**0.60**
2	7.56	5.56	**0.73**	7.77	5.91	**0.76**	6.17	2.69	**0.44**
3	6.88	6.00	**0.87**	5.96	5.16	**0.87**	6.62	3.84	**0.58**
4	6.20	5.32	**0.86**	7.58	5.33	**0.70**	6.51	4.63	**0.71**
Average	**6.85**	**5.46**	**0.80**	**6.85**	**5.54**	**0.82**	**6.15**	**3.58**	**0.58**
Paired T-test			**0.018**			**0.062**			**0.006**

p62

		Time of Denervation													
		8 hours			16 hours			24 hours			3 days			7 days		
	Sample Set	SHAM	DEN	Fold-Change (DEN / SHAM)	SHAM	DEN	Fold-Change (DEN / SHAM)	SHAM	DEN	Fold-Change (DEN / SHAM)	SHAM	DEN	Fold-Change (DEN / SHAM)	SHAM	DEN	Fold-Change (DEN / SHAM)
	1	134	141	**1.06**	133	133	**1.00**	137	141	**1.03**	125	148	**1.18**	129	141	**1.09**
	2	167	171	**1.02**	171	175	**1.02**	180	180	**1.00**	173	192	**1.11**	175	174	**1.00**
	3	123	122	**0.99**	130	138	**1.06**	121	123	**1.01**	132	144	**1.09**	120	133	**1.10**
	4	136	141	**1.03**	151	151	**1.00**	142	148	**1.04**	151	163	**1.08**	142	151	**1.06**
Average		**140**	**144**	**1.03**	**146**	**149**	**1.02**	**145**	**148**	**1.02**	**145**	**162**	**1.11**	**142**	**150**	**1.06**
SEM		**10**	**10**	**0.01**	**9**	**9**	**0.02**	**12**	**12**	**0.01**	**11**	**11**	**0.02**	**12**	**9**	**0.02**

GAPDH

		Time of Denervation													
		8 hours			16 hours			24 hours			3 days			7 days		
	Sample Set	SHAM	DEN	Fold-Change (DEN / SHAM)	SHAM	DEN	Fold-Change (DEN / SHAM)	SHAM	DEN	Fold-Change (DEN / SHAM)	SHAM	DEN	Fold-Change (DEN / SHAM)	SHAM	DEN	Fold-Change (DEN / SHAM)
	1	144	153	**1.06**	150	142	**0.95**	144	138	**0.96**	138	134	**0.97**	136	133	**0.98**
	2	140	144	**1.03**	149	151	**1.02**	157	157	**1.00**	159	154	**0.97**	152	159	**1.05**
	3	86	87	**1.01**	92	106	**1.15**	112	102	**0.91**	95	94	**0.99**	96	99	**1.03**
	4	92	93	**1.02**	94	102	**1.08**	107	96	**0.90**	84	93	**1.11**	96	89	**0.92**
Average		**116**	**119**	**1.03**	**121**	**125**	**1.03**	**130**	**123**	**0.95**	**119**	**119**	**1.00**	**120**	**120**	**1.00**
SEM		**15**	**17**	**0.01**	**16**	**13**	**0.04**	**12**	**15**	**0.02**	**18**	**15**	**0.03**	**14**	**16**	**0.03**

p62 corrected for GAPDH

		Time of Denervation													
		8 hours			16 hours			24 hours			3 days			7 days		
	Sample Set	SHAM	DEN	Fold-Change (DEN / SHAM)	SHAM	DEN	Fold-Change (DEN / SHAM)	SHAM	DEN	Fold-Change (DEN / SHAM)	SHAM	DEN	Fold-Change (DEN / SHAM)	SHAM	DEN	Fold-Change (DEN / SHAM)
	1	0.93	0.92	**1.00**	0.89	0.93	**1.05**	0.95	1.02	**1.07**	0.90	1.11	**1.22**	0.95	1.05	**1.11**
	2	1.19	1.18	**0.99**	1.15	1.16	**1.01**	1.14	1.15	**1.00**	1.09	1.25	**1.15**	1.15	1.10	**0.95**
	3	1.43	1.41	**0.99**	1.42	1.31	**0.92**	1.08	1.21	**1.12**	1.38	1.53	**1.11**	1.25	1.34	**1.07**
	4	1.49	1.51	**1.01**	1.60	1.49	**0.93**	1.32	1.54	**1.16**	1.80	1.75	**0.98**	1.48	1.70	**1.15**
Average		**1.26**	**1.26**	**1.00**	**1.26**	**1.22**	**0.97**	**1.13**	**1.23**	**1.09**	**1.29**	**1.41**	**1.09**	**1.21**	**1.30**	**1.08**
SEM		**0.13**	**0.13**	**0.01**	**0.16**	**0.12**	**0.03**	**0.08**	**0.11**	**0.03**	**0.19**	**0.14**	**0.05**	**0.11**	**0.15**	**0.04**
Paired T-Test				**0.766**			**0.382**			**0.105**			**0.123**			**0.215**

LC3-II

		Time of Denervation														
		8 hours			16 hours			24 hours			3 days			7 days		
	Sample Set	SHAM	DEN	Fold-Change (DEN / SHAM)	SHAM	DEN	Fold-Change (DEN / SHAM)	SHAM	DEN	Fold-Change (DEN / SHAM)	SHAM	DEN	Fold-Change (DEN / SHAM)	SHAM	DEN	Fold-Change (DEN / SHAM)
	1	77	76	**0.99**	68	64	**0.93**	68	68	**1.01**	76	85	**1.11**	80	113	**1.40**
	2	115	125	**1.08**	120	122	**1.02**	128	123	**0.97**	116	140	**1.21**	116	140	**1.21**
	3	103	103	**1.00**	98	101	**1.03**	117	101	**0.87**	98	134	**1.37**	113	154	**1.37**
	4	110	99	**0.90**	102	108	**1.06**	100	88	**0.89**	97	136	**1.41**	114	154	**1.34**
Average		**101**	**101**	**0.99**	**97**	**99**	**1.02**	**103**	**95**	**0.93**	**97**	**124**	**1.28**	**106**	**140**	**1.33**
SEM		**9**	**10**	**0.04**	**11**	**13**	**0.03**	**13**	**12**	**0.03**	**8**	**13**	**0.07**	**8**	**10**	**0.04**

GAPDH

		Time of Denervation														
		8 hours			16 hours			24 hours			3 days			7 days		
	Sample Set	SHAM	DEN	Fold-Change (DEN / SHAM)	SHAM	DEN	Fold-Change (DEN / SHAM)	SHAM	DEN	Fold-Change (DEN / SHAM)	SHAM	DEN	Fold-Change (DEN / SHAM)	SHAM	DEN	Fold-Change (DEN / SHAM)
	1	144	153	**1.06**	150	142	**0.95**	144	138	**0.96**	138	134	**0.97**	136	133	**0.98**
	2	140	144	**1.03**	149	151	**1.02**	157	157	**1.00**	159	154	**0.97**	152	159	**1.05**
	3	86	87	**1.01**	92	106	**1.15**	112	102	**0.91**	95	94	**0.99**	96	99	**1.03**
	4	92	93	**1.02**	94	102	**1.08**	107	96	**0.90**	84	93	**1.11**	96	89	**0.92**
Average		**116**	**119**	**1.03**	**121**	**125**	**1.03**	**130**	**123**	**0.95**	**119**	**119**	**1.00**	**120**	**120**	**1.00**
SEM		**15**	**17**	**0.01**	**16**	**13**	**0.04**	**12**	**15**	**0.02**	**18**	**15**	**0.03**	**14**	**16**	**0.03**

LC3-II corrected for GAPDH

		Time of Denervation														
		8 hours			16 hours			24 hours			3 days			7 days		
	Sample Set	SHAM	DEN	Fold-Change (DEN / SHAM)	SHAM	DEN	Fold-Change (DEN / SHAM)	SHAM	DEN	Fold-Change (DEN / SHAM)	SHAM	DEN	Fold-Change (DEN / SHAM)	SHAM	DEN	Fold-Change (DEN / SHAM)
	1	0.53	0.50	**0.93**	0.46	0.45	**0.98**	0.47	0.49	**1.05**	0.55	0.63	**1.15**	0.59	0.85	**1.43**
	2	0.82	0.86	**1.05**	0.81	0.81	**1.01**	0.81	0.79	**0.97**	0.73	0.91	**1.25**	0.76	0.88	**1.16**
	3	1.20	1.19	**0.99**	1.07	0.96	**0.89**	1.04	0.99	**0.95**	1.02	1.42	**1.39**	1.17	1.56	**1.33**
	4	1.20	1.06	**0.88**	1.09	1.07	**0.98**	0.93	0.92	**0.99**	1.15	1.46	**1.27**	1.19	1.73	**1.46**
Average		**0.94**	**0.90**	**0.96**	**0.86**	**0.82**	**0.96**	**0.81**	**0.80**	**0.98**	**0.86**	**1.11**	**1.28**	**0.93**	**1.25**	**1.35**
SEM		**0.16**	**0.15**	**0.04**	**0.15**	**0.14**	**0.02**	**0.12**	**0.11**	**0.02**	**0.14**	**0.20**	**0.05**	**0.15**	**0.23**	**0.07**
Paired T-Test				**0.430**			**0.291**			**0.348**			**0.039**			**0.036**

Beclin-1

		Time of Denervation											
		24 hours			3 days			5 days			7 days		
	Sample Set	SHAM	DEN	Fold-Change (DEN / SHAM)	SHAM	DEN	Fold-Change (DEN / SHAM)	SHAM	DEN	Fold-Change (DEN / SHAM)	SHAM	DEN	Fold-Change (DEN / SHAM)
	1	33152	50677	**1.53**	64656	123425	**1.91**	35929	127862	**3.56**	36746	133488	**3.63**

Atg7

		Time of Denervation											
		24 hours			3 days			5 days			7 days		
	Sample Set	SHAM	DEN	Fold-Change (DEN / SHAM)	SHAM	DEN	Fold-Change (DEN / SHAM)	SHAM	DEN	Fold-Change (DEN / SHAM)	SHAM	DEN	Fold-Change (DEN / SHAM)
	1	91971	96401	**1.05**	89671	80873	**0.90**	70126	83449	**1.19**	69534	106613	**1.53**

GAPDH

		Time of Denervation											
		24 hours			3 days			5 days			7 days		
	Sample Set	SHAM	DEN	Fold-Change (DEN / SHAM)	SHAM	DEN	Fold-Change (DEN / SHAM)	SHAM	DEN	Fold-Change (DEN / SHAM)	SHAM	DEN	Fold-Change (DEN / SHAM)
	1	293768	264021	**0.90**	248103	240189	**0.97**	212035	202700	**0.96**	244576	213993	**0.87**

Beclin-1 corrected for GAPDH

		Time of Denervation											
		24 hours			3 days			5 days			7 days		
	Sample Set	SHAM	DEN	Fold-Change (DEN / SHAM)	SHAM	DEN	Fold-Change (DEN / SHAM)	SHAM	DEN	Fold-Change (DEN / SHAM)	SHAM	DEN	Fold-Change (DEN / SHAM)
	1	0.11	0.19	**1.70**	0.26	0.51	**1.97**	0.17	0.63	**3.72**	0.15	0.62	**4.15**

Atg7 corrected for GAPDH

		Time of Denervation											
		24 hours			3 days			5 days			7 days		
	Sample Set	SHAM	DEN	Fold-Change (DEN / SHAM)	SHAM	DEN	Fold-Change (DEN / SHAM)	SHAM	DEN	Fold-Change (DEN / SHAM)	SHAM	DEN	Fold-Change (DEN / SHAM)
	1	0.31	0.37	**1.17**	0.36	0.34	**0.93**	0.33	0.41	**1.24**	0.28	0.50	**1.75**

Appendix D

Protocols and Extended Methods

Procedure for the denervation of the tibialis anterior (TA) and extensor digitorum longus (EDL) muscles of the rat

Materials:
Animal
Heating pad
1 pair each of sharp surgical scissors and blunt scissors.
Sterile ampicillin (dissolved in sterile saline)
Isoflourane anesthetic machine
Surgical forceps (multiple pairs)
Surgical needle driver (to aid in the wound suturing)
Surgical stapler and staples
Iodine
95% ethanol
Braided surgical silk 5-0 (Ethicon)
Tear gel (Novartis)
Surgical blade (Feather Safety Razor Co.) and scalpel

Procedure:
1. Sterilize surgical instruments in autoclave machine for 20 minutes.
2. Anaesthetize rat with gaseous isoflourane, keep animal on a warm heating pad throughout the duration of the surgery.
3. Shave both of the animal's hindlimbs, removing as much of the hair as possible.
4. Wipe the shaved areas with 1% topical iodine antiseptic solution, and then again with 95% ethanol solution.
5. Make a 2 cm incision in the skin approximately 1 cm posterior and 1 cm inferior to the knee.
6. Carefully blunt dissect through the exposed superficial muscle until the common peroneal nerve is visualized. This nerve innervates the TA and EDL muscles.
7. Cut out a small 5mm section of the nerve. This ensures that the nerve endings will not regenerate during the experiment and thus effectively remove any neural innervation to the TA and EDL muscles.
8. Inject a small volume (~0.1mls) of sterile ampicillin in the local incision site.
9. Using the 5.0 surgical silk, suture close the superficial muscle tear. Seal the overlying skin on the hindlimb using surgical staples.
10. Turn the animal over, and repeat the surgical procedure. However, when the nerve is encountered, simply expose it, without neurotomy. Suture the wound and treat with ampicillin as above.
11. While still under anaesthetic, the animal is given the analgesic *meloxicam* (stock solution of 5 mg/ml is diluted 10-fold in sterile saline to a concentration of 0.5mg/ml) in a subcutaneous injection. Post-surgery, the animal is given 2 mg/kg body weight, and is given 1.5 mg/kg and 1 mg/kg body weight at 24 hours and 48 hours (respectively) post-surgery, should the animal be kept for a denervation length of that time.
12. Monitor the animal (at minimum) over the next 72 hours to ensure recovery (shorter, if the length of denervation is less than 72 hours). The animal is free to move about the cage and feed/drink *ad libitum*.
13. Recovering animals are given amoxicillin in their drinking water (0.025% w/v) for up to one week post-surgery.

DNA injection and electroporation into rat hindlimb muscles

References:

Wolff JA, Malone RW, Williams P, Chong W, Ascadi G, Jani A, Felgner PL. Direct gene transfer into mouse muscle *in vivo*. *Science* 247(4949 Pt 1):1465-8, 1990.

Wolff JA, Williams P, Ascadi G, Jiao S, Jani A, Chong W. Conditions affecting direct gene transfer into rodent muscle *in vivo*. *Biotechniques* 11(4): 474-85, 1991.

Davis HL, Whalen RG, Demeneix BA. Direct gene transfer into skeletal muscle *in vivo*: factors affecting efficiency of transfer and stability of expression. *Hum Gen Ther* 4(2):151-9, 1993.

Materials:

29 gauge insulin syringe, ½" needle (Ultrafine, Becton Dickson)

Forceps (sterile)

Plasmid DNA: 50µg plasmid of interest + 1µg of pRL-CMV plasmid (use spectrophotometer to determine DNA concentration)

ECM 830 Electroporation system (BTX)

0.7cm tweezertrodes (BTX)

DNA preparation:

DNA is prepared using the alkaline lysis plasmid DNA preparation to produce plasmids inserted with the promoter of interest upstream of the luciferase gene, which can be used to both *in vivo* and *in vitro* transfections. DNA is stored in stab cultures, in glycerol at -80°C for long-term storage. Follow the manufacturer's instructions to isolate DNA from these stores, using a MaxiPrep isolation kit (Sigma-Aldrich, GenElute HP Plasmid Maxiprep kit). Transfection efficiency is determined through the co-transfection of the pRL-CMV (renilla luciferase) plasmid, as it is assumed that the cells transfected with the plasmids containing the promoter of interest have also been transfected with the pRL-CMV plasmid.

Sample calculation:

[1.1kb Tfam + pGL3] = 3.13µg/µl

(arbitrary concentration, measured by spectrophotometry after DNA isolation)

∴ 50µg of [1.1kb Tfam + pGL3] = 50/3.13=**15.79µl of plasmid DNA**

[pRL-CMV]=1.00µg/µl (measured by spectrophotometry, and solution is kept at this concentration)

∴ 1µg of [pRL-CMV] = 1/1 = **1µl of plasmid DNA**

Volume up to 30µl (3 units on the syringe) with 0.9% sterile saline.

15.79ul of plasmid DNA [1.1kb Tfam+pGL3] + 1µl of plasmid DNA [pRL-CMV] +13.21µl sterile saline = 30µl to be injected into muscle

*NOTE: to fill syringes, fill a 1.5ml sterile Eppendorf with a solution of all plasmid DNA and sterile saline sufficient for all injections to be performed in a single day. Insert the needle into the Eppendorf, and slowly withdraw fluid from the Eppendorf, ensure that **no air bubbles** are present in the syringe. Do not store syringes in the fridge after filling, but rather use them immediately.

Injection procedure:

1. Animals are anesthetized using isoflourane.
2. Set the appropriate parameters on the electroporator (100 V/cm, 20ms pulse duration, 200ms interval, 4 pulses, unipolarity).
3. The lower part of the limb in shaved, providing a clear view of the outline of the tibialis anterior muscle.
4. The injection site is sterilized by applying iodine (Providine solution) and subsequently ethanol to the shaved area.
5. The animal is turned slightly on its side to provide clear access to the injection site at the tibialis anterior (TA) muscle.
6. Take a prefilled syringe (containing 50µg of plasmid DNA of the gene of interest, 1µg of plasmid DNA of the control plasmid in a 30µl solution with 0.9% sterile saline) and perform the injection into the muscle. Take time to perform the injection (up to 30 seconds per injection), and maintain a very small angle between the muscle and the syringe. Do not insert the needle of the syringe more than 1-3mm into the muscle, and ensure injection takes places into the belly of the muscle.
7. Remove the needle from the muscle very slowly (take 10-15 seconds to do so). If the injection has been successfully completed, no leak from the site of injection will be visible to the eye.
8. Adjust the width of the tweezertrodes according to the size of the muscle. Tweezertrodes are positioned over the skin, and on either side of the muscle in a direction parallel to the muscle fiber orientation. Pulse the muscle, and observe contraction of the muscle. Repeat this if no contraction is observed. Switch the polarity by reversing the orientation of the electrodes and pulse the muscle again.
9. Repeat steps 6-9 on the contralateral hindlimb,
10. Remove the isoflourance anesthetic, and allow the animal to recover for 4 days without any further handling. Do not massage or put any pressure on the injected muscle, as this has been shown to markedly reduce expression of the reporter gene (Davis HL et al, *Hum Gen Ther*). Antibiotic water should be given to the animal during recovery.
11. Perform the denervation surgery after the animal has been left to recover for 4 days, and remove the TA muscle for analysis of promoter activity using a luciferase assay.

Whole muscle tissue preparation for luciferase assay

1. Add 1ml of 5X passive lysis buffer (PLB) into 4ml sterile water to dilute 5-fold. Add 100µl of this now diluted 1X PLB into 1.5ml eppendorfs.
2. Pound the tibialis anterior muscle tissue at the temperature of liquid nitrogen into a fine powder using a mortar and pestle. Weigh 30-50mg of this powdered tissue into the 1.5ml eppendorfs already containing 100µl of 1X PLB.
3. Dilute this 7-fold in more 1X PLB.
4. Mix samples by flicking the eppendorfs briefly, and sonicate samples 3 X 10 seconds on ice.
5. Centrifuge at max speed on a tabletop centrifuge for 5 minutes at 4°C.
6. Retain supernates and transfer them to new 1.5ml eppendorfs. Use these supernates for a luciferase assay on the same day.

RNA Isolation

Procedure:

Day 1

1. Homogenize tissues (100 mg, frozen and powdered) in 1 ml TRIzol reagent in a sterile 13 ml Sarstedt tube (approximately 3 x 10 seconds @ 30% power);
   Note: The homogenizer must be sterilized in 0.1M NaOH and rinsed in sterile water prior to use. Rinse homogenizer in sterile water between samples.

2. Transfer homogenized solution to a sterile 1.5ml Eppendorf, and let stand for 5 min at room temperature;

3. Add 400µ chloroform and shake vigorously for 15 sec, let stand for 2-3 min at room temperature;

4. Spin at 16100 *g* for 15 min at 4°C;

5. Transfer aqueous phase to a new sterile 1.5ml Eppendorf;

6. Add 500µl isopropanol, shake vigorously for 15 seconds and place in -20°C freezer to allow for RNA precipitation overnight,

Day 2

7. Allow RNA to thaw for 10 min at room temperature;

8. Spin at 16000 *g* for 10 min at 4°C;

9. Remove supernatant and add 700µl 75% ethanol, washing and resuspending the RNA pellet;

10. Spin again at 16,000 *g* for 10 min at 4°C;

11. Remove supernatant, and allow for pellet to air-dry for 40-45 minutes (or until all ethanol has evaporated);

12. Dissolve pellet in 30-40µl sterile distilled water and measure absorbance at 260 nm and 280 nm to determine RNA purity and concentration.

REAGENTS:

75% ethanol in sterile H_2O

(75 ml 100% ethanol + 25 ml dH_2O)

Reverse Transcription

First-strand cDNA synthesis is performed following the manufacturer's recommendations that are outlined below:

Reagents:

Total RNA (isolated as described above)
Oligo$(dT)_{20}$
10 mM each dATP, dTTP, dCTP, dGTP (diluted in sterile DEPC treated water)
Sterile DEPC treated ddH_20
RNAse OUT
0.1M Dithiothreitol (DTT)
5X First-strand Buffer
SuperScript III RT

Procedure:

1. Add following components to a nuclease/ RNA-free 500 µl eppendorf:

Oligo$(dT)_{20}$	1µl
1.5 µg of RNA	x µl
dNTP mix	1 µl
Sterile ddH_20	to 20 µl

2. Employ a thermal cycler to heat mixture to 65°C for 5 minutes. Collect the contents with a quick spin in a tabletop microcentrifuge and then add:

5X First-strand buffer	4 µl
0.1 M DTT	2 µl
RNAse OUT	1 µl
SuperScript III Reverse Transcriptase	1 µl

3. Using a thermal cycler, incubate at 55°C for 50 minutes, and then inactivate the reaction by heating at 70°C for 15 minutes.
4. cDNA is ready for use in PCR amplification.

Polymerase chain reaction (PCR)

The following protocol for semi-quantitative PCR uses GoTaq polymerases from Promega.

Reagents:

5X PCR buffer
25mM $MgCl_2$
10mM dNTPs (dATP, dTTP, dGTP, dCTP)
Forward primer
Reverse primer
Taq DNA polymerase
cDNA from Reverse Transcription reaction
Sterile double distilled water

Procedure:

The following procedure is only a starting point when using first-strand cDNA in PCR with GoTaq DNA polymerase. $MgCl_2$ will vary depending on the primer pair.

1. Combine the following into a 700µl Eppendorf, for each reaction:

5X PCR buffer	10µl
25mM $MgCl_2$	x µl
10mM dNTPs (dATP, dTTP, dGTP, dCTP)	1 µl
Forward primer (30µM)	1 µl
Reverse primer (30µM)	1 µl
cDNA from Reverse Transcription reaction	2 µl
sterile double distilled water	x µl
Taq DNA polymerase	1 µl
TOTAL REACTION VOLUME	**50 µl**

2. Mix gently by pipetting up and down, and layer 1-2 drops of mineral oil on top of the reaction to prevent evaporation during PCR.
3. Heat the samples to 94°C to dentaure the cDNA.
4. Perform 15-40 cycles of PCR using the recommended annealing and extension parameters for your chosen primers.
5. Optimize PCR conditions for your primers of interest (ie. $MgCl_2$ concentrations, cycle number, primer concentrations, annealing temperature).

***in vitro* mRNA Decay Assay**

Preparation of cytosolic extracts:

1. In a 13ml Sardtedt tube, homogenize skeletal muscle powders (50-100mg) 3 x 10 seconds (10mm probe, 40% maximum power) in 1 ml homogenization buffer*.
2. Transfer to a 1.5ml sterile eppendorf. Centrifuge the homogenates at 4°C for 15 minutes at 5000 *g*. Transfer the supernates to a sterile 1.5ml Eppendorf.
3. Centrifuge the supernates at 4°C for 15 minutes at 15000 *g* and transfer the resulting post-mitochondrial supernates (S15) to a sterile 1.5ml eppendorf.
4. Determine the protein concentration of the S15 fractions using the Braford total protein assay. These extracts can be used immediately in the assay, or store at -20°C.

***in vitro* decay reaction:**

1. Incubate total RNA (35µg) and S15 extract (20µg) in a sterile 700µl eppendorf. Volume up the reaction to a 100µl with sterile water, and incubate in a water bath set to 37°C. A baseline control must also be made, which allows for an estimation of the amount of RNA present in the sample not exposed to the S15 extract. This sample consists of total RNA (35µg) and homogenization buffer. Add 100µl phenol to his reaction immediately, and set aside on ice.
2. Remove aliquots after selected time points (15 and 45 minutes) and add 100µl of phenol to stop the decay of the mRNA substrate. Shake vigorously (~15 seconds) and place on ice.
3. Once all samples have been collected at all time points, spin in a table top centrifuge at max speed for 30 seconds.
4. Transfer the aqueous phase to a sterile 700µl Eppendorf. Add 100µl of phenol/chloroform/isoamyl alcohol (P:C:I) in a 25:24:1 ratio, and shake vigorously.
5. Spin in a table top centrifuge at max speed for 30 seconds.
6. Transfer the aqueous phase to a sterile 700µl Eppendorf . Add 100µl of chloroform/isoamyl alcohol (C:I) in a 24:1 ratio, and shake vigorously.
7. Spin in a table top centrifuge at max speed for 30 seconds.
8. Transfer the aqueous phase to a sterile 700µl Eppendorf. Add 10µl of 3M sodium acetate (pH 5.2) and 300µl of 100% anhydrous ethyl alcohol. Shake vigourously, precipitate at -20°C overnight .
7. Spin in a table top centrifuge at max speed for 15 minutes, at 4°C.
8. Wash and resuspend the pellet with 750µl of 75% ethanol and spin in a table top centrifuge at max speed for 5 minutes at 4°C.
9. Pour off the supernates, and air dry the pellets.
10. Resuspend the pellet in 20µl of sterile water. Use 5µl of RNA and combine this with 2.25µl of 0.5mg/ml EtBr and 9µl of RNA sample buffer. Volume up to 20µl with sterile water. Run on a 1% agarose-formaldehyde gel to determine RNA quality. Use 5µl to determine concentration of the RNA on the spectrophotometer. Utilize the remaining RNA for reverse transcription and semi-quantitative PCR to determine the relative quantity of mRNA remaining after the decay assay.

***Homogenization buffer (autoclave solution prior to use – this recipe makes 100ml):**

25% glycerol	25ml of sterile 100% stock solution
0.42M NaCl	10ml of a 4.2M stock solution
1.5mM $MgCl_2$	1ml of a 150mM stock solution
20mM HEPES (pH 7.9)	5ml of a 400mM stock solution
0.2mM EDTA	40µl of a 0.5M stock solution
0.5mM DTT	100µl of a 0.5M stock solution
0.5mM PMSF	100µl of a 0.5M stock solution
Sterile water	58.76ml

Bradford Protein Assay

Reference: Bradford MM. A rapid and sensitive method for the quantitation of microgram quantities of protein utilizing the principle of protein-dye binding. *Anal Biochem*, 72:248-254, 1976.

Reagents:

- Extraction buffer
  - 100 mM Na/K PO_4
  - 2 mM EDTA
  - pH to 7.2
- 5 X Bradford dye
  - 250 ml 85% Phosphoric acid
  - 250 ml 100% Ethanol
  - 500 ml ddH_2O
  - 0.235 g Comassie Brilliant Blue G250
- Bovine Serum Albumin (BSA)
  - 2 mg/ml in ddH_2O

Procedure:

1. Prepare the test tubes allowing for duplicates of each sample.
2. Add 95 µl of extraction buffer to each tube.
3. Add 5 µl of sample to each tube containing the extraction buffer.
4. To generate the standard curve, add the following volumes (in µl) of extraction buffer: BSA, each in separate tubes – 100:0, 95:5, 90:10, 85:15, 80:20, 75:25.
5. Dispense 5 ml of 1 X Bradford reagent into each tube and mix by gentle vortexing.
6. In duplicate, add 0.2 ml of each test tube to 96 well plate wells.
7. Measure absorbance of wells at 595 nm using a microplate reader; ensure that coefficient of determination (R^2) for standard curve is >0.99.
8. Calculate the protein concentration of each sample using the standard curve.

Cytochrome *c* oxidase (COX) assay for microplate reader

Cell extract containing cytochrome c oxidase is added to the test solution containing fully reduced cytochrome c. The rate of cytochrome c oxidation is measured over time as a reduction in absorbance at 550 nm. The reaction is carried out at 30^{o} C.

Reagents:

Horse Heart Cytochrome c (Sigma, C-2506)
Sodium Dithionite
100 mM K-Phosphate Buffer (KPO_4; pH to 7.0)
-make and mix equal proportions of 0.1 M KH_2PO_4 and 0.1 M $K_2HPO_4.3H_2O$
10 mM K-Phosphate Buffer
-dilute 100 mM K-Phosphate Buffer 1:10 with ddH_2O

Procedure:

1. Immediately following the completion of the enzyme extraction protocol from cells, proceed to making Test Solution. Add the following to a scintillation vial:

    - weigh out 20 mg of horses heart cytochrome c
    - add 1 ml of 10 mM KPO_4 buffer and fully dissolve cytochrome c
    - make up a small volume of 10 mg/ ml sodium dithionite- 10 mM KPO_4 stock solution (Note: make fresh each experiment and use within 20 minutes)
    - add 40 µl of dithionite stock solution to the Test Solution and observe the red to orange colour change
    - add 8 ml of ddH_2O
    - add 1 ml of 100 mM KPO_4 buffer (Note: the Test Solution becomes light sensitive at this step; make sure to the cover vial with aluminum foil).

2. Add 300 µl of Test Solution into 4-8 wells of a 96-well microplate and incubate at 30°C for 10 minutes to stabilize the temperature and absorbance.
3. Open KC4 plate reader program. Select CONTROL icon, then PRE-HEATING tab, enter 30°C and select ON (Do not run assay until KC4 temperature has reached 30°C).
4. Set-up COX activity protocol on computer.
5. Select WIZARD icon, then READING PARAMETERS icon.

    - Select Kinetic for Reading Type.
    - Select Absorbance for Reader and 550 nm for wavelength (drop-down).
    - Select Sweep for Read Mode.
    - Select 96 Well Plate (default) for Plate Type.
    - Enter first and last well to be read (eg. A1 and A4 if reading 4 samples simultaneously).
    - Select Yes and Pre-heating and enter 30 for Temperature Control.
    - For Shaking enter 0 for both intensity and duration (shaking is not necessary and it will delay the first reading).
    - Do not select either of the two options for Pre-reading.
    - Click on the KINETIC… rectangular tile to open the Kinetic window.
    - Enter run time (1 minute is recommended) and select MINIMUM for Interval

time (under these conditions the minimum Interval time should be 3 seconds).
- Select Allow Well Zoom During Read to see data in real time (optional).
- Under Scales, checkmarks should appear for both Auto check boxes. Do not select Individual Well Auto Scaling.
- Press OK to return to Reading Parameters window. Press OK to return to Wizard window. Press OK. Do not save the protocol.

6. Set the micropipette to 225 µl and secure 4-8 tips on the white projections (make sure they are on tight and all the same height).
7. In a second, clean 96 well plate, pipette samples into 4-8 empty wells (start with A1). *Recommended volumes:* 65 µl of enzyme extract from C2C12 cells.
8. Remove microplate with Test Solution from the incubator (as long as it has been incubating for 10 minutes). Place this plate beside the plate with the sample extracts in it.
9. On KC4 program, select the READ icon and press the START READING icon, then press the READ PLATE button. A box will appear that says, "Insert plate and start reading". Do not press OK yet, but move the mouse so that the cursor hovers over the OK button.
10. Using the micropipette (set to 225 µl) carefully draw up the Test Solution. Make sure the volume is equal in all the pipette tips, and that no significant air bubbles have entered any of the tips.
11. Pipette the Test Solution into the wells with the sample extracts (the second plate). As soon as all the Test Solution has been expelled from the tips (do not wait for the second push from the multipipette), place the plate onto the tray of the plate reader and with the other hand on the mouse, press the OK button. (Speed at this point is paramount, as there is an unavoidable latency period between the time of pressing the OK button and the time of the first reading.)
12. Once reading is complete, hold the CTRL key on the keyboard, and use the mouse to click once on each of the squares corresponding to a well that had sample in it. Once all the desired wells have been highlighted by a black square (up to a maximum of 8 wells), let go of the CTRL key and a large graph will appear with lines on it representing each sample.
13. To obtain the rate of change of absorbance over different time periods, select Options and enter the amount of time for which you would like a rate of change of absorbance to be calculated. The graph, along with one rate (at whichever time interval is selected) for each sample can be printed on a single sheet of paper, and the results can be saved.
14. The delta absorbance will appear in units of mOD/min and the number given will be negative. Convert this to OD/min by dividing by 1000 and omit the negative sign in the calculation. (eg. if Mean V: -394.8 mOD/mn, then use 0.395 OD/min)

Calculation:

CYTOX activity = $\frac{\text{mean dealta absorbance/ minute x total volume (ml) x 1000}}{\text{18.5 (µmol/ml extinction coeff.) x sample volume (ml) x total µg/ well}}$

Example Calculation:

55 µl of enzyme extraction
230 µl of Test Solution
Mean V: -584.30 mOD/mn
Protein concentration: 3.023 µg/ µl
Total µg/ well: 151.15

COX activity = $\frac{(0.5843)(0.285)(1000)}{(18.5)(0.055)(3.023 \times 55)}$

COX activity = 0.967 nmol/min/µg protein

Mitochondrial Isolation Protocol

Reagents:

All buffers are set to **pH 7.4** and stored at 4 °C.

Buffer 1
100 mM KCl
5 mM $MgSO_4$
5 mM EDTA
50 mM Tris base

Buffer 1 + ATP
Add 1 mM ATP to Buffer 1

Resuspension medium
100 mM KCl
10 mM MOPS
0.2% BSA

Procedure:

1. Remove the tibialis anterior (TA) muscle from the rat, and put it in a beaker containing 5 ml of Buffer 1(on ice) immediately.
2. Place TA on a watch glass (that is also on ice) and trim away fat and connective tissue. Proceed to thoroughly mince the muscle sample with forceps and scissors, until no large pieces are remaining.
3. Place the minced tissue in a plastic centrifuge tube and record the exact weight of tissue.
4. Add a 10-fold dilution of Buffer 1 + ATP to the tube.
5. Homogenize the samples using the Ultra-Turrax polytron with 40% power output and 10 s exposure time. Rinse the shaft with 0.5 ml of Buffer 1 + ATP (with a 1 ml pipette) to help minimize sample loss.
6. Using a Beckman JA 25.50 rotor, spin the homogenate at a centrifuge setting of 800 g for 10 min. This step divides the IMF and SS mitochondrial subfractions. The supernate will contain the SS mitochondria and the pellet will contain the IMF mitochondria.

→ Subsarcolemmal Mitochondria Isolation:

7. Filter the supernate through a single layer of cheesecloth into a second set of 50 ml plastic centrifuge tubes.
8. Spin tubes at 9000 g for 10 min. Upon completion of the spin, set aside the supernate (as the cytosols will can be recovered from these) and gently resuspend the pellet in 3.5 ml of Buffer 1 + ATP. Since the mitochondria are easily damaged, it is important that the resuspension of the pellet is done carefully.
9. Repeat the centifugation of the previous step (9000 g for 10 min) and discard the supernate.
10. Resuspend the pellet in 200 µl of Resuspension medium, being gentle so as to prevent damage to the SS mitochondria. Some extra time is needed during this final resuspension to ensure the SS pellet is completely resuspended.
11. Keep the SS samples on ice while proceeding to recover cytosols from these samples.

→ Cytosolic Fraction Recovery:

12. Using the supernate set aside in step 8, fill a centrifuge tube (Beckman Optiseal Polyallomer 8.9ml) using a Pasteur pipette and top up to the brim with Buffer 1 + ATP.

13. Place these tubes in a TI 70.1 rotor, and using an ultracentrifuge, spin for one hour at 100,000 x *g*.
14. Following centrifugation, transfer the supernate to a sterile 13 ml sample tube.
15. Transfer the entire contents of the recovered supernate to the chamber of the stirred filtration system (Millipore/Amicon Stirred Ultracell Filtration System Model 8010). At 4 °C, use compressed nitrogen to filter the supernate through the apparatus and ultrafiltration discs (Millipore Ultracell 10 kDa, 25mm diameter), which have been soaked in 10% ethanol.
16. The remaining concentrate can be assayed (along with the subsarcolemmal mitochondria) to determine protein concentration using the Bradford protein assay.

SDS polyacrylamide gel electrophoresis (SDS-PAGE)

Reagents:

- Polyacrylamide solution
  - 30% (w/v) Acrylamide
  - 0.8% (w/v) Bisacrylamide
  - Filter and store at 4 °C

- Ammonium Persulfate (APS)
  - 10% (w/v) in ddH_2O
  - Store at 4 °C

- Over Tris buffer
  - 1 M Tris•HCl
  - Spatula tip of Bromophenol Blue
  - pH to 6.8, store at 4 °C

- 15% Acrylamide separating gel
  - 5 ml 30% acrylamide
  - 1.8 ml ddH_2O
  - 3 ml Under Tris
  - 0.1 ml SDS
  - 0.1 ml APS
  - 0.01 ml TEMED

- 3% Acrylamide stacking gel
  - 0.5 ml 30% Acrylamide
  - 3.75 ml ddH_2O
  - 0.625 ml Over Tris
  - 0.05 ml SDS
  - 0.05 ml APS
  - 7.5 µl TEMED

- Sample dye
  - 40% (w/v) sucrose in electrophoresis buffer
  - spatula tip of Bromophenol Blue
  - (store at -20 °C)

- Under Tris buffer
  - 1 M Tris•HCl
  - pH to 8.8, store at 4 °C

- Sodium Dodecyl Sulfate (SDS)
  - 10% (w/v) in ddH_2O

- TEMED (Sigma, T-9281)
  - Store at 4 °C

- Electrophoresis buffer
  - 25 mM Tris
  - 192 mM Glycine
  - 0.1% (w/v) SDS
  - pH to 8.3

- Lysis buffer
  - 10% (w/v) glycerol
  - 2.3% (w/v) SDS
  - 62.5 mM Tris•HCl
  - pH to 6.8
  - add 5% β-mercaptoethanol

Procedure:

1. Prepare the separating gel solution and pour it between the glass plates of a gel apparatus assembly.
2. Add 100 µl of 2-butanol alcohol overlay and allow 30 min for gel polymerization.
3. Prepare the stacking gel.
4. Once the separating gel has polymerized, pour off the 2-butanol alcohol and wash with distilled water. Pour stacking gel on top of separating gel, and insert the lane comb. Allow 30 min for the stacking gel to polymerize.
5. Turn on the block heater to 95 °C.

6. Mix each sample with a 1:1 volume of 1 x lysis buffer.
7. Add 7 µl of sample dye to each sample and mix by vortexing.
8. Denature the samples at 95 °C for 5 min, followed by a quick cool on ice and a brief spin.
9. Remove the comb and place the gel in the electrophoresis chamber. Fill the chamber with electrophoresis buffer.
10. Add 10 µl of protein molecular weight marker to the first lane.
11. Load the samples into the remaining lanes by slowly ejecting the entire sample volume at the bottom of the lane.
12. Run the gel for the desired time at 120 V.
13. Once the Bromophenol Blue band has reached the bottom of the gel, turn off the power supply and remove the gel. The gel slab is ready for electroblotting (see Western Blot)

Western Blot

Reagents

- Transfer buffer
  - 0.025 M Tris•HCl
  - 0.15 M Glycine
  - 20% Methanol
  - pH to 8.3
- Wash buffer
  - 10 mM Tris•HCl
  - 100 mM NaCl
  - 0.1% TWEEN
  - pH to 7.5
- Ponceau stain (Sigma)
  - Dilute with 150 ml ddH_2O
- Blocking buffer
  - % skim milk powder in wash buffer
- Enhanced chemiluminescence (ECL) fluid (Santa Cruz)
  - Store at 4 °C

Procedure:

1. Remove the gel from the electrophoresis chamber, and separate the glass plates from the gel slab, keeping the gel moist at all times with transfer buffer.
2. Place three sheets of Whatman paper soaked in transfer buffer onto the plastic cassette, with a cloth. These sheets must be cut to the exact dimensions of the gel slab (8.5 x 6 cm).
3. Carefully place the gel on top of the Whatman paper.
4. Cut a piece of nitrocellulose membrane to the exact dimensions of the gel, soak it in transfer buffer, and place it on top of the gel slab.
5. Stack three more sheets of transfer buffer-soaked Whatman paper (same dimensions as gel) on top of membrane. Roll out any air bubbles with a glass test tube.
6. Secure the top of the sandwich with another cloth soaked in transfer buffer.
7. Transfer the proteins from the gel to the membrane for 1.5 hours at 120V.
8. Once the transfer is complete, place the membrane in Ponceau stain and gently agitate on a shaker plate. Pour off the stain and rinse with ddH_2O until the protein bands on the blot are revealed.
9. Wrap the membrane in plastic saran wrap and scan.
10. Remove the membrane from the wrap and rinse off the Ponceau stain with wash buffer.
11. Pour off the wash buffer and block the membrane in blocking solution (5% skim milk powder) on a shaker plate for 1 hour at room temperature.
12. Incubate the membrane with primary antibody diluted in blocking buffer (unless recommended otherwise by the antibody manufacturer) overnight at 4°C. This is done by laying the membrane face-up and pipetting the primary antibody solution on top of it.
13. The following morning, wash the membrane with rotation 3 x 5 min in wash buffer using a shaker plate.
14. Incubate the membrane with the appropriate secondary antibody for 1 hr at room temperature. This is done by laying the membrane face-up and pipetting the secondary antibody solution on top of it.
15. Wash the membrane with rotation 3 x 5 min in wash buffer using a shaker plate.
16. In the dark room, apply ECL fluids (1:1) to the membrane for 1 min.
17. Remove the membrane from the ECL fluid, wrap the membrane in plastic wrap, turn off the lights, and expose the blot to film.
18. Immerse in developing fluid until bands are visible and place the film into fixer fluid for 2 min.

Succinate Dehydrogenase Staining of Muscle Sections Protocol

Reagents:

0.2M Sodium Succinate Solution

Sodium Succiante: 5.4 g
Distilled Water: 100ml

0.2M Phosphate Buffer, pH 7.4

Na_2HPO_4 (mol wt. 141.98): 11.36 g/400ml distilled water
KH_2PO_4 (mol wt. 136.90): 2.72 g/100ml distilled water
Add Na_2HPO_4 to distilled water, otherwise a hard mass will form at the bottom of the beaker and will be difficult to dissolve. Dissolve each of the reagents separately, and then add them together to make a solution 500ml. pH solution to 7.4 and refrigerate at 4°C to preserve.

SDH Stock Solution (make fresh every two weeks)

0.2M Sodium Succinate: 100ml
0.2M Phosphate Buffer, pH 7.4: 100ml

SDH Incubating Solution (**pH 7.2-7.6**; adjust solution using 0.1N HCl or NaOH)

Nitroblue tetrazolium (NBT): 10mg
SDH Stock Solution: 10ml
*Cover jar containing solution in aluminum foil as the solution is light sensitive.

Procedure:

1. Preheat SDH incubating solution to 37°C in oven before staining in opaque plastic chamber.
2. Remove muscle sections (10µm) on slide from -20°C freezer and let thaw for 5-10 minutes.
3. Place slides in slide rack, and into opaque plastic chamber containing SDH incubating solution. Place cover on chamber and incubate at 37°C in oven for 30 minutes.
4. Remove chamber from oven, and inspect sections to ensure adequately stained. Place back in oven if they are not. Otherwise, remove slide rack and place in plastic chamber containing distilled water to rinse slides (put on shaker plate for 3 x 5 minutes, ~30-40rpm, change water after each 5 minute period).
5. After washing, place on kimwipe in fume hood to air dry.
6. Once dry, mount cover glass (FisherBrand microscope cover glass) on slides using DPX Mountant for histology (Fluka BioChemika no. 44581). Use a cut pipette tip to pipette mountant as it is highly viscous. Ensure no bubbles are formed when placing the cover glass on the slide. Allow to dry overnight.

Reference List for Literature Review

1. **Abruzzo PM, di Tullio S, Marchionni C, Belia S, Fanó G, Zampieri S, Carraro U, Kern H, Sgarbi G, Lenaz G, Marini M**. Oxidative stress in the denervated muscle. *Free Radic. Res.* 44: 563–76, 2010.

2. **Adhihetty PJ, Ljubicic V, Hood DA**. Effect of chronic contractile activity on SS and IMF mitochondrial apoptotic susceptibility in skeletal muscle. *Am. J. Physiol. Endocrinol. Metab.* 292: E748–755, 2007.

3. **Adhihetty PJ, Ljubicic V, Menzies KJ, Hood DA**. Differential susceptibility of subsarcolemmal and intermyofibrillar mitochondria to apoptotic stimuli. *Am. J. Physiol. Cell Physiol.* 3: C994–1001, 2005.

4. **Adhihetty PJ, O'Leary MFN, Chabi B, Wicks KL, Hood DA**. Effect of denervation on mitochondrially mediated apoptosis in skeletal muscle. *J. Appl. Physiol.* 3: 1143–1151, 2007.

5. **Adhihetty PJ, O'Leary MFN, Hood DA**. Mitochondria in skeletal muscle: adaptable rheostats of apoptotic susceptibility. *Exerc. Sport Sci. Rev.* 36: 116–21, 2008.

6. **Akimoto T, Pohnert SC, Li P, Zhang M, Gumbs C, Rosenberg PB, Williams RS, Yan Z**. Exercise stimulates Pgc-1alpha transcription in skeletal muscle through activation of the p38 MAPK pathway. *J. Biol. Chem.* 280: 19587–93, 2005.

7. **Altamura N, Capitanio N, Bonnefoy N, Papa S, Dujardin G**. The Saccharomyces cerevisiae OXA1 gene is required for the correct assembly of cytochrome c oxidase and oligomycin-sensitive ATP synthase. *FEBS Lett.* 382: 111–115, 1996.

8. **Ames BN**. Endogenous DNA damage as related to cancer and aging. *Mutat. Res.* 214: 41–6, 1989.

9. **Amirouche A, Tadesse H, Lunde JA, Bélanger G, Côté J, Jasmin BJ**. Activation of p38 signaling increases utrophin A expression in skeletal muscle via the RNA-binding protein KSRP and inhibition of AU-rich element-mediated mRNA decay: implications for novel DMD therapeutics. *Hum. Mol. Genet.* 22: 3093–111, 2013.

10. **Argadine HM, Hellyer NJ, Mantilla CB, Zhan W, Sieck GC**. The effect of denervation on protein synthesis and degradation in adult rat diaphragm muscle. *J. Appl. Physiol.* 107: 438–444, 2009.

11. **Argadine HM, Mantilla CB, Zhan W, Sieck GC**. Intracellular signaling pathways regulating net protein balance following diaphragm muscle denervation. *Am. J. Physiol. Cell Physiol.* 300: C318–C327, 2011.

12. **Asin-Cayuela J, Gustafsson CM**. Mitochondrial transcription and its regulation in mammalian cells. *Trends Biochem. Sci.* 32: 111–7, 2007.

13. **Axelsson B, Thesleff S**. A study of supersensitivity in denervated mammalian skeletal muscle. *J. Physiol.* 147: 178–193, 1959.

14. **Balagopal V, Fluch L, Nissan T**. Ways and means of eukaryotic mRNA decay. *Biochim. Biophys. Acta* 1819: 593–603, 2012.

15. **Becker T, Vögtle FN, Stojanovski D, Meisinger C**. Sorting and assembly of mitochondrial outer membrane proteins. *Biochim. Biophys. Acta* 1777: 557–63, 2008.

16. **Bengtsson J, Gustafsson T, Widegren U, Jansson E, Sundberg CJ**. Mitochondrial transcription factor A and respiratory complex IV increase in response to exercise training in humans. *Pflugers Arch.* 443: 61–6, 2001.

17. **Bergeron R, Ren JM, Cadman KS, Moore IK, Perret P, Pypaert M, Young LH, Semenkovich CF, Shulman GI**. Chronic activation of AMP kinase results in NRF-1 activation and mitochondrial biogenesis. *Am. J. Physiol. Endocrinol. Metab.* 281: E1340–1346, 2001.

18. **Bertaggia E, Coletto L, Sandri M**. Posttranslational modifications control FoxO3 activity during denervation. *Am. J. Physiol. Cell Physiol.* 302: C587–96, 2012.

19. **Bhattacharya A, Hamilton R, Jernigan A, Zhang Y, Sabia M, Rahman MM, Li Y, Wei R, Chaudhuri A, Van Remmen H**. Genetic ablation of 12/15-lipoxygenase but not 5-lipoxygenase protects against denervation-induced muscle atrophy. *Free Radic. Biol. Med.* 67C: 30–40, 2013.

20. **Bizeau ME, Willis WT, Hazel JR**. Differential responses to endurance training in subsarcolemmal and intermyofibrillar mitochondria. *J. Appl. Physiol.* 85: 1279–84, 1998.

21. **Bodine SC, Latres E, Baumhueter S, Lai VK, Nunez L, Clarke BA, Poueymirou WT, Panaro FJ, Na E, Dharmarajan K, Pan ZQ, Valenzuela DM, DeChiara TM, Stitt TN, Yancopoulos GD, Glass DJ**. Identification of ubiquitin ligases required for skeletal muscle atrophy. *Science* 294: 1704–8, 2001.

22. **Bogenhagen DF, Rousseau D, Burke S**. The layered structure of human mitochondrial DNA nucleoids. *J. Biol. Chem.* 283: 3665–75, 2008.

23. **Booth FW, Gollnick PD**. Effects of disuse on the structure and function of skeletal muscle. *Med. Sci. Sports Exerc.* 15: 415–20, 1983.

24. **Borisov AB, Carlson BM**. Cell death in denervated skeletal muscle is distinct from classical apoptosis. *Anat. Rec.* 258: 305–318, 2000.

25. **Borisov AB, Huang SK, Carlson BM**. Remodeling of the vascular bed and progressive loss of capillaries in denervated skeletal muscle. *Anat. Rec.* 258: 292–304, 2000.

26. **Brault JJ, Jespersen JG, Goldberg AL**. Peroxisome proliferator-activated receptor γ coactivator 1α or 1B overexpression inhibits muscle protein degradation, induction of ubiquitin ligases, and disuse atrophy. *J. Biol. Chem.* 285: 19460–71, 2010.

27. **Briata P, Forcales SV, Ponassi M, Corte G, Chen CY, Karin M, Puri PL, Gherzi R**. p38-dependent phosphorylation of the mRNA decay-promoting factor KSRP controls the stability of select myogenic transcripts. *Mol. Cell* 20: 891–903, 2005.

28. **Briata P, Lin WJ, Giovarelli M, Pasero M, Chou CF, Trabucchi M, Rosenfeld MG, Chen CY, Gherzi R**. PI3K/AKT signaling determines a dynamic switch between distinct KSRP functions favoring skeletal myogenesis. *Cell Death Differ.* 19: 478–87, 2012.

29. **Carter HN, Hood DA**. Contractile activity-induced mitochondrial biogenesis and mTORC1. *Am. J. Physiol. Cell Physiol.* 303: C540–7, 2012.

30. **Chan DC**. Fusion and fission: interlinked processes critical for mitochondrial health. *Annu. Rev. Genet.* 46: 265–87, 2012.

31. **Chan NC, Salazar AM, Pham AH, Sweredoski MJ, Kolawa NJ, Graham RLJ, Hess S, Chan DC**. Broad activation of the ubiquitin-proteasome system by Parkin is critical for mitophagy. *Hum. Mol. Genet.* 20: 1726–37, 2011.

32. **Chen CY, Gherzi R, Ong SE, Chan EL, Raijmakers R, Pruijn GJ, Stoecklin G, Moroni C, Mann M, Karin M**. AU binding proteins recruit the exosome to degrade ARE-containing mRNAs. *Cell* 107: 451–64, 2001.

33. **Chen CY, Shyu AB**. AU-rich elements: characterization and importance in mRNA degradation. *Trends Biochem. Sci.* 20: 465–470, 1995.

34. **Chen Y, Azad MB, Gibson SB**. Superoxide is the major reactive oxygen species regulating autophagy. *Cell Death Differ.* 16: 1040–52, 2009.

35. **Chin ER, Olson EN, Richardson JA, Yang Q, Humphries C, Shelton JM, Wu H, Zhu W, Bassel-Duby R, Williams RS**. A calcineurin-dependent transcriptional pathway controls skeletal muscle fiber type. *Genes Dev.* 12: 2499–2509, 1998.

36. **Chin ER**. Intracellular Ca2+ signaling in skeletal muscle: decoding a complex message. *Exerc. Sport Sci. Rev.* 38: 76–85, 2010.

37. **Ciciliot S, Rossi AC, Dyar KA, Blaauw B, Schiaffino S**. Muscle type and fiber type specificity in muscle wasting. *Int. J. Biochem. Cell Biol.* 45: 2191–9, 2013.

38. **Clarke BA, Drujan D, Willis MS, Murphy LO, Corpina RA, Burova E, Rakhilin S V, Stitt TN, Patterson C, Latres E, Glass DJ**. The E3 Ligase MuRF1 degrades myosin heavy chain protein in dexamethasone-treated skeletal muscle. *Cell Metab.* 6: 376–85, 2007.

39. **Cogswell AM, Stevens RJ, Hood DA**. Properties of skeletal muscle mitochondria isolated from subsarcolemmal and intermyofibrillar regions. *Am. J. Physiol.* 264: C383–9, 1993.

40. **Cohen S, Brault JJ, Gygi SP, Glass DJ, Valenzuela DM, Gartner C, Latres E, Goldberg AL**. During muscle atrophy, thick, but not thin, filament components are degraded by MuRF1-dependent ubiquitylation. *J. Cell Biol.* 185: 1083–95, 2009.

41. **Connor MK, Bezborodova O, Escobar CP, Hood DA**. Effect of contractile activity on protein turnover in skeletal muscle mitochondrial subfractions. *J. Appl. Physiol.* 88: 1601–6, 2000.

42. **Connor MK, Irrcher I, Hood DA**. Contractile activity-induced transcriptional activation of cytochrome C involves Sp1 and is proportional to mitochondrial ATP synthesis in C2C12 muscle cells. *J. Biol. Chem.* 276: 15898–904, 2001.

43. **Connor MK, Takahashi M, Hood DA**. Tissue-specific stability of nuclear- and mitochondrially encoded mRNAs. *Arch. Biochem. Biophys.* 333: 103–8, 1996.

44. **Csukly K, Ascah A, Matas J, Gardiner PF, Fontaine E, Burelle Y**. Muscle denervation promotes opening of the permeability transition pore and increases the expression of cyclophilin D. *J. Physiol.* 574: 319–27, 2006.

45. **Cullen MJ, Pluskal MG**. Early changes in the ultrastructure of denervated rat skeletal muscle. *Exp. Neurol.* 56: 115–131, 1977.

46. **Cunningham JT, Rodgers JT, Arlow DH, Vazquez F, Mootha VK, Puigserver P**. mTOR controls mitochondrial oxidative function through a YY1-PGC-1alpha transcriptional complex. *Nature* 450: 736–40, 2007.

47. **D'souza D, Lai RYJ, Shuen M, Hood DA**. mRNA stability as a function of striated muscle oxidative capacity. *Am. J. Physiol. Regul. Integr. Comp. Physiol.* 303: R408–17, 2012.

48. **Davies KJA, Quintanilhat AT, Brooks GA, Packer L**. Free radicals and tissue damage produced by exercise. *Biochem. Biophys. Res. Commun.* 107: 1198–1205, 1982.

49. **Delp MD, Duan C**. Composition and size of type I, IIA, IID/X, and IIB fibers and citrate synthase activity of rat muscle. *J. Appl. Physiol.* 80: 261–70, 1996.

50. **Díaz-Moreno I, Hollingworth D, Kelly G, Martin S, García-Mayoral M, Briata P, Gherzi R, Ramos A**. Orientation of the central domains of KSRP and its implications for the interaction with the RNA targets. *Nucleic Acids Res.* 38: 5193–205, 2010.

51. **Doller A, Huwiler A, Muller R, Radeke HH, Pfeilschifter J, Eberhardt W**. Protein Kinase C alpha-dependent phosphorylation of the mRNA-stabilizing Factor HuR: implications for posttranscriptional regulation of cyclooxygenase-2. *Mol. Biol. Cell* 18: 2137–2148, 2007.

52. **Echtay KS**. Mitochondrial uncoupling proteins - what is their physiological role? *Free Radic. Biol. Med.* 43: 1351–71, 2007.

53. **Eichner LJ, Giguère V**. Estrogen related receptors (ERRs): a new dawn in transcriptional control of mitochondrial gene networks. *Mitochondrion* 11: 544–52, 2011.

54. **Eisner V, Csordás G, Hajnóczky G**. Interactions between sarco-endoplasmic reticulum and mitochondria in cardiac and skeletal muscle - pivotal roles in Ca^{2+} and reactive oxygen species signaling. *J. Cell Sci.* 126: 2965–78, 2013.

55. **Eley HL, Tisdale MJ**. Skeletal muscle atrophy, a link between depression of protein synthesis and increase in degradation. *J. Biol. Chem.* 282: 7087–97, 2007.

56. **Eulalio A, Huntzinger E, Izaurralde E**. Getting to the root of miRNA-mediated gene silencing. *Cell* 132: 9–14, 2008.

57. **Falkenberg M, Larsson NG, Gustafsson CM**. DNA replication and transcription in mammalian mitochondria. *Annu. Rev. Biochem.* 76: 679–99, 2007.

58. **Fan X, Hussien R, Brooks GA**. H2O2-induced mitochondrial fragmentation in C2C12 myocytes. *Free Radic. Biol. Med.* 49: 1646–54, 2010.

59. **Fan XC, Steitz JA**. Overexpression of HuR, a nuclear-cytoplasmic shuttling protein, increases the in vivo stability of ARE-containing mRNAs. *EMBO J.* 17: 3448–60, 1998.

60. **Ferree A, Shirihai OS**. Mitochondrial oxidative phosphorylation: nuclear-encoded genes, enzyme regulation, and pathophysiology. In: *Advances in Experimental medicine and biology*, edited by Kadenbach B. 2012, p. 13–40.

61. **Ferreira R, Vitorino R, Alves RMP, Appell HJ, Powers SK, Duarte JA, Amado F**. Subsarcolemmal and intermyofibrillar mitochondria proteome differences disclose functional specializations in skeletal muscle. *Proteomics* 10: 3142–54, 2010.

62. **Fielitz J, Kim M, Shelton JM, Latif S, Spencer JA, Glass DJ, Richardson JA, Bassel-Duby R, Olson EN**. Myosin accumulation and striated muscle myopathy result from the loss of muscle RING finger 1 and 3. *J. Clin. Invest.* 117: 2486–2495, 2007.

63. **Finol HJ, Lewis DM, Owens R**. The effects of denervation on contractile properties of rat skeletal muscle. *J. Physiol.* 319: 81–92, 1981.

64. **Fisher RP, Lisowsky T, Parisi MA, Clayton DA**. DNA wrapping and bending by a mitochondrial high mobility group-like transcriptional activator protein. *J. Biol. Chem.* 267: 3358–67, 1992.

65. **Freyssenet D, Di Carlo M, Hood DA**. Calcium-dependent regulation of cytochrome c gene expression in skeletal muscle cells: Identification of a protein kinase c-dependent pathway. *J. Biol. Chem.* 274: 9305–9311, 1999.

66. **Freyssenet D, Connor MK, Takahashi M, Hood DA**. Cytochrome c transcriptional activation and mRNA stability during contractile activity in skeletal muscle. *Am. J. Physiol.* 277: E26–32, 1999.

67. **Fridovich I**. Fundamental aspects of reactive oxygen species, or what's the matter with oxygen? *Ann. N. Y. Acad. Sci.* 893: 13–8, 1999.

68. **Furukawa R, Yamada Y, Matsushima Y, Goto YI, Harashima H**. The manner in which DNA is packaged with TFAM has an impact on transcription activation and inhibition. *FEBS Open Bio* 2: 145–50, 2012.

69. **Furuno K, Goodman M, Goldberg AL**. Role of different proteolytic systems in the degradation of muscle proteins during denervation atrophy. *J. Biol. Chem.* 265: 8550–8557, 1990.

70. **Gao M, Fritz DT, Ford LP, Wilusz J**. Interaction between a poly(A)-specific ribonuclease and the 5' cap influences mRNA deadenylation rates in vitro. *Mol. Cell* 5: 479–88, 2000.

71. **Garneau NL, Wilusz J, Wilusz CJ**. The highways and byways of mRNA decay. *Nat. Rev. Mol. Cell Biol.* 8: 113–26, 2007.

72. **Gauthier GF, Dunn RA**. Ultrastructural and cytochemical features of mammalian skeletal muscle fibers following denervation. *J. Cell. Sci.* 12: 525–547, 1973.

73. **Geiger PC, Bailey JP, Zhan WZ, Mantilla CB, Sieck GC**. Denervation-induced changes in myosin heavy chain expression in the rat diaphragm muscle. *J. Appl. Physiol.* 95: 611–9, 2003.

74. **Geisler S, Holmström KM, Skujat D, Fiesel FC, Rothfuss OC, Kahle PJ, Springer W**. PINK1/Parkin-mediated mitophagy is dependent on VDAC1 and p62/SQSTM1. *Nat. Cell Biol.* 12: 119–31, 2010.

75. **Gherzi R, Lee KY, Briata P, Wegmüller D, Moroni C, Karin M, Chen CY**. A KH domain RNA binding protein, KSRP, promotes ARE-directed mRNA turnover by recruiting the degradation machinery. *Mol. Cell* 14: 571–83, 2004.

76. **Gherzi R, Trabucchi M, Ponassi M, Ruggiero T, Corte G, Moroni C, Chen CY, Khabar KS, Andersen JS, Briata P**. The RNA-binding protein KSRP promotes decay of beta-catenin mRNA and is inactivated by PI3K-AKT signaling. *PLoS Biol.* 5: e5, 2007.

77. **Gleyzer N, Vercauteren K, Scarpulla RC**. Control of mitochondrial transcription specificity factors (TFB1M and TFB2M) by nuclear respiratory factors (NRF-1 and NRF-2) and PGC-1 family coactivators. *Mol. Cell. Biol.* 25: 1354–1366, 2005.

78. **Goldberg AL, Goodman HM**. Effects of disuse and denervation on amino acid transport by skeletal muscle. *Am. J. Physiol.* 216: 1116–9, 1969.

79. **Goldspink DF**. The influence of activity on muscle size and protein turnover. *J. Physiol.* 264: 283–296, 1977.

80. **Golstrohm AC, Wickens M**. Multifunctional deadenylase complexes diversify mRNA control. *Nat. Rev. Mol. Cell Biol.* 9: 337–44, 2008.

81. **Gomes A V, Waddell DS, Siu R, Stein M, Dewey S, Furlow JD, Bodine SC**. Upregulation of proteasome activity in muscle RING finger 1-null mice following denervation. *FASEB J.* 26: 2986–99, 2012.

82. **Gordon JW, Rungi AA, Inagaki H, Hood DA**. Effects of contractile activity on mitochondrial transcription factor A expression in skeletal muscle. *J. Appl. Physiol.* 90: 389–396, 2001.

83. **Halees AS, El-Badrawi R, Khabar KSA**. ARED Organism: expansion of ARED reveals AU-rich element cluster variations between human and mouse. *Nucleic Acids Res.* 36: D137–40, 2008.

84. **Hawke TJ, Garry DJ**. Myogenic satellite cells: physiology to molecular biology. *J. Appl. Physiol.* 91: 534–551, 2001.

85. **He C, Klionsky DJ**. Regulation mechanisms and signaling pathways of autophagy. *Annu. Rev. Genet.* 43: 67–93, 2009.

86. **Heck CS, Davis HL**. Effect of denervation and nerve extract on ultrastructure of muscle. *Exp. Neurol.* 100: 139–153, 1988.

87. **Hell K, Herrmann JM, Pratje E, Neupert W, Stuart RA**. Oxa1p, an essential component of the N-tail protein export machinery in mitochondria. *Proc. Natl. Acad. Sci. U. S. A.* 95: 2250–5, 1998.

88. **Hindi SM, Mishra V, Bhatnagar S, Tajrishi MM, Ogura Y, Yan Z, Burkly LC, Zheng TS, Kumar A**. Regulatory circuitry of TWEAK-Fn14 system and PGC-1α in skeletal muscle atrophy program. *FASEB J.* 28: 1398–1411, 2014.

89. **Hood DA**. Invited Review: contractile activity-induced mitochondrial biogenesis in skeletal muscle. *J. Appl. Physiol.* 90: 1137–57, 2001.

90. **Hoppeler H, Howald H, Conley K, Lindstedt SL, Claassen H, Vock P, Weibel ER**. Endurance training in humans: aerobic capacity and structure of skeletal muscle. *J. Appl. Physiol.* 59: 320–7, 1985.

91. **Hoppeler H**. Exercise-induced ultrastructural changes in skeletal muscle. *Int. J. Sports Med.* 7: 187–204, 1986.

92. **Hornberger TA, Hunter RB, Kandarian SC, Esser KA**. Regulation of translation factors during hindlimb unloading and denervation of skeletal muscle in rats. *Am. J. Physiol. Cell Physiol.* 281: C179–87, 2001.

93. **Houseley J, LaCava J, Tollervey D**. RNA-quality control by the exosome. *Nat. Rev. Mol. Cell Biol.* 7: 529–39, 2006.

94. **Huxley A**. Muscular Contraction. *Annu. Rev. Physiol.* 50: 1–16, 1988.

95. **Iqbal S, Ostojic O, Singh K, Joseph AM, Hood DA**. Expression of mitochondrial fission and fusion regulatory proteins in skeletal muscle during chronic use and disuse. *Muscle Nerve* 48: 963–70, 2013.

96. **Irrcher I, Adhihetty PJ, Sheehan T, Joseph AM, Hood DA**. PPARγ coactivator-1α expression during thyroid hormone- and contractile activity-induced mitochondrial adaptations. *Am. J. Physiol. Cell Physiol.* 284: C1669–1677, 2003.

97. **Irrcher I, Hood DA**. Regulation of Egr-1, SRF, and Sp1 mRNA expression in contracting skeletal muscle cells. *J. Appl. Physiol.* 97: 2207–2213, 2004.

98. **Irrcher I, Ljubicic V, Hood DA**. Interactions between ROS and AMP kinase activity in the regulation of PGC-1α transcription in skeletal muscle cells. *Am. J. Physiol. Cell Physiol.* 3: C116–123, 2009.

99. **Jackson RJ, Standart N**. Do the poly(A) tail and 3' untranslated region control mRNA translation? *Cell* 62: 15–24, 1990.

100. **Jäger S, Handschin C, St-Pierre J, Spiegelman BM**. AMP-activated protein kinase (AMPK) action in skeletal muscle via direct phosphorylation of PGC-1alpha. *Proc. Natl. Acad. Sci. U. S. A.* 104: 12017–22, 2007.

101. **Joseph AM, Hood DA**. Plasticity of TOM complex assembly in skeletal muscle mitochondria in response to chronic contractile activity. *Mitochondrion* 12: 305–12, 2012.

102. **Kanki T, Nakayama H, Sasaki N, Takio K, Alam TI, Hamasaki N, Kang D**. Mitochondrial nucleoid and transcription factor A. *Ann. N. Y. Acad. Sci.* 1011: 61–68, 2004.

103. **Kedar V, McDonough H, Arya R, Li HH, Rockman HA, Patterson C**. Muscle-specific RING finger 1 is a bona fide ubiquitin ligase that degrades cardiac troponin I. *Proc. Natl. Acad. Sci. U. S. A.* 101: 18135–40, 2004.

104. **Keene JD, Tenenbaum SA**. Eukaryotic mRNPs may represent posttranscriptional operons. *Mol. Cell* 9: 1161–7, 2002.

105. **Keil M, Bareth B, Woellhaf MW, Peleh V, Prestele M, Rehling P, Herrmann JM**. Oxa1-ribosome complexes coordinate the assembly of cytochrome C oxidase in mitochondria. *J. Biol. Chem.* 287: 34484–93, 2012.

106. **Kelly DP, Scarpulla RC**. Transcriptional regulatory circuits controlling mitochondrial biogenesis and function. *Genes Dev.* 18: 357–68, 2004.

107. **Kirkland RA, Adibhatla RM, Hatcher JF, Franklin JL**. Loss of cardiolipin and mitochondria during programmed neuronal death: evidence of a role for lipid peroxidation and autophagy. *Neuroscience* 115: 587–602, 2002.

108. **Koopman WJH, Verkaart S, Visch HJ, van der Westhuizen FH, Murphy MP, van den Heuvel LWPJ, Smeitink JAM, Willems PHGM**. Inhibition of complex I of the electron transport chain causes O2-·-mediated mitochondrial outgrowth. *Am. J. Physiol. Cell Physiol.* 288: C1440–1450, 2005.

109. **Koves TR, Noland RC, Bates AL, Henes ST, Muoio DM, Cortright RN**. Subsarcolemmal and intermyofibrillar mitochondria play distinct roles in regulating skeletal muscle fatty acid metabolism. *Am. J. Physiol. Cell Physiol.* 288: C1074–1082, 2005.

110. **Kowaltowski AJ, de Souza-Pinto NC, Castilho RF, Vercesi AE**. Mitochondria and reactive oxygen species. *Free Radic. Biol. Med.* 47: 333–43, 2009.

111. **Krieger DA, Tate CA, McMillin-Wood J, Booth FW**. Populations of rat skeletal muscle mitochondria after exercise and immobilization. *J. Appl. Physiol.* 48: 23–28, 1980.

112. **Kukat C, Wurm CA, Spåhr H, Falkenberg M, Larsson NG**. Super-resolution microscopy reveals that mammalian mitochondrial nucleoids have a uniform size and frequently contain a single copy of mtDNA. *Proc. Natl. Acad. Sci. U. S. A.* 108: 13534–13539, 2011.

113. **Kumar A, Bhatnagar S, Paul PK**. TWEAK and TRAF6 regulate skeletal muscle atrophy. *Curr. Opin. Clin. Nutr. Metab. Care* 15: 233–239, 2012.

114. **Kuyumcu-Martinez NM, Wang GS, Cooper TA**. Increased steady-state levels of CUGBP1 in myotonic dystrophy 1 are due to PKC-mediated hyperphosphorylation. *Mol. Cell* 28: 68–78, 2007.

115. **Lai RYJ, Ljubicic V, D'souza D, Hood DA**. Effect of chronic contractile activity on mRNA stability in skeletal muscle. *Am. J. Physiol. Cell Physiol.* 299: C155–163, 2010.

116. **Lal A, Mazan-Mamczarz K, Kawai T, Yang X, Martindale JL, Gorospe M**. Concurrent versus individual binding of HuR and AUF1 to common labile target mRNAs. *EMBO J.* 23: 3092–102, 2004.

117. **Laplante M, Sabatini DM**. mTOR signaling in growth control and disease. *Cell* 149: 274–93, 2012.

118. **Larsson NG, Wang J, Wilhelmsson H, Oldfors A, Rustin P, Lewandowski M, Barsh GS, Clayton DA**. Mitochondrial transcription factor A is necessary for mtDNA maintenance and embryogenesis in mice. *Nature* 18: 231–236, 1998.

119. **Lazarou M, Jin SM, Kane LA, Youle RJ**. Role of PINK1 binding to the TOM complex and alternate intracellular membranes in recruitment and activation of the E3 ligase Parkin. *Dev. Cell* 22: 320–33, 2012.

120. **Lebedeva S, Jens M, Theil K, Schwanhäusser B, Selbach M, Landthaler M, Rajewsky N**. Transcriptome-wide analysis of regulatory interactions of the RNA-binding protein HuR. *Mol. Cell* 43: 340–52, 2011.

121. **Lecker SH, Goldberg AL, Mitch WE**. Protein degradation by the ubiquitin-proteasome pathway in normal and disease states. *J. Am. Soc. Nephrol.* 17: 1807–19, 2006.

122. **Lecker SH, Jagoe RT, Gilbert A, Gomes M, Baracos V, Bailey J, Price SR, Mitch WE, Goldberg AL**. Multiple types of skeletal muscle atrophy involve a common program of changes in gene expression. *FASEB J.* 18: 39–51, 2004.

123. **Lee HC, Yin PH, Chi CW, Wei YH**. Increase in mitochondrial mass in human fibroblasts under oxidative stress during replicative cell senescence. *J. Biomed. Sci.* 9: 517–526, 2002.

124. **Lee HC, Yin PH, Lu CY, Chi CW, Wei YH**. Increase of mitochondria and mitochondrial DNA in response to oxidative stress in human cells. *Biochem. J.* 348: 425–32, 2000.

125. **Lee JE, Lee JY, Wilusz J, Tian B, Wilusz CJ**. Systematic analysis of cis-elements in unstable mRNAs demonstrates that CUGBP1 is a key regulator of mRNA decay in muscle cells. *PLoS One* 5: e11201, 2010.

126. **Lee WJ, Kim M, Park HS, Kim HS, Jeon MJ, Oh KS, Koh EH, Won JC, Kim M-S, Oh GT, Yoon M, Lee KU, Park JY**. AMPK activation increases fatty acid oxidation in skeletal muscle by activating PPARalpha and PGC-1. *Biochem. Biophys. Res. Commun.* 340: 291–5, 2006.

127. **Legros F, Malka F, Frachon P, Lombès A, Rojo M**. Organization and dynamics of human mitochondrial DNA. *J. Cell Sci.* 117: 2653–62, 2004.

128. **Lerin C, Rodgers JT, Kalume DE, Kim S, Pandey A, Puigserver P**. GCN5 acetyltransferase complex controls glucose metabolism through transcriptional repression of PGC-1alpha. *Cell Metab.* 3: 429–38, 2006.

129. **Li H, Park S, Kilburn B, Jelinek MA, Henschen-Edman A, Aswad DW, Stallcup MR, Laird-Offringa IA**. Lipopolysaccharide-induced methylation of HuR, an mRNA-stabilizing protein, by CARM1. *J. Biol. Chem.* 277: 44623–30, 2002.

130. **Lin J, Wu H, Tarr PT, Zhang CY, Wu Z, Boss O, Michael LF, Puigserver P, Isotani E, Olson EN, Lowell BB, Bassel-Duby R, Spiegelman BM**. Transcriptional co-activator PGC-1alpha drives the formation of slow-twitch muscle fibres. *Nature* 418: 797–801, 2002.

131. **Lipsky NG, Pedersen PL**. Mitochondrial turonver in animals cells: Half-lives of mitochondria and mitochondrial subfractions of rat liver based on [14C]bicarbonate incorporation. *J. Biol. Chem.* 256: 8652–8657, 1981.

132. **Litonin D, Sologub M, Savkina M, Anikin M, Gustafsson CM**. Human mitochondrial transcription revisited: Only Tfam and Tfb2m are required for the transcription of mitochondrial genes in vitro. *J. Biol. Chem.* 285: 18129–18133, 2010.

133. **Liu H, Rodgers ND, Jiao X, Kiledjian M**. The scavenger mRNA decapping enzyme DcpS is a member of the HIT family of pyrophosphatases. *EMBO J.* 21: 4699–708, 2002.

134. **Liu J, Peng Y, Feng Z, Shi W, Qu L, Li Y, Liu J, Long J**. Reloading functionally ameliorates disuse-induced muscle atrophy by reversing mitochondrial dysfunction, and similar benefits are gained by administering a combination of mitochondrial nutrients. *Free Radic. Biol. Med.* 69C: 116–128, 2014.

135. **Lokireddy S, Wijesoma IW, Sze SK, McFarlane C, Kambadur R, Sharma M**. Identification of atrogin-1-targeted proteins during the myostatin-induced skeletal muscle wasting. *Am. J. Physiol. Cell Physiol.* 303: C512–29, 2012.

136. **Lokireddy S, Wijesoma IW, Teng S, Bonala S, Gluckman PD, McFarlane C, Sharma M, Kambadur R**. The ubiquitin ligase Mul1 induces mitophagy in skeletal muscle in response to muscle-wasting stimuli. *Cell Metab.* 16: 613–24, 2012.

137. **Lu B, Lee J, Nie X, Li M, Morozov YI, Venkatesh S, Bogenhagen DF, Temiakov D, Suzuki CK**. Phosphorylation of human TFAM in mitochondria impairs DNA binding and promotes degradation by the AAA+ Lon protease. *Mol. Cell* 49: 121–32, 2013.

138. **Lu DX, Huang SK, Carlson BM**. Electron microscopic study of long-term denervated rat skeletal muscle. *Anat. Rec.* 248: 355–65, 1997.

139. **Lu JY, Schneider RJ**. Tissue distribution of AU-rich mRNA-binding proteins involved in regulation of mRNA decay. *J. Biol. Chem.* 279: 12974–9, 2004.

140. **Ma WJ, Cheng S, Campbell C, Wright A, Furneaux H**. Cloning and characterization of HuR, a ubiquitously expressed Elav-like protein. *J. Biol. Chem.* 271: 8144–8151, 1996.

141. **Madrazo JA, Kelly DP**. The PPAR trio: regulators of myocardial energy metabolism in health and disease. *J. Mol. Cell. Cardiol.* 44: 968–75, 2008.

142. **Mammucari C, Milan G, Romanello V, Masiero E, Rudolf R, Del Piccolo P, Burden SJ, Di Lisi R, Sandri C, Zhao J, Goldberg AL, Schiaffino S, Sandri M**. FoxO3 controls autophagy in skeletal muscle in vivo. *Cell Metab.* 6: 458–71, 2007.

143. **Maniura-Weber K, Goffart S, Garstka HL, Montoya J, Wiesner RJ**. Transient overexpression of mitochondrial transcription factor A (TFAM) is sufficient to stimulate mitochondrial DNA transcription, but not sufficient to increase mtDNA copy number in cultured cells. *Nucleic Acids Res.* 32: 6015–27, 2004.

144. **Masiero E, Agatea L, Mammucari C, Blaauw B, Loro E, Komatsu M, Metzger D, Reggiani C, Schiaffino S, Sandri M**. Autophagy is required to maintain muscle mass. *Cell Metab.* 10: 507–15, 2009.

145. **Matsushima Y, Goto Y, Kaguni LS**. Mitochondrial Lon protease regulates mitochondrial DNA copy number and transcription by selective degradation of mitochondrial transcription factor A (TFAM). *Proc. Natl. Acad. Sci. U. S. A.* 107: 18410–18415, 2010.

146. **McArdle F, Pattwell DM, Vasilaki A, McArdle A, Jackson MJ**. Intracellular generation of reactive oxygen species by contracting skeletal muscle cells. *Free Radic. Biol. Med.* 39: 651–7, 2005.

147. **Mcgee SL, Hargreaves M**. Exercise and myocyte enhancer factor 2 regulation in human skeletal muscle. *Diabetes* 53: 1208–1214, 2004.

148. **Midrio M**. The denervated muscle: facts and hypotheses. A historical review. *Eur. J. Appl. Physiol.* 98: 1–21, 2006.

149. **Minczuk M, He J, Duch AM, Ettema TJ, Chlebowski A, Dzionek K, Nijtmans LGJ, Huynen MA, Holt IJ**. TEFM (c17orf42) is necessary for transcription of human mtDNA. *Nucleic Acids Res.* 39: 4284–99, 2011.

150. **Ming X, Stoecklin G, Lu M, Looser R, Moroni C**. Parallel and independent regulation of interleukin-3 mRNA turnover by phosphatidylinositol 3-kinase and p38 mitogen-activated protein kinase. *Mol. Cell. Biol.* 21: 5778–5789, 2001.

151. **Minich WB, Balasta ML, Goss DJ, Rhoads RE**. Chromatographic resolution of in vivo phosphorylated and nonphosphorylated eukaryotic translation initiation factor eIF-4E: increased cap affinity of the phosphorylated form. *Proc. Natl. Acad. Sci. U. S. A.* 91: 7668–72, 1994.

152. **Mittal A, Bhatnagar S, Kumar A, Lach-Trifilieff E, Wauters S, Li H, Makonchuk DY, Glass DJ, Kumar A**. The TWEAK-Fn14 system is a critical regulator of denervation-induced skeletal muscle atrophy in mice. *J. Cell Biol.* 188: 833–49, 2010.

153. **Miwa S, Lawless C, von Zglinicki T**. Mitochondrial turnover in liver is fast in vivo and is accelerated by dietary restriction: application of a simple dynamic model. *Aging Cell* 7: 920–3, 2008.

154. **Montoya J, Christianson T, Levens D, Rabinowitz M, Attardi G**. Identification of initiation sites for heavy-strand and light-strand transcription in human mitochondrial DNA. *Proc. Natl. Acad. Sci. U. S. A.* 79: 7195–9, 1982.

155. **Moraes KCM, Wilusz CJ, Wilusz J**. CUG-BP binds to RNA substrates and recruits PARN deadenylase. *RNA* 12: 1084–1091, 2006.

156. **Morey-Holton ER, Globus RK**. Hindlimb unloading of growing rats: a model for predicting skeletal changes during space flight. *Bone* 22: 83S–88S, 1998.

157. **Morey-Holton ER, Globus RK**. Hindlimb unloading rodent model: technical aspects. *J. Appl. Physiol.* 92: 1367–77, 2002.

158. **Moro F, Sirrenberg C, Schneider HC, Neupert W, Brunner M**. The TIM17.23 preprotein translocase of mitochondria: composition and function in protein transport into the matrix. *EMBO J.* 18: 3667–75, 1999.

159. **Mukherjee D, Gao M, O'Connor JP, Raijmakers R, Pruijn G, Lutz CS, Wilusz J**. The mammalian exosome mediates the efficient degradation of mRNAs that contain AU-rich elements. *EMBO J.* 21: 165–74, 2002.

160. **Muller FL, Song W, Jang YC, Liu Y, Sabia M, Richardson A, Van Remmen H**. Denervation-induced skeletal muscle atrophy is associated with increased mitochondrial ROS production. *Am. J. Physiol. Regul. Integr. Comp. Physiol.* 293: R1159–1168, 2007.

161. **Musacchia XJ, Steffen JM, Fell RD**. Disuse atrophy of skeletal muscle: animal models. *Exerc. Sport Sci. Rev.* 16: 61–87, 1988.

162. **Narendra D, Tanaka A, Suen D, Youle RJ**. Parkin is recruited selectively to impaired mitochondria and promotes their autophagy. *J. Cell Biol.* 183: 795–803, 2008.

163. **Narendra DP, Jin SM, Tanaka A, Suen D, Gautier CA, Shen J, Cookson MR, Youle RJ**. PINK1 is selectively stabilized on impaired mitochondria to activate Parkin. *PLoS Biol.* 8: e1000298, 2010.

164. **Nemoto S, Fergusson MM, Finkel T**. SIRT1 functionally interacts with the metabolic regulator and transcriptional coactivator PGC-1alpha. *J. Biol. Chem.* 280: 16456–60, 2005.

165. **Neupert W, Herrmann JM**. Translocation of proteins into mitochondria. *Annu. Rev. Biochem.* 76: 723–49, 2007.

166. **Ngo HB, Kaiser JT, Chan DC**. The mitochondrial transcription and packaging factor Tfam imposes a U-turn on mitochondrial DNA. *Nat. Struct. Mol. Biol.* 18: 1290–6, 2011.

167. **Ngo HB, Lovely GA, Phillips R, Chan DC**. Distinct structural features of TFAM drive mitochondrial DNA packaging versus transcriptional activation. *Nat. Commun.* 5: 3077, 2014.

168. **O'Leary MF, Vainshtein A, Iqbal S, Ostojic O, Hood DA**. Adaptive plasticity of autophagic proteins to denervation in aging skeletal muscle. *Am. J. Physiol. Cell Physiol.* 304: C422–30, 2013.

169. **O'Leary MFN, Hood DA**. Denervation-induced oxidative stress and autophagy signaling in muscle. *Autophagy* 5: 230–231, 2009.

170. **O'Leary MFN, Vainshtein A, Carter HN, Zhang Y, Hood DA**. Denervation-induced mitochondrial dysfunction and autophagy in skeletal muscle of apoptosis-deficient animals. *Am. J. Physiol. Cell Physiol.* 303: C447–54, 2012.

171. **Ojala D, Montoya J, Attardi G**. tRNA punctuation model of RNA processing in human mitochondria. *Nature* 290: 470–474, 1981.

172. **Okamoto K, Brinker A, Paschen SA, Moarefi I, Hayer-Hartl M, Neupert W, Brunner M**. The protein import motor of mitochondria: a targeted molecular ratchet driving unfolding and translocation. *EMBO J.* 21: 3659–71, 2002.

173. **Ornatsky OI, Connor MK, Hood DA**. Expression of stress proteins and mitochondrial chaperonins in chronically stimulated skeletal muscle. *Biochem. J.* 311: 119–23, 1995.

174. **Ostojic O, O'Leary MFN, Singh K, Menzies KJ, Vainshtein A, Hood DA**. The effects of chronic muscle use and disuse on cardiolipin metabolism. *J. Appl. Physiol.* 114: 444–52, 2013.

175. **Parker R, Sheth U**. P bodies and the control of mRNA translation and degradation. *Mol. Cell* 25: 635–46, 2007.

176. **Pastore S, Hood DA**. Endurance training ameliorates the metabolic and performance characteristics of circadian Clock mutant mice. *J. Appl. Physiol.* 114: 1076–84, 2013.

177. **Patterson MF, Stephenson GMM, Stephenson DG**. Denervation produces different single fiber phenotypes in fast- and slow-twitch hindlimb muscles of the rat. *Am. J. Physiol. Cell Physiol.* 291: C518–528, 2006.

178. **Paul PK, Gupta SK, Bhatnagar S, Panguluri SK, Darnay BG, Choi Y, Kumar A**. Targeted ablation of TRAF6 inhibits skeletal muscle wasting in mice. *J. Cell Biol.* 191: 1395–411, 2010.

179. **Pellegrino C, Franzini C**. An electron microscope study of denervation atrophy in red and white skeletal muscle fibers. *J. Cell Biol.* 17: 327–349, 1963.

180. **Peng SS, Chen CY, Xu N, Shyu AB**. RNA stabilization by the AU-rich element binding protein, HuR, an ELAV protein. *EMBO J.* 17: 3461–70, 1998.

181. **Pette D, Staron RS**. Myosin isoforms, muscle fiber types, and transitions. *Microsc. Res. Tech.* 50: 500–9, 2000.

182. **Philips A V, Timchenko LT, Cooper TA**. Disruption of splicing regulated by a CUG-regulated protein in myotonic dystrophy. *Science (80-.).* 280: 737–741, 1998.

183. **Picard M, White K, Turnbull DM**. Mitochondrial morphology, topology, and membrane interactions in skeletal muscle: a quantitative three-dimensional electron microscopy study. *J. Appl. Physiol.* 114: 161–71, 2013.

184. **Piccirillo R, Goldberg AL**. The p97/VCP ATPase is critical in muscle atrophy and the accelerated degradation of muscle proteins. *EMBO J.* 31: 3334–50, 2012.

185. **Pilegaard H, Saltin B, Neufer PD**. Exercise induces transient transcriptional activation of the PGC-1 gene in human skeletal muscle. *J. Physiol.* 546: 851–858, 2003.

186. **Poole AC, Thomas RE, Yu S, Vincow ES, Pallanck L**. The mitochondrial fusion-promoting factor mitofusin is a substrate of the PINK1/parkin pathway. *PLoS One* 5: e10054, 2010.

187. **Primeau AJ, Adhihetty PJ, Hood DA**. Apoptosis in heart and skeletal muscle. *Can. J. Appl. Physiol.* 27: 349–95, 2002.

188. **Puigserver P, Adelmant G, Wu Z, Fan M, Xu J, O'Malley B, Spiegelman BM**. Activation of PPAR coactivator-1 through transcription factor docking. *Science (80-.).* 286: 1368–1371, 1999.

189. **Puigserver P, Rhee J, Lin J, Wu Z, Yoon JC, Zhang C, Krauss S, Mootha VK, Lowell BB, Spiegelman BM**. Cytokine Stimulation of Energy Expenditure through p38 MAP Kinase Activation of PPARγ Coactivator-1. *Mol. Cell* 8: 971–982, 2001.

190. **Quy PN, Kuma A, Pierre P, Mizushima N**. Proteasome-dependent activation of mammalian target of rapamycin complex 1 (mTORC1) is essential for autophagy suppression and muscle remodeling following denervation. *J. Biol. Chem.* 288: 1125–34, 2013.

191. **Raffaello A, Laveder P, Romualdi C, Bean C, Toniolo L, Germinario E, Megighian A, Danieli-Betto D, Reggiani C, Lanfranchi G**. Denervation in murine fast-twitch muscle: short-term physiological changes and temporal expression profiling. *Physiol. Genomics* 25: 60–74, 2006.

192. **Raghavan A, Ogilvie RL, Reilly C, Abelson ML, Raghavan S, Vasdewani J, Krathwohl M, Bohjanen PR**. Genome-wide analysis of mRNA decay in resting and activated primary human T lymphocytes. *Nucleic Acids Res.* 30: 5529–38, 2002.

193. **Rattenbacher B, Beisang D, Wiesner DL, Jeschke JC, von Hohenberg M, St Louis-Vlasova IA, Bohjanen PR**. Analysis of CUGBP1 targets identifies GU-repeat sequences that mediate rapid mRNA decay. *Mol. Cell. Biol.* 30: 3970–80, 2010.

194. **Riva A, Tandler B, Loffredo F, Vazquez E, Hoppel C**. Structural differences in two biochemically defined populations of cardiac mitochondria. *Am. J. Physiol. Hear. Circ. Physiol.* 289: H868–872, 2005.

195. **Röckl KSC, Witczak CA, Goodyear LJ**. Signaling mechanisms in skeletal muscle: acute responses and chronic adaptations to exercise. *IUBMB Life* 60: 145–53, 2008.

196. **Romanello V, Guadagnin E, Gomes L, Roder I, Sandri C, Petersen Y, Milan G, Masiero E, Del Piccolo P, Foretz M, Scorrano L, Rudolf R, Sandri M**. Mitochondrial fission and remodelling contributes to muscle atrophy. *EMBO J.* 29: 1774–85, 2010.

197. **Rubio-Cosials A, Sidow JF, Jiménez-Menéndez N, Fernández-Millán P, Montoya J, Jacobs HT, Coll M, Bernadó P, Solà M**. Human mitochondrial transcription factor A induces a U-turn structure in the light strand promoter. *Nat. Struct. Mol. Biol.* 18: 1281–9, 2011.

198. **Sacheck JM, Hyatt JP, Raffaello A, Jagoe RT, Roy RR, Edgerton VR, Lecker SH, Goldberg AL**. Rapid disuse and denervation atrophy involve transcriptional changes similar to those of muscle wasting during systemic diseases. *FASEB J.* 21: 140–55, 2007.

199. **Sacheck JM, Ohtsuka A, McLary SC, Goldberg AL**. IGF-I stimulates muscle growth by suppressing protein breakdown and expression of atrophy-related ubiquitin ligases, atrogin-1 and MuRF1. *Am. J. Physiol. Endocrinol. Metab.* 287: E591–601, 2004.

200. **Saleem A, Hood DA**. Acute exercise induces tumour suppressor protein p53 translocation to the mitochondria and promotes a p53-Tfam-mitochondrial DNA complex in skeletal muscle. *J. Physiol.* 591: 3625–36, 2013.

201. **Sandri M, Lin J, Handschin C, Yang W, Arany ZP, Lecker SH, Goldberg AL, Spiegelman BM**. PGC-1alpha protects skeletal muscle from atrophy by suppressing FoxO3 action and atrophy-specific gene transcription. *Proc. Natl. Acad. Sci. U. S. A.* 103: 16260–5, 2006.

202. **Sandri M, Sandri C, Gilbert A, Skurk C, Calabria E, Picard A, Walsh K, Schiaffino S, Lecker SH, Goldberg AL**. Foxo transcription factors induce the atrophy-related ubiquitin ligase atrogin-1 and cause skeletal muscle atrophy. *Cell* 117: 399–412, 2004.

203. **Sandri M**. Apoptotic signaling in skeletal muscle fibers during atrophy. *Curr. Opin. Clin. Nutr. Metab. Care* 5: 249–53, 2002.

204. **Satoh M, Kuroiwa T**. Organization of multiple nucleoids and DNA molecules in mitochondria of a human cell. *Exp. Cell Res.* 196: 137–140, 1991.

205. **Sayir F, Kavak S, Meral I, Demir H, Cengiz N, Çobanoğlu U**. Effect of crush and axotomy of phrenic nerves on oxidative stress in diaphragm muscle of rats. *Muscle Nerve* 45: 412–5, 2012.

206. **Scarpulla RC**. Transcriptional paradigms in mammalian mitochondrial biogenesis and function. *Physiol. Rev.* 88: 611–638, 2008.

207. **Scherz-Shouval R, Shvets E, Fass E, Shorer H, Gil L, Elazar Z**. Reactive oxygen species are essential for autophagy and specifically regulate the activity of Atg4. *EMBO J.* 26: 1749–60, 2007.

208. **Schiaffino S, Reggiani C**. Fiber types in mammalian skeletal muscles. *Physiol. Rev.* 91: 1447–531, 2011.

209. **Schulte L, Peters D, Taylor J, Kandarian S**. Sarcoplasmic in denervated reticulum skeletal Ca2+ pump expression muscle. *Am. J. Physiol. Cell Physiol.* 267: C617–622, 1994.

210. **Schwerzmann K, Hoppeler H, Kayar SR, Weibel ER**. Oxidative capacity of muscle and mitochondria: correlation of physiological, biochemical, and morphometric characteristics. *Proc. Natl. Acad. Sci. U. S. A.* 86: 1583–7, 1989.

211. **Senf SM, Dodd SL, Judge AR**. FOXO signaling is required for disuse muscle atrophy and is directly regulated by Hsp70. *Am. J. Physiol. Cell Physiol.* 298: C38–45, 2010.

212. **Senf SM, Sandesara PB, Reed SA, Judge AR**. p300 acetyltransferase activity differentially regulates the localization and activity of the FOXO homologues in skeletal muscle. *Am. J. Physiol. Cell Physiol.* 300: C1490–1501, 2011.

213. **Shi Y, Dierckx A, Wanrooij PH, Wanrooij S, Larsson NG, Wilhelmsson LM, Falkenberg M, Gustafsson CM**. Mammalian transcription factor A is a core component of the mitochondrial transcription machinery. *Proc. Natl. Acad. Sci. U. S. A.* 109: 16510–5, 2012.

214. **Shyu AB, Belasco JG, Greenberg ME**. Two distinct destabilizing elements in the c-fos message trigger deadenylation as a first step in rapid mRNA decay. *Genes Dev.* 5: 221–231, 1991.

215. **Sieck GC, Zhan W, Han YS, Prakash YS**. Effect of denervation on ATP consumption rate of diaphragm muscle fibers. *J. Appl. Physiol.* 103: 858–866, 2007.

216. **Singh K, Hood DA**. Effect of denervation-induced muscle disuse on mitochondrial protein import. *Am. J. Physiol. Cell Physiol.* 300: C138–145, 2011.

217. **Sirrenberg C, Bauer MF, B G, Neupert W, Brunner M**. Import of carrier proteins into the mitochondrial inner membrane mediated by Tim22. *Nature* 384: 582–585, 1996.

218. **Siu PM, Alway SE**. Mitochondria-associated apoptotic signalling in denervated rat skeletal muscle. *J. Physiol.* 565: 309–23, 2005.

219. **Stitt TN, Drujan D, Clarke BA, Panaro F, Timofeyva Y, Kline WO, Gonzalez M, Yancopoulos GD, Glass DJ**. The IGF-1/PI3K/Akt pathway protects expression of muscle atrophy-induced ubiquitin ligases by inhibiting FOXO transcription factors. *Mol. Cell* 14: 395–403, 2004.

220. **Takahashi M, Chesley A, Freyssenet D, Hood DA**. Contractile activity-induced adaptations in the mitochondrial protein import system. *Am. J. Physiol.* 274: C1380–7, 1998.

221. **Takahashi M, Hood DA**. Protein import into subsarcolemmal and intermyofibrillar muscle mitochondria: differential import regulation in distinct subcellular regions. *J. Biol. Chem.* 271: 27285–27291, 1996.

222. **Tanaka A, Cleland MM, Xu S, Narendra DP, Suen D, Karbowski M, Youle RJ**. Proteasome and p97 mediate mitophagy and degradation of mitofusins induced by Parkin. *J. Cell Biol.* 191: 1367–80, 2010.

223. **Tawa NE, Odessey R, Goldberg AL**. Inhibitors of the proteasome reduce the accelerated proteolysis in atrophying rat skeletal muscles. *J. Clin. Invest.* 100: 197–203, 1997.

224. **Taylor AB, Smith BS, Kitada S, Kojima K, Miyaura H, Otwinowski Z, Ito A, Deisenhofer J**. Crystal structures of mitochondrial processing peptidase reveal the mode for specific cleavage of import signal sequences. *Structure* 9: 615–25, 2001.

225. **Taylor RW, Turnbull DM**. Mitochondrial DNA mutations in human disease. *Nat. Rev. Genet.* 6: 389–402, 2005.

226. **Terjung RL**. The turnover of cytochrome c in different skeletal-muscle fibre types of the rat. *Biochem. J.* 178: 569–74, 1979.

227. **Teyssier C, Ma H, Emter R, Kralli A, Stallcup MR**. Activation of nuclear receptor coactivator PGC-1alpha by arginine methylation. *Genes Dev.* 19: 1466–73, 2005.

228. **Timchenko LT, Miller JW, Timchenko NA, DeVore DR, Datar K V, Lin L, Roberts R, Caskey CT, Swanson MS**. Identification of a (CUG)n triplet repeat RNA-binding protein and its expression in myotonic dystrophy. *Nucleic Acids Res.* 24: 4407–14, 1996.

229. **Timchenko NA, Wang G, Timchenko LT**. RNA CUG-binding protein 1 increases translation of 20-kDa isoform of CCAAT/enhancer-binding protein beta by interacting with the alpha and beta subunits of eukaryotic initiation translation factor 2. *J. Biol. Chem.* 280: 20549–57, 2005.

230. **Tomanek RJ, Lund DD**. Degeneration of different types of skeletal muscle fibres. I. Denervation. *J. Anat.* 116: 395–407, 1973.

231. **Turrens JF**. Mitochondrial formation of reactive oxygen species. *J. Physiol.* 552: 335–44, 2003.

232. **Twig G, Elorza A, Molina AJA, Mohamed H, Wikstrom JD, Walzer G, Stiles L, Haigh SE, Katz S, Las G, Alroy J, Wu M, Py BF, Yuan J, Deeney JT, Corkey BE, Shirihai OS**. Fission and selective fusion govern mitochondrial segregation and elimination by autophagy. *EMBO J.* 27: 433–46, 2008.

233. **Tyml K, Mathieu-Costello O, Cheng L, Noble EG**. Differential microvascular response to disuse in rat hindlimb skeletal muscles. *J. Appl. Physiol.* 87: 1496–505, 1999.

234. **Uguccioni G, Hood DA**. The importance of PGC-1α in contractile activity-induced mitochondrial adaptations. *Am. J. Physiol. Endocrinol. Metab.* 300: E361–371, 2011.

235. **Vavvas D, Apazidis A, Saha AK, Gamble J, Patel A, Kemp BE, Witters LA, Ruderman NB**. Contraction-induced changes in acetyl-CoA carboxylase and 5'-AMP-activated kinase in skeletal muscle. *J. Biol. Chem.* 20: 13255–13261, 1997.

236. **Vega RB, Huss JM, Kelly DP**. The coactivator PGC-1 cooperates with peroxisome proliferator-activated receptor alpha in transcriptional control of nuclear genes encoding mitochondrial fatty acid oxidation enzymes. *Mol. Cell. Biol.* 20: 1868–1876, 2000.

237. **Vlasova IA, Tahoe NM, Fan D, Larsson O, Rattenbacher B, Sternjohn JR, Vasdewani J, Karypis G, Reilly CS, Bitterman PB, Bohjanen PR**. Conserved GU-rich elements mediate mRNA decay by binding to CUG-binding protein 1. *Mol. Cell* 29: 263–70, 2008.

238. **Wagatsuma A, Kotake N, Mabuchi K, Yamada S**. Expression of nuclear-encoded genes involved in mitochondrial biogenesis and dynamics in experimentally denervated muscle. *J. Physiol. Biochem.* 67: 359–70, 2011.

239. **Wagatsuma A, Osawa T**. Time course of changes in angiogenesis-related factors in denervated muscle. *Acta Physiol. (Oxf).* 187: 503–9, 2006.

240. **Wallace DC**. Diseases of the mtDNA. *Annu. Rev. Biochem.* 61: 1175–1212, 1992.

241. **Wallace DC**. A mitochondrial paradigm of metabolic and degenerative diseases, aging, and cancer: a dawn for evolutionary medicine. *Annu. Rev. Genet.* 39: 359–407, 2005.

242. **Wallberg AE, Yamamura S, Malik S, Spiegelman BM, Roeder RG**. Coordination of p300-mediated chromatin remodeling and TRAP/mediator function through coactivator PGC-1alpha. *Mol. Cell* 12: 1137–49, 2003.

243. **Walsh C, Barrow S, Voronina S, Chvanov M, Petersen OH, Tepikin A**. Modulation of calcium signalling by mitochondria. *Biochim. Biophys. Acta* 1787: 1374–82, 2009.

244. **Wang W, Fan J, Yang X, Fürer-Galban S, Lopez de Silanes I, Von Kobbe C, Guo J, Georas SN, Foufelle F, Hardie DG, Carling D, Gorospe M**. AMP-activated kinase regulates cytoplasmic HuR. *Mol. Cell. Biol.* 22: 3425–3436, 2002.

245. **Weitzel JM, Radtke C, Seitz HJ**. Two thyroid hormone-mediated gene expression patterns in vivo identified by cDNA expression arrays in rat. *Nucleic Acids Res.* 29: 5148–55, 2001.

246. **Wicks KL, Hood DA**. Mitochondrial adaptations in denervated muscle: relationship to muscle performance. *Am. J. Physiol.* 260: C841–50, 1991.

247. **Winder WW, Hardie DG**. Inactivation of acetyl-CoA carboxylase and activation of AMP-activated protein kinase in muscle during exercise. *Am. J. Physiol. Endocrinol. Metab.* 270: E299–304, 1996.

248. **Winder WW, Holmes BF, Rubink DS, Jensen EB, Chen M, Holloszy JO**. Activation of AMP-activated protein kinase increases mitochondrial enzymes in skeletal muscle. *J. Appl. Physiol.* 88: 2219–26, 2000.

249. **Wing SS, Haas AL, Goldberg AL**. Increase in ubiquitin-protein conjugates concomitant with the increase in proteolysis in rat skeletal muscle during starvation and atrophy denervation. *Biochem. J.* 307: 639–45, 1995.

250. **Winzen R, Kracht M, Ritter B, Wilhelm A, Chen CY, Shyu AB, Müller M, Gaestel M, Resch K, Holtmann H**. The p38 MAP kinase pathway signals for cytokine-induced mRNA stabilization via MAP kinase-activated protein kinase 2 and an AU-rich region-targeted mechanism. *EMBO J.* 18: 4969–80, 1999.

251. **Wittenberg JB, Wittenberg BA**. Mechanisms of cytoplasmic hemoglobin and myoglobin function. *Annu. Rev. Biophys. Biophys. Chem.* 19: 217–241, 1990.

252. **Wright DC, Geiger PC, Han D-H, Jones TE, Holloszy JO**. Calcium induces increases in peroxisome proliferator-activated receptor gamma coactivator-1alpha and mitochondrial biogenesis by a pathway leading to p38 mitogen-activated protein kinase activation. *J. Biol. Chem.* 282: 18793–9, 2007.

253. **Wu JJ, Quijano C, Chen E, Liu H, Cao L, Fergusson MM, Rovira II, Gutkind S, Daniels MP, Komatsu M, Finkel T**. Mitochondrial dysfunction and oxidative stress mediate the physiological impairment induced by the disruption of autophagy. *Aging (Albany. NY).* 1: 425–37, 2009.

254. **Wu Z, Puigserver P, Andersson U, Zhang C, Adelmant G, Mootha V, Troy A, Cinti S, Lowell B, Scarpulla RC, Spiegelman BM**. Mechanisms controlling mitochondrial biogenesis and respiration through the thermogenic coactivator PGC-1. *Cell* 98: 115–24, 1999.

255. **Xia Y, Buja LM, Scarpulla RC, McMillin JB**. Electrical stimulation of neonatal cardiomyocytes results in the sequential activation of nuclear genes governing mitochondrial proliferation and differentiation. *Proc. Natl. Acad. Sci. U. S. A.* 94: 11399–11404, 1997.

256. **Yakes FM, Van Houten B**. Mitochondrial DNA damage is more extensive and persists longer than nuclear DNA damage in human cells following oxidative stress. *Proc. Natl. Acad. Sci. U. S. A.* 94: 514–9, 1997.

257. **Yakubovskaya E, Guja KE, Eng ET, Choi WS, Mejia E, Beglov D, Lukin M, Kozakov D, Garcia-Diaz M**. Organization of the human mitochondrial transcription initiation complex. *Nucleic Acids Res.* 42: 4100–12, 2014.

258. **Yamashita A, Chang TC, Yamashita Y, Zhu W, Zhong Z, Chen CY, Shyu A Bin**. Concerted action of poly(A) nucleases and decapping enzyme in mammalian mRNA turnover. *Nat. Struct. Mol. Biol.* 12: 1054–63, 2005.

259. **Young JC, Hoogenraad NJ, Hartl FU**. Molecular chaperones Hsp90 and Hsp70 deliver preproteins to the mitochondrial import receptor Tom70. *Cell* 112: 41–50, 2003.

260. **Yu T, Robotham JL, Yoon Y**. Increased production of reactive oxygen species in hyperglycemic conditions requires dynamic change of mitochondrial morphology. *Proc. Natl. Acad. Sci. U. S. A.* 103: 2653–8, 2006.

261. **Zhao J, Brault JJ, Schild A, Cao P, Sandri M, Schiaffino S, Lecker SH, Goldberg AL**. FoxO3 coordinately activates protein degradation by the autophagic/lysosomal and proteasomal pathways in atrophying muscle cells. *Cell Metab.* 6: 472–83, 2007.

262. **Zheng D, Ezzeddine N, Chen CY, Zhu W, He X, Shyu AB**. Deadenylation is prerequisite for P-body formation and mRNA decay in mammalian cells. *J. Cell Biol.* 182: 89–101, 2008.

Reference List for Manuscript

1. **Adams V, Mangner N, Gasch A, Krohne C, Gielen S, Hirner S, Thierse HJ, Witt CC, Linke A, Schuler G, Labeit S**. Induction of MuRF1 is essential for TNF-alpha-induced loss of muscle function in mice. *J. Mol. Biol.* 384: 48–59, 2008.

2. **Adhihetty PJ, O'Leary MFN, Chabi B, Wicks KL, Hood DA**. Effect of denervation on mitochondrially mediated apoptosis in skeletal muscle. *J. Appl. Physiol.* 3: 1143–1151, 2007.

3. **Akimoto T, Pohnert SC, Li P, Zhang M, Gumbs C, Rosenberg PB, Williams RS, Yan Z**. Exercise stimulates Pgc-1alpha transcription in skeletal muscle through activation of the p38 MAPK pathway. *J. Biol. Chem.* 280: 19587–93, 2005.

4. **Amirouche A, Tadesse H, Lunde JA, Bélanger G, Côté J, Jasmin BJ**. Activation of p38 signaling increases utrophin A expression in skeletal muscle via the RNA-binding protein KSRP and inhibition of AU-rich element-mediated mRNA decay: implications for novel DMD therapeutics. *Hum. Mol. Genet.* 22: 3093–111, 2013.

5. **Argadine HM, Hellyer NJ, Mantilla CB, Zhan W, Sieck GC**. The effect of denervation on protein synthesis and degradation in adult rat diaphragm muscle. 107: 438–444, 2009.

6. **Bergeron R, Ren JM, Cadman KS, Moore IK, Perret P, Pypaert M, Young LH, Semenkovich CF, Shulman GI**. Chronic activation of AMP kinase results in NRF-1 activation and mitochondrial biogenesis. *Am. J. Physiol. Endocrinol. Metab.* 281: E1340–1346, 2001.

7. **Bizeau ME, Willis WT, Hazel JR**. Differential responses to endurance training in subsarcolemmal and intermyofibrillar mitochondria. *J. Appl. Physiol.* 85: 1279–84, 1998.

8. **Briata P, Forcales SV, Ponassi M, Corte G, Chen CY, Karin M, Puri PL, Gherzi R**. p38-dependent phosphorylation of the mRNA decay-promoting factor KSRP controls the stability of select myogenic transcripts. *Mol. Cell* 20: 891–903, 2005.

9. **Chen CA, Shyu AB**. AU-rich elements: characterization and importance in mRNA degradation. *Trends Biochem. Sci.* 20: 465–470, 1995.

10. **Cogswell AM, Stevens RJ, Hood DA**. Properties of skeletal muscle mitochondria isolated from subsarcolemmal and intermyofibrillar regions. *Am. J. Physiol.* 264: C383–9, 1993.

11. **Connor MK, Takahashi M, Hood DA**. Tissue-specific stability of nuclear- and mitochondrially encoded mRNAs. *Arch. Biochem. Biophys.* 333: 103–8, 1996.

12. **D'souza D, Lai RYJ, Shuen M, Hood DA**. mRNA stability as a function of striated muscle oxidative capacity. *Am. J. Physiol. Regul. Integr. Comp. Physiol.* 303: R408–17, 2012.

13. **Derbre F, Ferrando B, Gomez-Cabrera MC, Sanchis-Gomar F, Martinez-Bello VE, Olaso-Gonzalez G, Diaz A, Gratas-Delamarche A, Cerda M, Viña J**. Inhibition of xanthine oxidase by allopurinol prevents skeletal muscle atrophy: role of p38 MAPKinase and E3 ubiquitin ligases. *PLoS One* 7: e46668, 2012.

14. **Donà M, Sandri M, Rossini K, Dell'Aica I, Podhorska-Okolow M, Carraro U**. Functional in vivo gene transfer into the myofibers of adult skeletal muscle. *Biochem. Biophys. Res. Commun.* 312: 1132–1138, 2003.

15. **Egan DF, Shackelford DB, Mihaylova MM, Gelino S, Kohnz RA, Mair W, Vasquez DS, Joshi A, Gwinn DM, Taylor R, Asara JM, Fitzpatrick J, Dillin A, Viollet B, Kundu M, Hansen M, Shaw RJ**. Phosphorylation of ULK1 (hATG1) by AMP-activated protein kinase connects energy sensing to mitophagy. *Science* 331: 456–61, 2011.

16. **Ekstrand MI, Falkenberg M, Rantanen A, Park CB, Gaspari M, Hultenby K, Rustin P, Gustafsson CM, Larsson NG**. Mitochondrial transcription factor A regulates mtDNA copy number in mammals. *Hum. Mol. Genet.* 13: 935–44, 2004.

17. **Falkenberg M, Larsson NG, Gustafsson CM**. DNA replication and transcription in mammalian mitochondria. *Annu. Rev. Biochem.* 76: 679–99, 2007.

18. **Figueroa A, Cuadrado A, Fan J, Atasoy U, Muscat GE, Muñoz-Canoves P, Muñoz A**. Role of HuR in skeletal myogenesis through coordinate regulation of muscle differentiation genes. *Mol. Cell. Biol.* 23: 2003, 2003.

19. **Freyssenet D, Connor MK, Takahashi M, Hood DA**. Cytochrome c transcriptional activation and mRNA stability during contractile activity in skeletal muscle. *Am. J. Physiol.* 277: E26–32, 1999.

20. **Furuno K, Goodman M, Goldberg AL**. Role of Different Proteolytic Proteins during Denervation Systems in the Degradation Atrophy. *J. Biol. Chem.* 265: 8550–8557, 1990.

21. **Gherzi R, Lee KY, Briata P, Wegmüller D, Moroni C, Karin M, Chen CY**. A KH domain RNA binding protein, KSRP, promotes ARE-directed mRNA turnover by recruiting the degradation machinery. *Mol. Cell* 14: 571–83, 2004.

22. **Gordon JW, Rungi AA, Inagaki H, Hood DA**. Effects of contractile activity on mitochondrial transcription factor A expression in skeletal muscle. *J. Appl. Physiol.* 90: 389–396, 2001.

23. **Handschin C, Spiegelman BM**. Peroxisome proliferator-activated receptor gamma coactivator 1 coactivators, energy homeostasis, and metabolism. *Endocr. Rev.* 27: 728–35, 2006.

24. **Jäger S, Handschin C, St-Pierre J, Spiegelman BM**. AMP-activated protein kinase (AMPK) action in skeletal muscle via direct phosphorylation of PGC-1alpha. *Proc. Natl. Acad. Sci. U. S. A.* 104: 12017–22, 2007.

25. **Kim J, Kundu M, Viollet B, Guan KL**. AMPK and mTOR regulate autophagy through direct phosphorylation of Ulk1. *Nat. Cell Biol.* 13: 132–41, 2011.

26. **Koves TR, Noland RC, Bates AL, Henes ST, Muoio DM, Cortright RN**. Subsarcolemmal and intermyofibrillar mitochondria play distinct roles in regulating skeletal muscle fatty acid metabolism. *Am. J. Physiol. Cell Physiol.* 288: C1074–1082, 2005.

27. **Kukat C, Larsson NG**. mtDNA makes a U-turn for the mitochondrial nucleoid. *Trends Cell Biol.* 23: 457–63, 2013.

28. **Kukat C, Wurm CA, Spåhr H, Falkenberg M, Larsson NG**. Super-resolution microscopy reveals that mammalian mitochondrial nucleoids have a uniform size and frequently contain a single copy of mtDNA. *Proc. Natl. Acad. Sci. U. S. A.* 108: 13534–13539, 2011.

29. **Lai RYJ, Ljubicic V, D'souza D, Hood DA**. Effect of chronic contractile activity on mRNA stability in skeletal muscle. *Am. J. Physiol. Cell Physiol.* 299: C155–163, 2010.

30. **Lal A, Mazan-Mamczarz K, Kawai T, Yang X, Martindale JL, Gorospe M**. Concurrent versus individual binding of HuR and AUF1 to common labile target mRNAs. *EMBO J.* 23: 3092–102, 2004.

31. **Larsson NG, Wang J, Wilhelmsson H, Oldfors A, Rustin P, Lewandowski M, Barsh GS, Clayton DA**. Mitochondrial transcription factor A is necessary for mtDNA maintenance and embryogenesis in mice. *Nature* 18: 231–236, 1998.

32. **Lee JE, Lee JY, Wilusz J, Tian B, Wilusz CJ**. Systematic analysis of cis-elements in unstable mRNAs demonstrates that CUGBP1 is a key regulator of mRNA decay in muscle cells. *PLoS One* 5: e11201, 2010.

33. **Li YP, Chen Y, John J, Moylan J, Jin B, Mann DL, Reid MB**. TNF-alpha acts via p38 MAPK to stimulate expression of the ubiquitin ligase atrogin1/MAFbx in skeletal muscle. *FASEB J.* 19: 362–70, 2005.

34. **Maniura-Weber K, Goffart S, Garstka HL, Montoya J, Wiesner RJ**. Transient overexpression of mitochondrial transcription factor A (TFAM) is sufficient to stimulate mitochondrial DNA transcription, but not sufficient to increase mtDNA copy number in cultured cells. *Nucleic Acids Res.* 32: 6015–27, 2004.

35. **Moraes KCM, Wilusz CJ, Wilusz J**. CUG-BP binds to RNA substrates and recruits PARN deadenylase. *RNA* 12: 1084–1091, 2006.

36. **Ngo HB, Kaiser JT, Chan DC**. The mitochondrial transcription and packaging factor Tfam imposes a U-turn on mitochondrial DNA. *Nat. Struct. Mol. Biol.* 18: 1290–6, 2011.

37. **O'Leary MFN, Hood DA**. Denervation-induced oxidative stress and autophagy signaling in muscle. *Autophagy* 5: 230–231, 2009.

38. **O'Leary MFN, Vainshtein A, Carter HN, Zhang Y, Hood DA**. Denervation-induced mitochondrial dysfunction and autophagy in skeletal muscle of apoptosis-deficient animals. *Am. J. Physiol. Cell Physiol.* 303: C447–54, 2012.

39. **Paul PK, Gupta SK, Bhatnagar S, Panguluri SK, Darnay BG, Choi Y, Kumar A**. Targeted ablation of TRAF6 inhibits skeletal muscle wasting in mice. *J. Cell Biol.* 191: 1395–411, 2010.

40. **Rattenbacher B, Beisang D, Wiesner DL, Jeschke JC, von Hohenberg M, St Louis-Vlasova IA, Bohjanen PR**. Analysis of CUGBP1 targets identifies GU-repeat sequences that mediate rapid mRNA decay. *Mol. Cell. Biol.* 30: 3970–80, 2010.

41. **Rubio-Cosials A, Sidow JF, Jiménez-Menéndez N, Fernández-Millán P, Montoya J, Jacobs HT, Coll M, Bernadó P, Solà M**. Human mitochondrial transcription factor A induces a U-turn structure in the light strand promoter. *Nat. Struct. Mol. Biol.* 18: 1281–9, 2011.

42. **Sacheck JM, Hyatt JP, Raffaello A, Jagoe RT, Roy RR, Edgerton VR, Lecker SH, Goldberg AL**. Rapid disuse and denervation atrophy involve transcriptional changes similar to those of muscle wasting during systemic diseases. *FASEB J.* 21: 140–55, 2007.

43. **Sandri M, Lin J, Handschin C, Yang W, Arany ZP, Lecker SH, Goldberg AL, Spiegelman BM**. PGC-1alpha protects skeletal muscle from atrophy by suppressing FoxO3 action and atrophy-specific gene transcription. *Proc. Natl. Acad. Sci. U. S. A.* 103: 16260–5, 2006.

44. **Scarpulla RC**. Transcriptional Paradigms in Mammalian Mitochondrial Biogenesis and Function. *Physiol. Rev.* 88: 611–638, 2008.

45. **Shi Y, Dierckx A, Wanrooij PH, Wanrooij S, Larsson NG, Wilhelmsson LM, Falkenberg M, Gustafsson CM**. Mammalian transcription factor A is a core component of the mitochondrial transcription machinery. *Proc. Natl. Acad. Sci. U. S. A.* 109: 16510–5, 2012.

46. **Singh K, Hood DA**. Effect of denervation-induced muscle disuse on mitochondrial protein import. *Am. J. Physiol. Cell Physiol.* 300: C138–145, 2011.

47. **Taylor AB, Smith BS, Kitada S, Kojima K, Miyaura H, Otwinowski Z, Ito A, Deisenhofer J**. Crystal structures of mitochondrial processing peptidase reveal the mode for specific cleavage of import signal sequences. *Structure* 9: 615–25, 2001.

48. **Vlasova IA, Tahoe NM, Fan D, Larsson O, Rattenbacher B, Sternjohn JR, Vasdewani J, Karypis G, Reilly CS, Bitterman PB, Bohjanen PR**. Conserved GU-rich elements mediate mRNA decay by binding to CUG-binding protein 1. *Mol. Cell* 29: 263–70, 2008.

49. **Wagatsuma A, Kotake N, Mabuchi K, Yamada S**. Expression of nuclear-encoded genes involved in mitochondrial biogenesis and dynamics in experimentally denervated muscle. *J. Physiol. Biochem.* 67: 359–70, 2011.

50. **Wagatsuma A, Osawa T**. Time course of changes in angiogenesis-related factors in denervated muscle. *Acta Physiol. (Oxf).* 187: 503–9, 2006.

51. **Wicks KL, Hood DA**. Mitochondrial adaptations in denervated muscle: relationship to muscle performance. *Am. J. Physiol.* 260: C841–50, 1991.

52. **Wredenberg A, Wibom R, Wilhelmsson H, Graff C, Wiener HH, Burden SJ, Oldfors A, Westerblad H, Larsson NG**. Increased mitochondrial mass in mitochondrial myopathy mice. *Proc. Natl. Acad. Sci. U. S. A.* 99: 15066–71, 2002.

53. **Wu Z, Puigserver P, Andersson U, Zhang C, Adelmant G, Mootha V, Troy A, Cinti S, Lowell B, Scarpulla RC, Spiegelman BM**. Mechanisms controlling mitochondrial biogenesis and respiration through the thermogenic coactivator PGC-1. *Cell* 98: 115–24, 1999.

54. **Yakubovskaya E, Guja KE, Eng ET, Choi WS, Mejia E, Beglov D, Lukin M, Kozakov D, Garcia-Diaz M**. Organization of the human mitochondrial transcription initiation complex. *Nucleic Acids Res.* 42: 4100–12, 2014.

55. **Zhao J, Brault JJ, Schild A, Cao P, Sandri M, Schiaffino S, Lecker SH, Goldberg AL**. FoxO3 coordinately activates protein degradation by the autophagic/lysosomal and proteasomal pathways in atrophying muscle cells. *Cell Metab.* 6: 472–83, 2007.